IMPROVING THE PERFORMANCE OF FBG SENSING SYSTEM

A thesis submitted in fulfillment of the requirement for the award of the degree of

Master of Engineering Research

from

University of Wollongong

By

XINGYUAN XU

B.E, University of Electronic Science and Technology of China

Maser of Internet Technology, University of Wollongong

School of Electrical, Computer & Telecommunications Engineering

2006

CERTIFICATION

I, Xingyuan Xu, declare that this thesis, submitted in partial fulfillment of the requirements for the award of Master of Engineering Research, in the School of Electrical, Computer & Telecommunications Engineering, University of Wollongong, is wholly my own work unless otherwise referenced or acknowledged. The document has not be submitted for qualifications at any other academic institution.

Xingyuan Xu

26 June 2006

TABLE OF CONTENT

LIST OF FIGURES

ABSTRACT

The Fiber Bragg Grating (FBG) is a periodic perturbation of the refractive index inside the fiber formed by exposure of the fiber core to an intense optical interference pattern. The most important property of FBG is that it will reflect the incident light with particularly predetermined wavelengths, while passing all the other wavelengths of light at the same time. As the wavelength of the reflected light varies with the strain, temperature and other environmental factors, detection of the wavelength will yield information about these quantities. Recently, FBG has attracted much research and development effort due to their potential enormous potential of strain and temperature sensing in smart structures and polymeric materials, thereby several FBG sensing systems have been developed.

This research aims to develop new approaches to improve the performance of FBG sensing system. Firstly, we have demonstrated a novel demodulation system based on wavelength-multiplexed FBG sensors and the Fabry-Perot (FP) tunable filter for measurement of vibration/dynamic strain. By using such a system, the restricted scanning frequency of FP tunable filter is overcome. Furthermore, signal processing methods are proposed to achieve more reliable and accurate measurement. In the experiment, program controlled multipoint dynamic strain detection is successfully implemented by this system. The second task involved in this research work is to develop signal processing methods for improving the measurement precision of FBG sensing system. In practical applications, various types of noise will occur that significantly limit the accuracy of wavelength detection. Therefore, proper signal processing method is required, especially for long-term applications. In this thesis, classical digital filter, adaptive digital filter and neural network were investigated to solve this problem.

The last issue of this thesis is to improve the performance of the FBG sensing system

which using intensity and wavelength-division multiplexing (IWDM) technique. IWDM technique has the advantages of low complexity and enabling the system to contain twice the number of FBGs as the conventional WDM technique. However, this technique requires long processing times to get high detection accuracy. In this chapter, three optimization algorithms: gradient algorithm, tabu search algorithm and tabu-gradient algorithm are developed to improve the performance of IWDM based FBG sensing system.

ACKNOWLEDGEMENTS

I wish to express my deepest appreciation to all the people that have contributed to the completion of this thesis. Fist of all, I would like to express my genuine gratitude to Associate Professor Jiangtao Xi and Professor Joe Chicharo , my supervisors, for their invaluable guidance and encouragement in the research and preparation of this thesis. Without their patience, this work would not been possible.

I sincerely thank Dr. Enbang Li for sharing his wonderful knowledge and experience in the area of fiber optical sensing. He gave me patient and valuable direction throughout the experiment process.

I would like to thank the colleagues in PESPG group for many informative discussions. In particularly, my special thanks go to Mr. Yingsong Hu for his useful advices on preparing the thesis.

I am also indebted to all my best friends for their friendship and support.

Finally, I would like to thank my grandmother and my parents for their endless love, which encourages me to overcome all problems.

LIST OF PUBLICATION

Xingyuan Xu, Enbang Li, Jiangtao Xi and Joe Chicharo, "Signal Processing Methods Implemented in a Novel FBG Sensing System for Vibration/Dynamic Strain Measurement", *Proceeding of first international conference on sensing technology*, New Zealand, 2005.

Xingyuan Xu, Jiangtao Xi, and Joe Chicharo, "Improving the performance of IWDM based FBG sensing system using tabu search algorithm," Submitted to *Optical Communication.*

Xingyuan Xu, Jiangtao Xi, and Joe Chicharo, "Improving the Measurement Accuracy of FBG Sensor Using Adaptive filters," Submitted to *Proceeding of international topic meeting on microwave photonics.* France, 2006.

CHAPTER 1 INTRODUCTION

In recent years, fiber Bragg grating (FBG) has attracted much research and development effort. FBG is considered to have a critical impact on the field of the optical sensing technology due to the enormous potential of strain and temperature sensing in smart structures and polymeric materials. Compared with other traditional sensors, FBG sensors have a number of distinguishing advantages: The FBG sensor devices are small size, light weight, high temperature tolerance; The FBG sensor devices are simple and have all the advantages normally attributed to optical fiber sensors, such as electrically passive operation, EMI immunity, high sensitivity, and potential low cost; The FBG sensing system is immune to source power and connector loss which plague other types of optical sensors; FBG sensors can easily be multiplexed and build a distributed sensing network. Due to the superiority of FBG senor, various FBG sensing systems have been developed.

This research seeks to develop new approaches to improve the performance of FBG sensing system. This chapter provides general introduction and background knowledge of this thesis, which is organized as follows. Section 1 gives a general introduction for FBG. Section 2 includes a comprehensive literature review that provides the background knowledge of FBG and FBG sensing systems. Section 3 discusses the existing issues of FBG sensing system. Section 4 presents the contribution of research work. Section 5 gives a review of how this thesis is organized.

1.1 General Introduction

1.1.1 Fiber Bragg grating

FBG is a periodic perturbation of the refractive index inside the fiber formed by exposure of the fiber core to an intense optical interference pattern. FBG can perform many functions such as reflection, diffraction and filtering in a high effect and low loss mode. The most important property of FBG is that it will reflect the incident light with particularly predetermined wavelengths, while passing all the other wavelengths of light at the same time. As the wavelength of the reflected light varies with the strain, temperature and other environmental factors, detection of the wavelength will yield information about these quantities. Therefore, FBG is an ideal candidate in the sensing field.

1.1.2 FBG applications in sensing field

FBG has found wide applications for measuring temperature, strain, pressure and other environment factors in the field of sensing technology such as:

- Civil engineering structural monitor
- Pressure, strain, temperature sensor for aerospace application
- Optical fiber thermometers for thermocouple and thermistor device
- Deep Bore-hole application
- Real time strain gauge for glass reinforced lock gate
- Acoustic measurement in marine application
- Detector for high frequency ultrasonic field
- Medical application
- Steam Pipe monitor
- Nuclear shield monitor
- Waste conditioning and disposal monitoring
- Multiplexed load monitoring system for power transmission lines

1.1.3 Aims of the thesis work

This thesis work aims to deal with the following research issues associated with the FBG sensing systems:

- Design a simple FBG distributed sensing system for vibration/dynamic strain measurement.
- Improving the measurement precision of FBG sensing system using signal processing algorithms
- Improving the performance of Multiplexing techniques for FBG sensing system.

1.2 Literature Review

1.2.1 Introduction

The literature review provides a critical overview of the background knowledge of the FBG sensor and the FBG sensing system. It looks around the existing literatures in this field and determines the strengths and weaknesses in what has been done in this area.

In this section, we firstly introduce the fundamentals of FBG, including fabrication, properties and types of FBGs. Then we present a brief review of the FBG sensor including basic Bragg gratings quasi-distributed sensors, the chirped Bragg grating sensor, Bragg grating laser sensors and the application of the FBG senor. Also, multiplexing and demodulating technology of Fiber Bragg grating systems are introduced. Finally we address the existing issues of FBGs sensing system.

1.2.2 Fundamental of FBG

In 1978, a significant phenomenon was discovered by Dr. Kenneth Hill *et al*. at the Canadian Communication Research Center (CRC). Through exposing the fiber under light with characteristic wavelength and intensity, a corresponding index perturbation occurs in the core of the waveguide. Then they got an index grating which is

photo-imprinted in the optical waveguide and an entire class of in-fiber components - fiber Bragg grating was introduced. This kind of grating is subject to the perturbation of temperature and strain, which lead to wavelength dependent reflectivity. Thus, by tracking the wavelength of the Bragg reflection light, we will acquire the information of external environment. A brief overview of fabrication, property and types of FBG will be given in this section.

1.2.2.1 Grating fabrication

The Fiber Bragg Grating is formed by changing the refractive index of the single-mode Ge-mixed fiber core. Putting the fiber under the periodically-space changing UV laser source, perturbation of the refractive index will occur in the fiber core. Because the periodical perturbation of refractive index only influences a very narrow spectrum, the FBG plays the function of speculum of choosing the light wave. Essentially, Bragg Grating can be classified as the internal and external fabrication. Hill and co-worker (1978) firstly demonstrated the internal fabrication technique. Internal fabrication use single frequency laser light as the source. By coupling the light into the fiber core, the incident laser light interferes with the reflection light (from the cleaved end of the fiber) and forms an intensity pattern within the core of fiber. The high-intensity points alter the index of the refraction permanently that forms Bragg gating (Hill *et al.*, 1978). This technique is simple and the requirement of experimental equipment is minimal. However, the Bragg wavelength is limited by the excitation laser wavelength (Othonos, *et al*., 1999). Therefore, far more useful gratings are inscribed using external techniques such as the interferometric fabrication (Meltz and co-workers *et al.*, 1989), phase mark fabrication (Hill and co-worker *et al.*, 1993) and point-by-point fabrication (Malo and co-worker *et al.*, 1993). Instead of coupling the light into the fiber core, the external fabrication technique forms the interference pattern by side exposing the photosensitive fiber under light. External fabrication technique overcomes the fundamental limitation of internal fabrication and has been widely used today.

1.2.2.2 Properties of FBG

FBG consists of a periodic modulation of the refractive index in the core of a single-mode optical fiber. The phase fronts of the uniform fiber grating are vertical to the longitudinal axis of the fiber. Incident light will be scattered by each grating plane when it is guided along the core of the optical fiber as shown in Figure 1.1. If the Bragg condition is fulfilled, reflected light from each grating will produce a back-reflected peak.

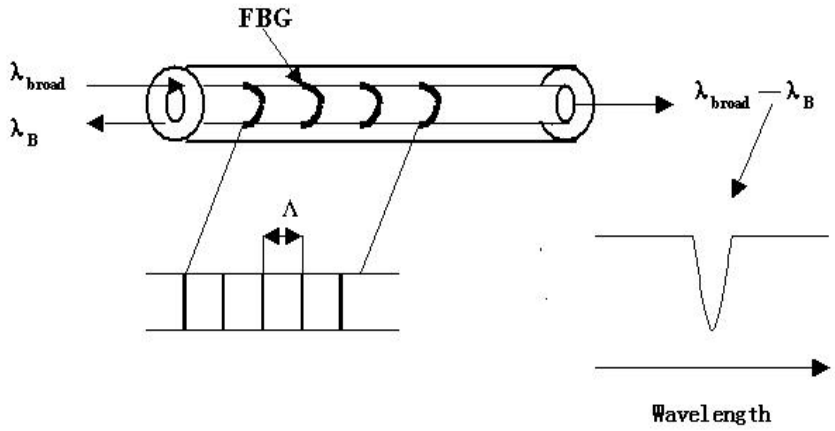

Figure 1.1 Properties of the uniform Bragg Grating

The requirement of the Bragg Condition is to satisfy momentum conservation. The momentum conservation condition can be expressed as following Equation (Othonos, *et al.*, 1999):

$$\frac{4\pi n_{eff}}{\lambda_B} = 2\pi / \Lambda \tag{1.1}$$

and it can be simplified to

$$\lambda_B = 2n_{eff}\Lambda \tag{1.2}$$

where λ_B is the reflectivity peaks (Bragg wavelength) of the input light which will be back- reflected, n_{eff} is the efficient refractive index of the core and Λ is the period of index modulation of FBG. Typically, the gauge length of fiber Bragg grating is 5 mm.

The length up to 100 cm is used for civil-engineering applications and the reflected spectral component has a bandwidth of 0.05 – 0.3 nm (Grattan and Meggitt, 2000).

A very important character of fiber Bragg grating is that the wavelength of reflected light will change when there is a change in strain, temperature and other environment factor. The reason is that change of the strain of the grating or its environmental temperature can result in change in the efficient refractive index of the core n_{eff} as well as the period of index modulation Λ. Therefore, the change of n_{eff} and Λ leads to offset of Bragg wavelength λ_B. Now, strain and temperature sensitivity for a 1550-nm FBG can reach 8.87 pm/μstrain (K.Zhou, *et al.*, 2004) and 9.62 pm/° C respectively (Jharna Mandal, *et al.*, 2005). By examining the excursion of λ_B, corresponding strain and temperature can be obtained that makes the FBG as a sensor.

The shift in Bragg wavelength with strain and temperature is expressed using (Morey, *et al.*, 1989):

$$\frac{\Delta\lambda_B}{\lambda_B} = \left(1 - \frac{n^2}{2}\left[\rho_{12} - \nu(\rho_{11} - \rho_{12})\right]\right)\Delta\varepsilon + (\alpha + \xi)\Delta T \qquad (1.3)$$

where, $\Delta\varepsilon$ is applied strain, $P_{i,j}$ is Pockel's coef. of the stress-optic tensor, ν is Pisson's ratio , α is coefficient of thermal expansion, ξ is thermo-optic coefficient, ΔT is temperature change.

For a typical germanosilicate fiber, the coefficients $P_{i,j,}$ ν, ξ and α are almost fixed. Therefore, Bragg Wavelength is approximately has linear relationship with the environment factors.

FBG has been regarded as an excellent element for use as sensors to measure strain, temperature, and other physical parameters. However, FBG's are sensitive to both strain and temperature, and thus independent measurement of these two measurements

using a single FBG is very difficult. Therefore, the major drawback of FBG sensors is that temperature variations along the fiber will be indistinguishable from strain (Kersey *et al.*, 1997, Othonos *et al.*, 1999). It is very necessary to find an approach to separate the temperature-induced and strain-induced wavelength shifts. A simple technique (Morey, *et al.*, 1989) is to use a reference grating along the fiber. The reference grating is only influenced by temperature but does not respond to the strain. The reference FBG and the common FBG are located close to each other so that they are almost in the same thermal environment. The temperature-induced wavelength shift of the dual-sensitive common FBG can be compensated by subtracting the wavelength shift of the reference FBG.

The advantage of this method is simple and of low cost. However, this method needs two absolutely identical FBG for a measurement system. In addition, for the applications that require compact operation space, adding the reference sensor may not be practicable. Recently, many other advanced discrimination measurement methods are introduced such as dual-wavelength superimposed FBGs method (Xu *et al.*, 1994), combined FBG and LPG method (Bhatia *et al.*, 1996), different cladding-diameter FBGs method (James *et al.*, 1996), FBG Febry–Perot cavity method (Du *et al.*, 1999) and superstructure FBG method (Guan *et al.*, 2000). These methods can achieve better performance than reference grating method and suitable for different FBG applications.

1.2.2.3 Types of fiber Bragg grating

There are three main types of fiber Bragg grating structures: common Bragg grating (Hill *et al.*, 1978), blazed Bragg grating (Meltz *et al.*, 1991), and chirped Bragg grating (Outllette, *et al.*, 1991). These fiber Bragg grating are distinguished by the spacing between grating plane (grating pitch) and tilt. Common fiber Bragg grating has a constant pitch. Non-periodic pitch chirped grating display increased space between grating planes. As for blazed Bragg grating, it has phase front tilted to the fiber axis,

therefore the angle between the grating planes and the fiber axis is not perpendicular.

- Common fiber Bragg grating

The common Bragg Grating has periodic modulation of refractive index and constant period of the grating plane. This type of grating is very simple and used widely. The common Bragg grating can be used as a narrow band transmission of reflection filter depending on adjusting the grating length and magnitude of induced index change. Figure 1.2 shows that the Bragg grating is used to remove the discrete wavelength to modify a broadband spectrum.

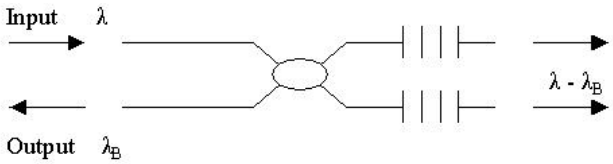

Figure 1.2 Filter arranged in a Michelson type configuration

As Bragg grating has wavelength-encoded characteristics, Bragg grating is considered to be good strain and temperature sensing devices. The appearance of common Bragg grating eliminates the problems of intensity and amplitude fluctuations that happened in other types of fiber-based sensor system. Also, a series of grating can be written in the same fiber, because each Bragg grating can be designed to having its own wavelength character. This configuration can be used for wavelength division multiplexing of quasi-distributed sensing (Kershyap *et al.*, 1996). In addition, common Bragg grating can serve as one or both ends of the laser cavity. Changing the Bragg wavelength will vary the lasing wavelength. Using this method, single mode erbium fiber laser can be made with two Bragg grating (Ball *et al*, 1992).

- Chirped Bragg grating

Chirper Bragg grating refers to the grating that has aperiodic pitch. Chirped Bragg grating has attracted more and more interest in the sensing and telecommunication

field. A chirped Bragg grating is a grating that has a varying grating period as show in Figure 1.3.

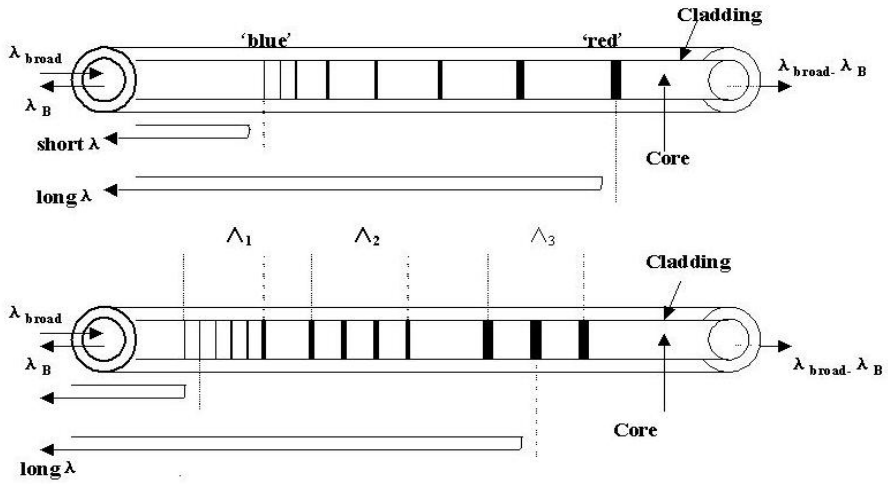

Figure 1.3 (a) Chirped grating with an aperiodic pitch, (b) A cascade of several grating with increasing period.

Interest in chirped gratings focused originally on their potential for dispersion compensation in telecommunications systems and the stable synthesis ability in multiple wavelength sources (Ouellette *et al.*, 1991). These types of grating can be realized by axially varying either period of the grating or the index of refraction of the core or both. Figure 1.4 shows a linear chirped Bragg grating in which the period of the grating varies linearly with the position. With this characteristic, the grating can reflect different wavelengths along its length.

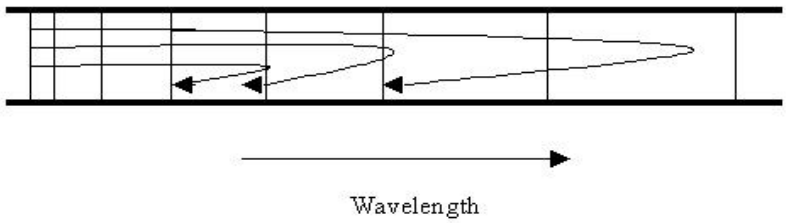

Figure 1.4 Linear chirped Bragg grating

Linear variation of the grating period is the simplest type of chirped grating structure (Ouellette *et al.*,1987):

$$\Lambda(z) = \Lambda_0 + \Lambda_1 z \qquad (1.4)$$

where z is the length of grating, Λ_0 is the starting period and Λ_1 is the linear change along the length of the grating. Therefore, the chirped Bragg grating can be considered as a series of small length common Bragg Grating in period.

- Blazed Bragg grating

Baek *et al.* (1990) proposed another structure of fiber Bragg grating. This grating has a tilt angle with the fringes of the Bragg grating along the core of fiber. The incident light guided in the fiber core will be coupled into a loosely bound, guided cladding or radiation modes by the blazed grating (Othonos *et al.*, 1999). The tilt angle of the grating planes and the strength of the index modulation determined the coupling efficiency and the bandwidth of the trapped out light. In a single-mode fiber Bragg grating, the grating tilt can effectively reduce fringe visibility. However, coupling of the cladding mode can be influenced by the tilt angle of a grating seriously (Baek *et al.*, 1990). Figure 1.5 shows the principle of the blazed fiber Bragg grating as follows:

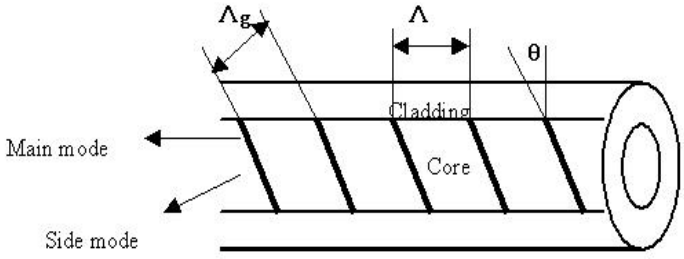

Figure1.5 Blazed fiber Bragg grating

where

θ is the tilt angle of the blazed fiber Bragg grating

Λ*g* is grating periods with axes

Λ is grating periods unprimed axes

In order to understand the theory of a tilt angle influencing a FBG, it is necessary to assume that a tilt angle causes the change of the refractive index in the core of the fiber, as described by the following Equation (Kashyap and Wyatt, 1994),

$$\delta n_{co}(x,z) = \delta n_{\infty}(z')\left\{1 + v\cos\left[\frac{2\pi}{\Lambda_g}z' + \phi(z')\right]\right\} \quad (1.5)$$

where δn_{∞} is the spatially averaged index change in a grating period, v is the fringe visibility that describes the index change, and $\phi(z')$ describes the situation of grating chirp. It is clear that for blazed gratings not only different wavelengths emerge at different angle, but also different modes of the same wavelength emerge at slightly different angles for their different propagation constant.

The most important applications of blazed Bragg grating are mode conversion and acting as gain flatteners in amplifiers. Kashyap has demonstrated the use of multiple blazed gratings to flatten the gain spectrum of erbium-doped fiber amplifier in 1993. This is important in fiber communications that use signals at different wavelengths. Blaze Bragg grating also can be used in other application such as: Narrow band transmission filter, Reflection filter or mirror in WDM, FBG sensors Building industry, pump stabilizers and Add/Drop filter (Morey *et al.*, 1991).

- Novel Bragg grating structure

With the development of fabrication technology of FBG, there are some atypical gratings were demonstrated that have significant value to sensing and telecommunication devices. These structure include superstructure Bragg gratings, superimposed multiple Bragg gratings and phase-shifted Bragg Grating.

The superstructure Bragg grating refers to a special grating fiber structure, which is fabricated with a modulated exposure over the length of the grating (Eggleton *et al.,* 1994). The resulting period of the grating envelope was approximately 5.65mm and forming several periods of the superstructure. These superstructures grating can be used for signal processing and for increasing the tunability of the fiber laser grating reflector.

The superimposed multiple Bragg grating was demonstrated by Othonos and Co-workers (1994) that several Bragg grating can be fabricated at the same location on a piece of optical fiber. This is a very important discovery for the device in sensing system, because the multiple Bragg grating is very suitable for multiplexing and de-multiplexing signals.

The principle of the phase-shifted Bragg grating was demonstrated by Alferness (1986). The phase shifted grating is formed by exposing the grating region to pulses of UV laser radiation. The phase-shifted Bragg grating can act as the basic component of the single-mode semiconductor distributed feedback (DFB) laser, which is used to tailor the transmission spectrum to suit specific requirement (Agrawal *et al.*, 1993). This technology can be used to design the FBG as the narrowband transmission filter that is widely used in a multi-channel telecommunication system.

1.2.3 Fiber Bragg grating sensor

FBG has been considered as an excellent sensor element in recent years, which are currently receiving more and more research interest. The FBG attracts wide attention for its wavelength-based algorithms, which make the sensor self-referencing with less power/conductor loss. Furthermore, FBG sensor has the advantages of low cost, ease to fabricate and small volume. Therefore, the Bragg grating sensors are very important component for the development of smart structure sensing technology (Chavez, *et al.*, 1998). This section presents a comprehensive discuss of existing FBG sensor including Bragg grating point sensor, Chirped Bragg grating sensor and Bragg grating laser sensor.

1.2.3.1 Bragg grating point sensor

Today, the Bragg grating senor is widely used for providing sensing of strain and temperature. One of the most important advantages of FBG is that the wavelength coded sensed information does not depend directly on the light level or losses along the

fiber. Kersey *et al.* (1997) concluded that this property enable FBG suitable for processing quasi-distributed point sensing of strain and temperature or other measurands. The temperature response relies on the refractive index of FBG while the strain response is based on the fractional change in grating pitch and fiber index which is influenced by photo-elastic effects. The measured temperature response at a constant strain is found to be (Kersey, *et al.*, 1997):

$$\frac{1}{\lambda_B}\frac{\delta\lambda_B}{\lambda\delta T} = 6.667 \times 10^{-6} {}^{\circ}C^{-1} \tag{1.6}$$

The measured strain response at a constant temperature is found to be:

$$\frac{1}{\lambda_B}\frac{\xi\lambda_B}{\lambda\xi\varepsilon} = 0.78 \text{ x } 10^{-6}\,\mu\varepsilon^{-1} \tag{1.7}$$

Normally, using laboratory instrumentation, Bragg wavelength λ_B = 1300nm can achieve the resolution of 1 pm (0.001 NM) to resolve the strain change of 1 μ strain or temperature change of 0.1 $^{\circ}C$ (Kersey *et al.*, 1997). However, to achieving this resolution using small packaged optics unit in practical environment is still very difficult (Kersey *et al.*, 1997).

1.2.3.2 Chirped Bragg grating sensor

The recent attention of chirped Bragg grating is its application in optical fiber sensor systems. Chirped Bragg grating sensor refers to the sensor based on the non-periodic pitch chirped grating. The basic principle of this application is the measurement of the change of the reflection wavelength and the measurand can be temperature, pressure, strain etc (Hill *et al.*, 1994).

$$\lambda_B(z) = 2n_{eff}(z)\Lambda(z) \tag{1.8}$$

where n_{eff} and $\Lambda(z)$ may vary along the grating due to the effects of the measurand (Hill *et al.*, 1994):.

$$\Delta\lambda = 2n_{eff}\Lambda + 2n_{eff}\Delta\Lambda \tag{1.9}$$

The shift of the reflection wavelength is caused by changes in the refractive index n_{eff} and in the Bragg period. Typically there are two important chirped sensors: broadband chirped grating sensor and tapered chirped grating sensor. The following paragraphs will give a brief introduction to these two chirped grating sensor.

The FBG sensing system using normal narrowband Bragg grating always relies on the optical filter to demodulate its wavelength-encoded signal. Chirped Bragg gratings possess a broadband, step-function chip profile. This property can provide many advantages, particularly as an alternative to matched-grating demodulation. A demodulation method called identical chirped Bragg grating (ICGI) which is based on the matched-grating of two identical and broadband chirped that was demonstrated by Fallon *et al.* (1997). This technology eliminates the requirement of high-quality piezoelectric actuators or tunable filters and it is particularly attractive for aerospace application. The process of this method can be described as: light coming from a broad source is reflected by the sensing chirped grating to the reference grating. The reference grating acts as a rejection filter to minimally transmit the reflected light to the detector. If perturbation affects the sensing grating, its spectral profile is almost linearly shifted. This phenomena result in a fraction of the reflected light from the sensing grating falling outside the rejection band of the rejection filter and being transmitted to the detector. By measuring the output power of detector, the strain or temperature information can be determined. Also ICGI can be in the multiplexing scheme that the sensor is interrogated simultaneously and the speed of interrogation can be very fast.

Another very important chirped grating sensor introduced by Putnam *et al.* (1995) is the tapered grating sensor. The tapered chirped grating is written on a first tapered fiber and this taped fiber is under a tension load during the fabrication process. The most important property of taper grating sensor is that it has different response with temperature and strain. Strain leads to the widening of the spectrum and the shift of the Bragg wavelength of reflected light. Temperature only leads to the shift of the Bragg

wavelength. As the tapered grating sensor applied in the environment with cross-sensitivity, temperature and strain can be measured separately by measurement of the spectral shift and broadening. Therefore, these devices are widely used to simultaneous measurement strain and temperature.

1.2.3.3 Bragg grating laser sensor

Fiber Bragg grating can also act as narrowband reflector for forming in-fiber laser cavities. Ball *et al.* (1993) first introduced Bragg grating laser sensor. The basic Bragg grating laser sensor is formed by two FBG with matched Bragg wavelength and Er-doped fiber. Two FBGs can create an in fiber cavity and the Er-doped fiber between FBGs acts as the gain medium allows the system to be optically pumped thus lasing. If an external perturbation acts on the FBGs, the lasing wavelength will change as well. By measuring the lasing wavelength, measurand information can be acquired. FBG laser sensor has a very important meaning for the particular high-resolution dynamic temperature and strain monitoring in the sensing field. The Bragg grating laser sensor can be implemented through various ways and operated in both a single frequency and multimode fashion (Dong *et al.*, 2000).

The main advantage of laser-based sensors is that it can significantly increase the signal to noise ratio of FBG sensing system. Therefore, laser-based FBG sensor offers greater measurement resolution than common FBG sensor. And an important application of the tunable and calibrated fiber laser can be used as the source and demodulator to the passive grating array.

1.2.3.4 Applications of FBG sensors

The use of the FBG sensor appears to have many benefits in various fields. However, some applications are not mature, and some are under developed. The most recently discussed FBG sensor applications are geophysical monitoring, petroleum and civil structure protection.

It is very important to monitor and obtain environmental data for both protecting ecosystems and the environment and limiting damage in city and village infrastructure. FBG sensor is very useful in the geophysical field, such as flood forecasting, defense and estimation, wetlands management and drainage, river level and wave height monitoring, conservation, power generation (Gornall *et al.*, 2003) and reservoir safety, etc.

It is necessary for the petroleum industry to apply FBG sensor. Both the temperature and strain are important parameters in searching for oil and gas and testing their boundaries. Furthermore, it is crucial to monitor the environment of wells and their trends in order to avoid well disaster. Well-monitored systems are designed for down-hole application to measure temperature and pressure in extreme conditions which exceed 150 $^{\circ}C$ and 1000 bar respectively (Liquime *et al.*, 1997). FBG sensors are potentially useful for this application for their ability to work in high-pressure and high temperature environments with limited space. Also FBG sensors can fulfill the requirement of long working distance and lifetimes. However, in terms of achieving ultra-high wavelength resolution and pressure resolution, FBG sensor is left behind compared to the conventional sensing system (Gornall *et al.*, 2003). Therefore, FBG sensors still need to be developed in this application.

FBG sensors are drawing attention from civil infrastructure all over the world. In civil structures such as bridges and important architectural buildings, the measurement of strain is critical so that can carry out earlier detection of erosion. Optical fiber strain sensing systems on the basis of FBGs greatly benefits the civil structures like the above mentions. For instance, integrating a fiber optic sensor network with any composite structure can provide an immediate strain analysis. It is critical for the appropriate examination and certification of the structure (Meissner *et al.*, 1997). Also, carbon fibers and steel are being utilized for strengthening and stiffening structures (Dewynter

et al., 1998). In these cases, it is also important to monitor and measure the conditions of structures. Because of the early detection of occurrences of problems, maintenance costs can be heavily reduced and the awareness of safety is brought to the fore.

1.2.4 Demodulation technique of optical sensing system

The signal demodulation is one of the key technologies of the sensing system that researchers always pay close attentions to. The signal demodulation technique of fiber Bragg sensing system is to track the environment factors-induced Bragg wavelength-shifts of the sensors. The measurand information can be determined through the shift in Bragg wavelength that has a direct correlation with corresponding change of environment factor. At present, there are various kinds of fiber grating sensing signal demodulation systems including fixed filter demodulation (Nunes *et al.*, 2004), spectrum coding/ratiometric demodulation (Davis *et al.*, 1994), interferometric demodulation (Koo *et al.*, 1995) and tunable Fabry-Perot filter demodulation (Kersey, *et al.*, 1993) etc. Considering from the aspect of the time response, there are both dynamic and static (or semi-static) demodulations (Zhang *et al.*, 2000) and analysis from the aspect of the nature of the parameter demodulation, intensity, phase position, polarization and wavelength exist (Rao *et al.*, 1997). Out of the demodulation techniques, tunable Fabry-Perot filter demodulation and interferometric demodulation are the most popular and have been widely used.

1.2.4.1 Reference filter demodulation (Zhang, 2004)

This demodulation system utilizes another FBG (reference fiber grating) to track the wavelength's change. It enables the reflected wavelength of the reference FBG in accordance with that of the sensing FBG at a certain time or within a certain period of time. Figure 1.6 shows the realization of the demodulation.

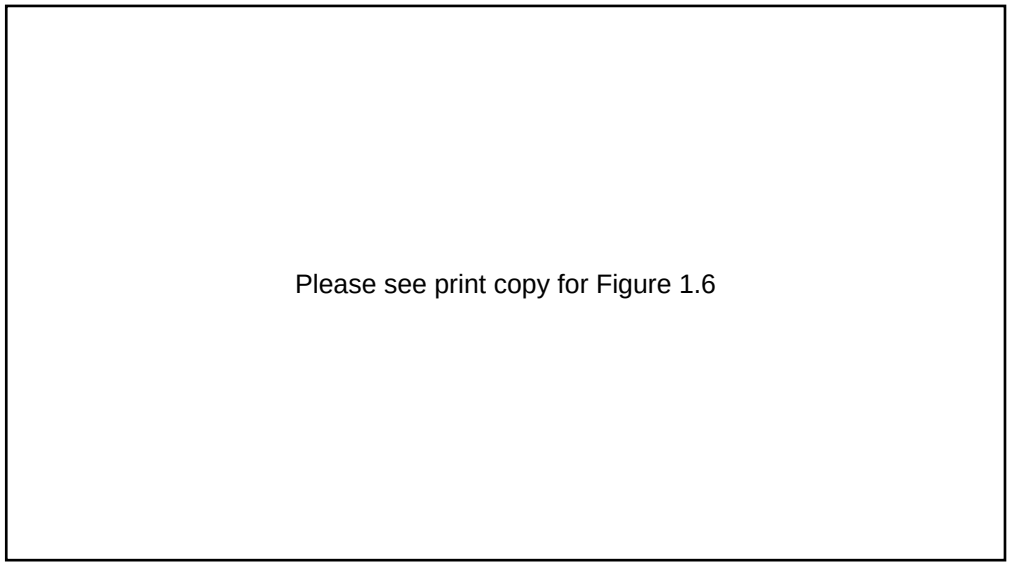

Figure 1.6 Reference filter demodulation (Zhang *et al.*, 2004)

The reflected light from the sensing FBG reaches the reference FBG. When the reflected wavelength of the reference FBG is consistent with that of the sensing FBG, the light is reflected instead of transmitted. The displacement of the wavelength of the sensing FBG can be measured through measuring the maximum reflected power or the minimum transmission power. When the wavelength of the reference fiber grating is equal to the wavelength of the sensing FBG, the driving signal of the driving organ is corresponding with the reflected wavelength of the sensing FBG. The measured strain or temperature can be gained by measuring the driving signal of the driving organ. This kind of sensor has the advantages of simple structure and low cost. However, the sensitivity and range of this approach is limited and the portability is reduced for it's based on bulk optic components.

1.2.4.2 Ratiometric demodulation (Melle *et al.*, 1992)

The principle of the radiometric demodulation system is shown in Figure 1.7. The reflected light from FBG is split into two beams of equal intensity. One of the beams is filtered by an edge filter before being detected by a photo detector. The edge filter has a wavelength dependent transmittance property that is linear with the wavelength range. The other beam that acts as a reference signal is directly detected by a photo detector. The reference signal is used to eliminate the measurement error caused by the intensity

fluctuations of the light source and the fiber. The ratio between the filtered beam and the reference beam provides the information of the Bragg wavelength. Supposing the narrowband reflected Bragg grating has a spectrum width $\triangle\lambda$ of the Gauss function, the central wavelength of the spectrum is λ_B, and the filtering function is

$$F(\lambda) = A(\lambda - \lambda_p) \tag{1.10}$$

and the proportion between the signal of the filtering-wave light I_F and that of the reference light I_R can be expressed as (Melle *et al.*, 1992):

$$\frac{I_F}{I_R} = A(\lambda_B - \lambda_0 + \frac{\Delta\lambda}{\sqrt{\pi}}) \tag{1.11}$$

where A is the slope of filtering wave. The above formulation is a linear function of the reflected Bragg wave obviously. Because the detection system of this method applies the self-adjustment principle, the fluctuation and change of the light source's intensity, coupling loss and connector's alignment do not influence the output of the system. However, there is a disadvantage of this demodulation technique that it is not an all fiber approach and the alignment of the edge filter will reduce the measurement precision (Zhao, *et al.*, 2004). Davis has proposed an all fiber system to solve this problem. This improved system using a WDM fiber coupler to replace the edge filter (Davis, *et.al*, 1994).

Please see print copy for Figure 1.7

Figure 1.7 Ratio metric Demodulation (Zhang *et al.*, 2004)

1.2.4.3 Interferometric demodulation (Kersey *et al.*, 1992)

The interferometric demodulation system using interferometer to convert the wavelength shifts into a phase change at the interferometer output. Figure 1.8 shows the principle of this type of demodulation system. In this method, the reflected light from the FBG is directed through the interferometer with unequal path. FBG wavelength shift can be converted into phase shift by the unbalanced interferometer. The band pass filter is used to eliminate slowly varying thermal phase drifts of the interferometer. Through controlling the path balance between the interferometer arms, the output of interferometer can be assessed. The correlation of the output phase and FBG wavelength shift is given (Melle *et al.*, 1992):

$$\Delta \phi = \frac{2 \pi nd}{\lambda} \Delta \lambda \tag{1.12}$$

The primary advantage of this system is it has very high sensitivity and is suitable for measuring the dynamic signal. However, the random phase shifting makes this method only suitable for dynamic strain sensing and problematic for quasi-strain sensing. Furthermore, the range of the phase shift will limit the measurement range, and the wastage of the measured wavelength will appear in this case.

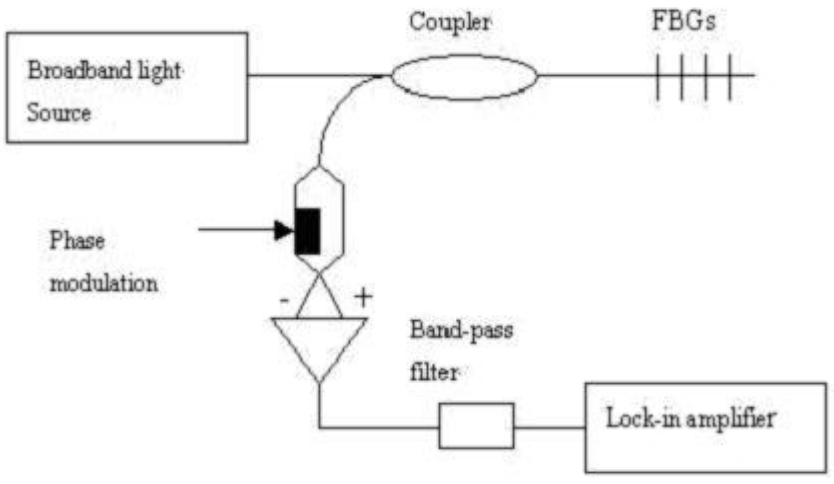

Figure 1.8 Interferometric demodulation system for FBG sensor

1.2.4.4 Fabry-Perot filter demodulation (Kersey *et al.*, 1993)

The most popular demodulation technology is based on tunable Fabry-Perot (FP) filter. This method has many advantages including compact size, reasonable price and directly wavelength-voltage transfer. The theory of tunable FP filter demodulation is shown in Figure 1.9.

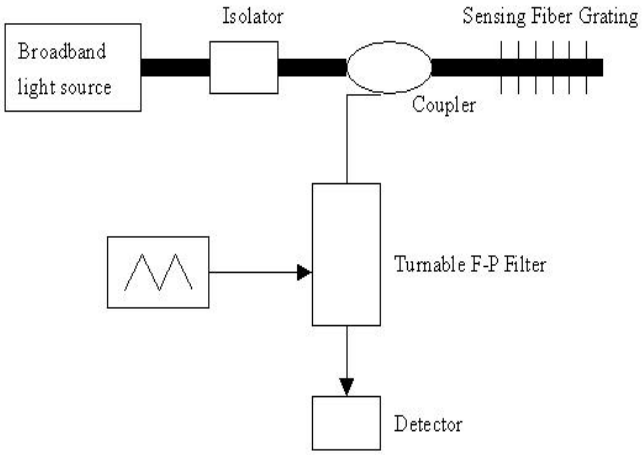

Figure 1.9 Tuneable FP filter demodulation

The light reflected from the FBG is transmitted to the tunable FP filter via the coupler. The FP filter only passes one narrowband wavelength depending on the space between two FP filter mirrors, which can be electrically controlled. Therefore, if the pass band scanner detects the maximum intensity of the transmission light from FP filter, the wavelength can be determined from the voltage applied to the filter at that time.

1.2.5 Multiplexing techniques

One distinctive feature offered by FBG's is their excellent multiplexing capability. Multiplexing of FBG sensors enables the distributed measurement along the fiber. The multipoint configuration reduces the costs of system. Therefore, FBG sensor has a very wide prospect of applications in the field of safety inspection of the large structures, such as dams, bridges, architectures and aircrafts, etc. The following multiplexing techniques have been applied to optical sensor: time, wavelength, spatial, and frequency. Among these different multiplexing techniques, the wavelength division multiplexing technique is most widely used. However, the maximum number of sensors is limited by

the ratio of the source spectral width over the spacing between the Bragg wavelengths variation range of the FBGs. In order to increase the multiplexing number of the fiber grating, techniques were introduced such as intensity and wavelength-division multiplexing (IWDM) (Zhang *et al.*, 1999), mixed WDM/TDM multiplexing (Kersey *et al.*, 1997), code-division multiplexing access (CDMA) multiplexing (Koo *et al.*, 1999) and frequency-modulated continuous-wave (FMCW) multiplexing (Chan *et al.*, 2000). Among all, IWDM and mixed WDM/TDM are easy to implement and extendible to embrace gratings with larger numbers thereby further enhancing capacity of the sensing system. In this section, an overview of two fundamental multiplexing techniques (WDM and TDM) are given, and two advanced multiplexing techniques (IWDM and WDM/TDM) are discussed thereafter.

1.2.5.1 Wavelength division-multiplexed (WDM) systems

WDM was defined as a technique used in optical fiber communications that allows two or more samples in different wavelengths can be combined and transmitted with the same direction at the same time (Putnam *et al.*, 1990). As shows in Figure 1.10, the different wavelengths λ_1, λ_2, λ_3, λ_4, and λ_5 of optical signals can be simultaneously multiplexed and transmitted in the same direction along a single optical fiber cable.

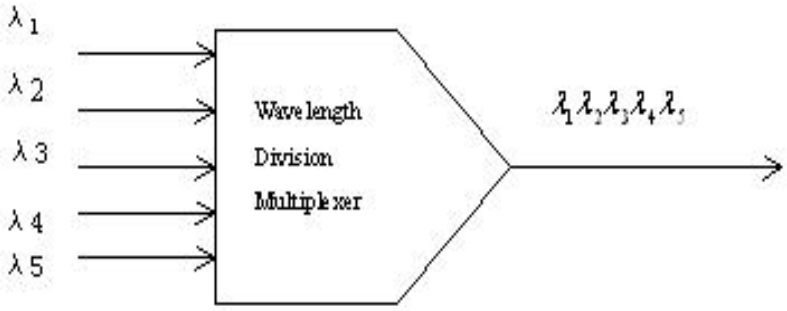

Figure 1.10 Wavelength-division Multiplexing

Because FBG has wavelength-encoded property, it is easy for implementing wavelength-division multiplexing (WDM). The theory of the multiplexed FBG is that the working wavelengths of each FBG are inter-separated, the reflected signal is gained

through the 3-dB coupler, and the wavelength detecting technology is used to measure the wavelength (or the movement of the wavelength) of each FBG.

In the mode of the wavelength multiplexing, because multiple FBGs use the same source and the reflected wavelength of each FBG moves linearly with the change of the strain (or the temperature) within a certain scope of the spectrum, the spectrum space of each fiber grating must not be overlapped each other, and the measurement of them can be guaranteed without interrupting each other within that scope. Therefore, the spectrum space of the single FBG sensor and the spectrum scope of the source determine the aim of the multiplexing. The general LED sources allow the multiplexing of over 10 FBGs (Othonos *et al.*,1999). Thus, only using a set of the system can realize the strain measurement of multiple positions that extremely reduces costs.

1.2.5.2 Time-division-multiplexed (TDM) systems

Time-division multiplexing (TDM) is the method of combining several sampled signals in a definite time sequence. The main advantage of TDM is it allows many simultaneous signals to be transmitted over a single link in which each sampled signal rises to a continuous signal after filtering.

In a TDM FBG sensing system, a pulsed laser source acts as the light source. The reflected light from the gratings can be separated in time domain (Weis *et al.*, 1994). The minimum distance between two gratings is determined by the emitted pulse time width. This technique requires fast time domain signal analysis to discriminate the reflected signal from different individual FBG sensors. Comparing with WDM technique, TDM technique can increase the sensor number for a FBG sensing system (Rao *et al.*, 1997). The limitation for TDM is that the requirement of a laser source is very high. It demands very high source power and very short laser pulses to get high values of SNR. Also, as the coherence length of the laser is long, parasitic interferometric signals will affect the measurement accuracy of system (Chan *et al.*,

2000).

1.2.5.3 Intensity and wavelength division multiplexing

Zhang (1999 *et al.*) has proposed an intensity and wavelength division multiplexing to increase the sensor number of FBG sensing system. In such a system, a series of wavelength stepped FBG's with high reflectivity and low reflectivity are alternately placed along a fiber (Zhang *et al.*, 1999). In a conventional WDM system, the total usable bandwidth of the light source and the required operation wavelength range of each FBG sensor determine the maximum number of FBG sensors. The operation wavelength range of adjacent gratings is not permitted to cross each other. In contrast, in the reflectivity-encoded IWDM FBG sensing system, the spectrum of adjacent gratings can overlap each other. Therefore, an extra set of gratings with different reflected intensity can be inserted alternately into the original FBG sensor array. This system can contain twice the number of FBGs as the original sensor array and keeping the same dynamic range for each FBG sensor.

However, the wavelength of the reflected signal cannot be identified when the low reflectivity FBG and high reflectivity FBG totally overlap. To solve this problem, dual-peak structure gratings are used in the sensor array (Zhang, *et al.*, 1999). All the low reflectivity FBG have dual peak spectral feature and the bandwidth of each spectrum is the same as that of high reflectivity FBG. When the dual peak FBG is affected by the environment factors, both peaks of grating will shift simultaneously with same distance. If one peak is overlapped with the high reflectivity FBG, the shift of the wavelength can be read from another peak.

This system requires specifically fabricated dual peak FBG sensors. Gong *et al.* (2002) have demonstrated a signal processing method named minimum variance shift (MVS) for the IWDM scheme based on common FBG sensors. By this method, wavelength detection can be achieved by scanning through specified ranges at small steps. However,

the computation time is long, making it difficult to apply in practical situations where a large number of FBG sensors are involved.

1.2.5.4 The Combination of TDM and WDM

Berkoff *et al.* (1995) demonstrated an effective method to reuse the spectrum is combining TDM and WDM that can enlarge the number of sensors. Figure 1.11 shows three principal configurations of the combination of WDM and TDM. A serial configuration using a set of wavelength-stepped arrays is shown in Figure 1.11(a). Each of these FBG arrays has a greater distance with another along the fiber. The pulse light is emitted from the light source and reflected by the FBG arrays then retuned to the detector. The detection system only responds to the reflected signal during a selected time window after the pulse is generated. Thus, a single WDM FBG array is selected for detection. This method has the ability of addressing very large arrays. However, it has some deadly drawbacks because reflected light signals are separated in time, but the overlap in wavelength will lead to multiple-reflection and spectral shadowing cross-talk (Kersey *et al.*, 1997). Both multiple-reflection and spectral-shadowing will cause large errors appearing in the measurement.

The parallel and branching TDM/WDM optical fiber network topologies (Kersey *et al.*, 1997) are shown in Figure 11(b) and (c). By using these kind of configuration, the deleterious effects can be eliminated. However they increase the price and the need for additional couplers and stronger reflecting grating.

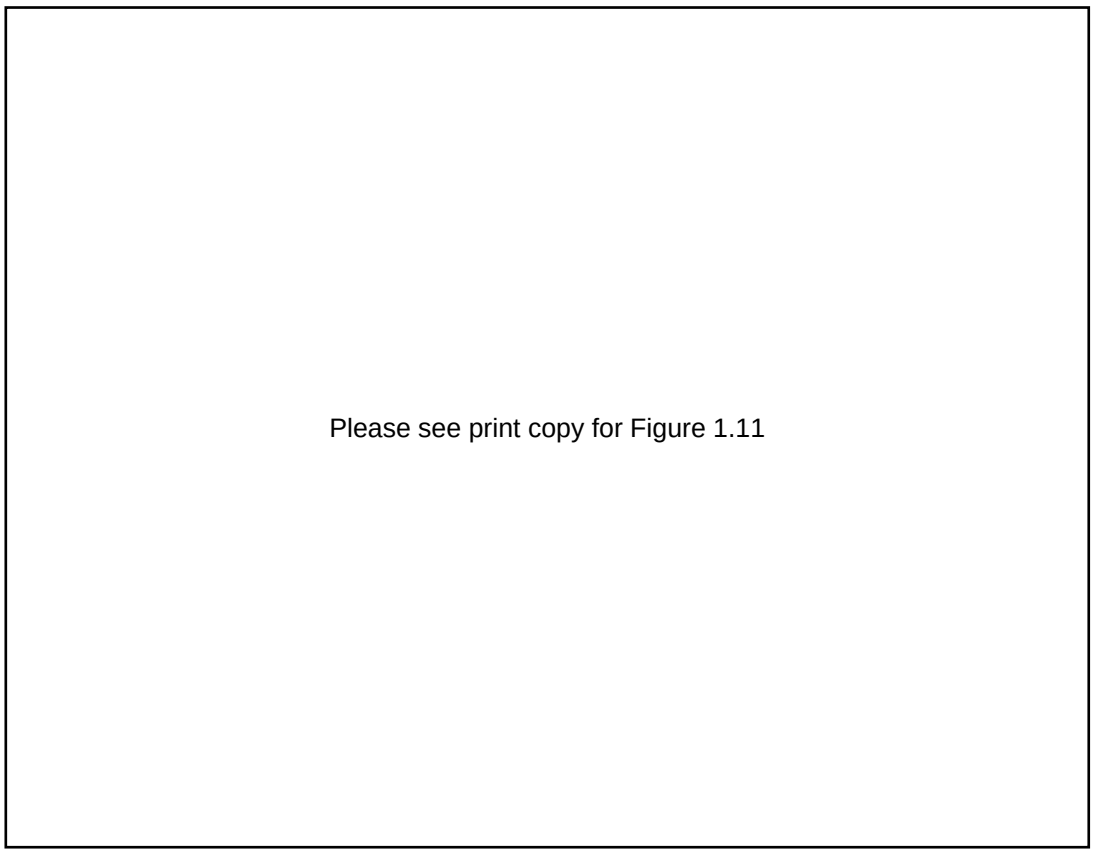

Figure 1.11 WDM/TDM addressing topologies for FBG arrays.

(Kersey, *et al.*, 1997)

(a) Serial system with lower festivity gratings

(b)Parallel network

(c) Branching network

1.3 Existing Issues

In last section, we look at the existing research work of the area of FBG sensing. Through evaluating the strengths, weaknesses and the gaps of other researchers' work, the following existing issues have been found out.

How to implement an efficient vibration/dynamic strain measurement in distributed sensing network

Vibration/dynamic strain measurement is critical to monitor the performance and

lifetime of mechanical systems. FBG has been considered as an excellent sensor element in the area of strain measurement. However, few practical systems provide a flexible and exact way to address the fast time varying vibration/dynamic strain. The FBG sensing system based on interferometric encoding via optical phase modulation offered high sensitivity. But, few practical systems based on interferometric demodulation techniques have been demonstrated for multiplexed sensor systems due to their relative complexity. The sensing system based on the tunable filter is easy to implement distributed sensing, but the scanning rate is limited. Thus, it is difficult to track the fast time varying FBG wavelength perturbation. Therefore, a distributed sensing system for processing vibration/dynamic strain measurement needs to be developed.

How to enhance the measurement accuracy in FBG sensing system

Another problem of FBG sensing system is that various types of noise will occur in the practical application. The existing FBG sensing systems have demonstrated that the detection accuracy can achieve 1 *pm* in laboratory environment and the signal-to-noise ratio (SNR) is high. However, in practical applications, the wavelength detection error could be much larger due to the various types of noise. Hence, post-processing algorithms needs to be developed to eliminate the noise from the measured signal.

How to improve the multiplexing capability of FBG sensing system

Multiplexing of the sensors is also an important technology that can provide the measurement that is distributed along the fiber. It reduces both the cost and the complexity in a multipoint configuration and increases the competitiveness of these sensors against conventional electrical sensors. Traditional multiplexing techniques based on time and wavelength have limited multiplexing capability. Therefore, efficient multiplexing technique should be proposed.

1.4 Contributions of The Thesis Work

The contribution of this research work is to improve the performance of FBG sensing system as shown in the following fronts:

Developed a new distributed FBG sensing system for dynamic strain/vibration measurement

We have demonstrated a novel demodulation system based on wavelength-multiplexed FBG sensors and the FP tunable filter for measurement of dynamic strain. In such a system, a series predetermined reference driving voltages are set to the FP tunable filter at an interval of few seconds. In that case, pass band central wavelength λ_S of FP tunable filter is fixed during the measurement process for each sensor. Therefore, it will release from the restricted scanning frequency and it is suitable for multipoint vibration/dynamic strain detection. Furthermore, two signal-processing methods are used to deal with the measured signal to obtain stable measurement of the vibration/dynamic strain over the response time of Fabry-Perot tunable filter. In the experiment, program controlled multipoint dynamic strain detection is successfully implemented by this system with these signal processing methods.

Developed signal processing methods for improving the measurement precision of FBG sensing system

Detection of a small Bragg wavelength shift signal is essential for accurately measuring the variation of strain. The FBG sensing system which uses broadband sources, the power of reflected signal is always very low. As for FBG sensing systems using the laser source, the signal power is relatively high. However, the interferometric noise will occur in the system. Digital filters have been reported to improve the measurement accuracy of FBG sensing system. However, the improvement is limited because the noise components within the filter band remain after filtering which will still affect the measurement accuracy. Therefore, in this thesis, classical digital filter, adaptive digital

filter and neural networks were investigated and compared to eliminate the noise from the measured signal.

Developed an on-line IWDM algorithm

Recently, some advanced multiplexing techniques have been introduced such as intensity and wavelength-division multiplexing (IWDM), mixed WDM/TDM multiplexing, code-division multiplexing access (CDMA) multiplexing and frequency-modulated continuous-wave (FMCW) multiplexing. Among all, IWDM provide superior performance due to its uncomplex implementation and large capability. However, it is an off-line algorithm and the computational time is very long for getting high detection accuracy. In this thesis, the IWDM technique was investigated and optimization algorithms such as gradient algorithm, Tabu search and a Tabu-gradient combination algorithm were developed for improving the performance of IWDM based FBG sensing system.

1.5 Organization of thesis

The remainder of this thesis is organized as follows: Chapter Two describes a novel FBG distributed sensing system for dynamic/static strain measurement. In additional, two data processing algorithms are introduced to deal with the measured signal to obtain stable measurement of the vibration/dynamic strain. Chapter Three presents advanced signal processing methods to eliminate the measurement error due to the various types of noise in the practical application. Chapter Four provides optimization algorithms to improve the performance of the IWDM based FBG sensing system. Finally, Chapter Five concludes the finding of the thesis and gives a suggestion for the further research

1.6 Conclusions

This chapter presented an introduction to this research work including general introduction, literature review, existing issues and contribution. The general introduction provided a basic understanding of fiber Bragg grating and pointed out the organization of this thesis. Literature review included a comprehensive review of the research work in the related field. It provided background knowledge of the FBG sensor and the FBG sensing system. Contribution concluded the objective of this thesis and summarized the contribution of the research work.

CHAPTER 2 FBG SENSING SYSTEM FOR DYNAMIC STRAIN MEASUREMENT

2.1 Introduction

Dynamic strain or vibration measurement is critical to monitoring the performance and lifespan of mechanical systems. If a monitoring system records the vibration history and warns the engineer in time, serious damage or breakdown of the mechanical system can be prevented. There are various FBG vibration/dynamic strain sensing systems have been explored. In particular, those based on interferometric encoding via optical phase modulation offer high sensitivity. The FBG vibration sensing system based on Mach-Zehnder, Michelson, Sagnac, and Fabry-Perot (FP) interferometers have been reported in recent years. However, until now, few of practical multiplexed sensors systems based on interferometric demodulation technique have been implemented due to their relative complexity.

Distributed sensing can be easily implemented using a tunable filter. Traditional FP tunable filter demodulation method perform continuous scanning in the wavlength range of the sensors and determine the instantaneous value of the Bragg wavelength for every sensor by locating the peaks of the scanned curve. Therefore, in order to track the variation of the Bragg wavelength in real time, the scanning frequency must be as fast as the frequency of the perturbation. However, as reported (Othonos *et al.*, 1999), the fastest scanning frequency can rarely exceed 1KHz. So, traditional method will not be suitable for tracking high frequency variation because of the limitation of the scanning rate.

In this chapter, we present a novel demodulation mechanism based on

wavelength-multiplexed FBG sensors and a FP tunable filter for measuring vibration/dynamic strain at a series of fixed operation points. During the measurement process for each sensor, instead of continuous scanning, the passband central wavelength λ_S of FP tunable filter is tuned to a fixed operation point and the FBG wavelength changes can be tracked by measuring the perturbation of the intensity of the reflected light. By using this kind of working mode, the restriction of the scanning frequency will be overcome. Hence, this system is very suitable for multipoint vibration or dynamic strain measurement. In addition, signal processing will also be required to achieve more reliable and accurate measurement.

This chapter is organized as follows: Section 2.2 introduces the typical demodulation technique based on a FP tunable filter. In this section, the principle of the typical FP filter demodulation approach is introduced and the problem of this approach is pointed out. Section 2.3 presents a novel demodulation scheme based FP tunable filter to overcome the limitation of the convention method. Section 2.4 describes the system implementation experiment results includes both static and dynamic measurement. Also, we point out the measurement error induced by the response time of tunable FP filter and signal processing methods are introduced to solve this problem. Finally, Section 2.5 provides the conclusion of this chapter.

2.2 FBG Wavelength Determination Using FP Tunable Filter: A Review

A typical FBG sensing system based on tunable FP filter is depicted in Figure 2.1. Light from a broadband source is transmitted to the sensor FBG. The reflected light from FBG is directed to a FP tunable filter by the three port circulator. The output of the FP filter is connected to a photo detector by which the optical signal is converted to an electrical signal.

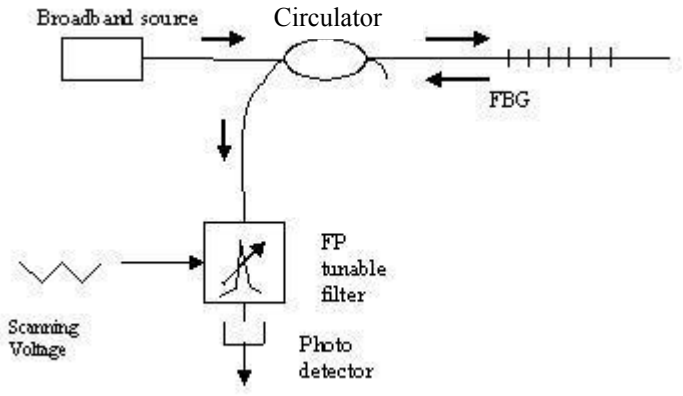

Figure 2.1 Typical FP filter based sensing system

The FP filter works like a tunable band-pass filter, which picks up the individual narrowband components of reflected light from the FBG. The band pass wavelength is determined by the cavity gap of the FP filter and the cavity gap is controlled by a piezoelectric actuator driven by an electrical signal. If the driving signal has the triangular waveform shown in Figure 2.2(a), then the cavity gap and the central wavelength of the filter will vary as shown in Figure 2.2 (b) and (c). As the driving voltage varies with time, the FP filter will conduct a continuous scanning within its free spectral range (FSR). In half a period of driving voltage, the FP filter completes an individual scanning process.

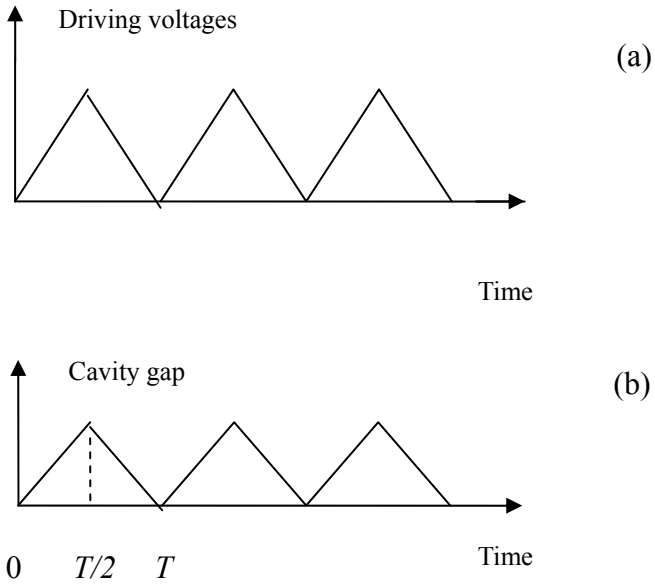

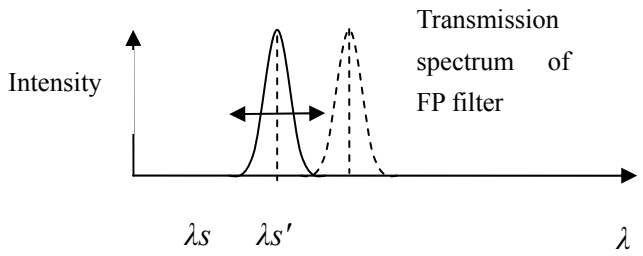

Figure 2.2 Working principle of FP tunable filter

The transmittance of a FP filter can be expressed approximately by the modified Lorentzian Function $T(\lambda,\lambda_S)$ (Suzuki, 1993), where, λ_S is the peak transmission wavelength. The spectral shape of reflected light from FBG can be expressed using the Gaussian expression (Nues, 2004):

$$S_{FBG}(\lambda,\lambda_B) = I_0 R_0 \exp(\frac{-4\ln 2}{a^2{}_{FBG}}(\lambda-\lambda_B)^2) \tag{2.1}$$

where I_0 is the output intensity of the light source, R_0 is the reflectivity of FBG, a_{FBG} is the full width at half maximum (FWHM) of the spectrum shape of reflect light, λ_B is the Bragg wavelength. According to the working principal of photo detector, the output voltage from the photo detector is expressed as:

$$V(\lambda_B,\lambda_S) = \int_{-\infty}^{+\infty} \beta S_{FBG}(\lambda,\lambda_B) T(\lambda,\lambda_S) d\lambda \tag{2.2}$$

where β is the constant which presents the optical to electric conversion factor of the photo detector. In order to show the working principle of FP tunable filter, we assume that FP tunable filter has very narrow FWHM compared with FBG. The transmittance of FP filter $T(\lambda,\lambda_S)$ can be regarded as an impulse signal $k\delta(\lambda-\lambda_S)$. Therefore, $V(\lambda_B,\lambda_S)$ can be expressed as:

$$V(\lambda_S,\lambda_B) = \int_{-\infty}^{+\infty} \beta k S_{FBG}(\lambda,\lambda_B)\delta(\lambda-\lambda_S) d\lambda = \beta k S_{FBG}(\lambda_S,\lambda_B) \tag{2.3}$$

As the FP filter scans across the spectrum of FBG, the output voltages can be expressed as:

$$U(\lambda_S, \lambda_B) = \beta k S_{FBG}(\lambda_S, \lambda_B) \tag{2.4}$$

It is assumed that the time varying driving voltages $v_d(t)$ has a linear relationship with λ_S during an individual scanning process, that is:

$$\lambda_S(t) = k_1 v_d(t) = k_1 k_2 t = Kt \qquad t \in [kT, k + \frac{T}{2}], k = 1,2...n \tag{2.5}$$

where k_1, k_2 are constants. T is the time period of the periodic driving voltage. Thus, the output voltages can be expressed in time domain as:

$$U(t) = \beta k S_{FBG}(\lambda_S, \lambda_B) = \beta k S_{FBG}(Kt, \lambda_B) \tag{2.6}$$

Hence, the output voltage signal $U(t)$ has a waveform that is the same as the shape of S_{FBG}. Therefore, by detecting the time instant where $U(t)$ exhibits the peak value, we have

$$\lambda_B = Kt_p \tag{2.7}$$

where $U(t)|_{t=t_p} = Max(U(t))$, $t \in [kT, k + \frac{T}{2}], k = 1,2...n$

Then, λ_B can be determined by the following stages:

1. FP tunable filter is driven by periodic driving voltages to conduct continuous and repetitive scanning within the FSR of the FP filter
2. The output voltages signal $U(t)$ is recorded. Within each individual scanning period, the maximum output voltage and the corresponding arisen time is located.

   $$V_{i\max} = U(t)|_{t=t_p}$$

   where, i stands for an individual scanning process.
3. Using Equation (2.5), corresponding λ_S can be determined by:

$$\lambda_{S\_\max}(i) = K(t_{i\max} - (i-1)\frac{T}{2}), i = (1,2,3,...n) \tag{2.8}$$

4. For each scanning process, the Bragg wavelength λ_B has the same value as $\lambda_{S\_\max}$. By observing the variation of $\lambda_{S\_\max}(i)$, the perturbation of λ_B can be determined.

With traditional measurement methods, the Bragg wavelength, which is what we are interested in during the measurement procedure, is determined by locating the maximum value of the spectral curve expressed by Equation(2.7), and the whole spectral curve is obtained by a spectral scanning process. This method is a very direct, but not an efficient method by which to implement Bragg wavelength measurement, because all the values of the spectral curve must be determined before measuring its maximum value. It requires that the Bragg wavelength λ_B be kept constant during the scanning process. Otherwise, the location of the maximum output voltage can not be located accurately and serious measurement error will take place. For static measurements, i.e. when the Bragg width does not vary or varies slowly enough during the scanning process, it is not a problem to obtain the spectral curve by scanning the whole spectrum in the measurement range. However, due to the limitations of the maximum scanning frequency, which has been reported as lower than 1KHz (Othonos, *et al.*, 1999), this traditional method is not suitable for dynamic measurements. Hence, we have to find a fast and efficient measurement technique for those dynamic or real-time applications.

2.3 A Novel Demodulation Technique Based On FP Tunable Filter

In order to achieve vibration/dynamic strain measurement, an alternative demodulation method based on a FP tunable filter is proposed. Instead of using continuous scanning process, a fixed point scheme is designed. In contrast to the conventional scanning method, the FP filter is set to a fixed reference operation point during the measurement process. Reconsidering the spectral curve expressed by Equation (2.4), we can find that the shape of curve does not vary and the location of the curve is actually

determined by the current Bragg wavelength of the grating, which is shown in Figure 2.3.

When the Bragg wavelength changes, the spectral curve will move along the spectral axis without change to its shape. Thus, we arbitrarily select a wavelength as our reference operation point - point λ_C shown in Figure 2.3. As the Bragg wavelength changes from $\lambda_{B\min}$ to $\lambda_{B\max}$, the observed output voltage will vary accordingly from $V_{\max}$ to $V_{\min}$, although the point $(\lambda_c, V_{\max})$ and the point $(\lambda_c, V_{\min})$ actually belong to two different spectral curves C_1 and C_2. Consequently, the variation of the voltage output at the operation point λ_C reflects the movement of the spectral curve caused by the change of the Bragg wavelength. In other words, as the shape of the curve does not change during the measurement, the variation of the output voltage at an arbitrary operation point is uniquely determined by the perturbation of the Bragg wavelength to be measured.

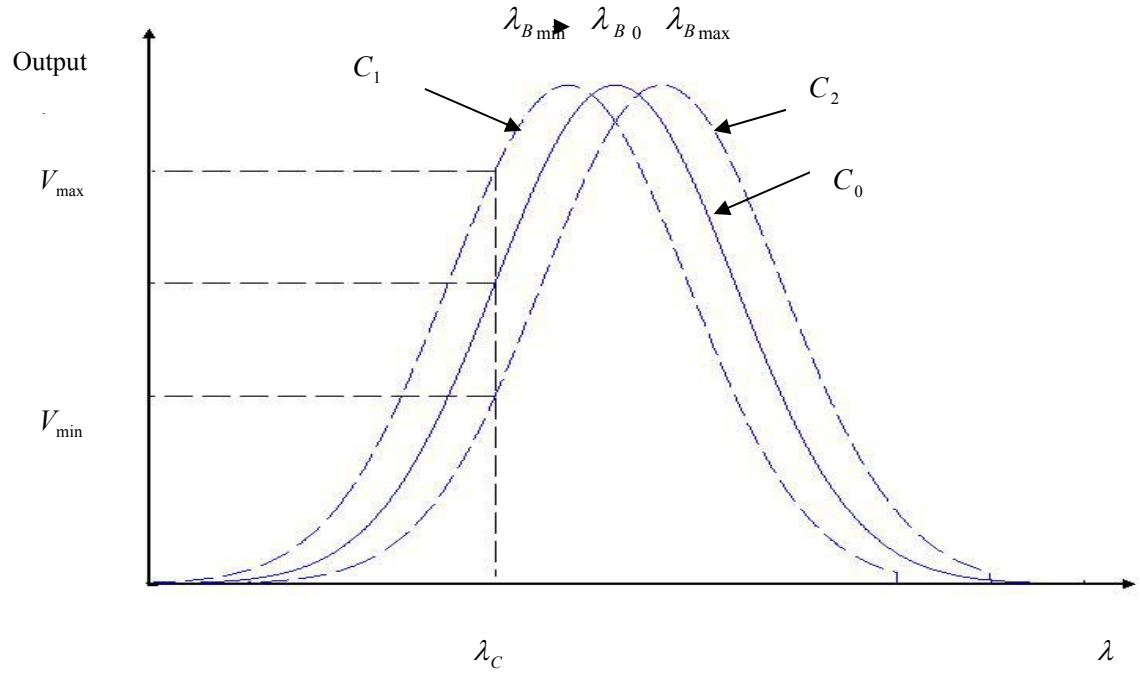

Figure 2.3 Output voltages change versus $\Delta\lambda_B$ when λ_S is set to a operation point λ_C

Hence, the measurement of the relative variation of the Bragg wavelength can be carried out by tracking the change in the output voltage. The relationship between output voltage and the Bragg wavelength can be expressed as:

$$U(\lambda_S, \lambda_B) = \alpha k S_{FBG}(\lambda_S, \lambda_B) = \alpha k S_{FBG}(\lambda_B, \lambda_C) = \beta k I_0 R_0 \exp(\frac{-4\ln 2}{a_{FBG}^2}(\lambda_B - \lambda_C)^2) \quad (2.9)$$

Additionally, the absolute Bragg wavelength can be calculated, so long as we have a reference Bragg wavelength λ_{B_0}, which can be easily obtained either by making a traditional measurement, or with some prior knowledge about the Bragg grating sensor. In order to implement the above approach, following issues must be studied:

2.3.1 Selection of reference Bragg wavelength

In order to implement the measurement by using our proposed method, a reference curve determined by a reference Bragg wavelength has to be selected in advance. In fact, the relative variation of the Bragg wavelength is independent from its absolute value. Therefore, any Bragg wavelength can be equally used as a reference Bragg wavelength. Hence, the process of obtaining the reference curve can be easily completed by making once of scanning over the spectrum at any time. Accordingly, the reference Bragg wavelength λ_{B_0} can be determined by locating the peak of the curve, which is just like the traditional method does, but the difference is that this process is used to determine the reference operation point of FP tunable filter.

2.3.2 Selection of reference operation point

Although any point can be used to measure the variation of the output voltage, different points will have different sensitivity to the movement of the Bragg wavelength. Therefore, the selection of the operation point is a necessary step in improving the performance of the measurement.

In fact, in practical applications, dynamic strain-induced Bragg wavelength

perturbation has very low amplitude, i.e. it has only a very small dynamic range around the reference wavelength λ_{B_0}. Therefore, the relationship between the variation of the instantaneous Bragg wavelength and the output voltage at the measurement point can be approximated by a linear relationship

$$\Delta U(\lambda_S, \lambda_B) = G(\lambda_S, \lambda_B) \cdot \Delta\lambda_B \tag{2.10}$$

where $G(\lambda_S, \lambda_B) = \frac{\partial U(\lambda_S, \lambda_B)}{\partial(\lambda_B)}|_{\lambda_B=\lambda_{B0}}$. Obviously, the sensitivity of the measurement depends on the value of $G(\lambda_S, \lambda_B)$, and further, as the reference wavelength λ_{B_0} has been pre-determined, the value of $G(\lambda_S, \lambda_B)$ relies on the location of the operation point. Therefore, we must find the optimal measurement point at which the greatest gradient value appears. $G(\lambda_S, \lambda_B)$ can be expressed as:

$$G(\lambda_S, \lambda_{B0}) = \frac{\partial U(\lambda_S, \lambda_B)}{\partial(\lambda_B)}|_{\lambda_B=\lambda_{B0}} = \frac{8\ln 2}{a_{FBG}^{\ 2}} \beta k I_0 R_0 \exp\left(\frac{-4\ln 2}{a_{FBG}^{\ 2}}(\lambda_S - \lambda_{B0})^2\right)(\lambda_S - \lambda_{B0}) \tag{2.11}$$

In order to find the exact λ_S that makes $G(\lambda_S, \lambda_{B0})$ reach its extremum point, the gradient of G with respect to λ_S is calculated and made equal to zero.

$$\begin{aligned}\frac{\partial G(\lambda_S, \lambda_{B0})}{\partial \lambda_S} &= \frac{8\ln 2}{a_{FBG}^{\ 2}} \beta k I_0 R_0 \left[\frac{8\ln 2}{a_{FBG}^{\ 2}} \exp\left(\frac{-4\ln 2}{a_{FBG}^{\ 2}}(\lambda_S - \lambda_{B0})^2\right)(\lambda_S - \lambda_{B0})^2\right. \\ &\quad \left. - \exp\left(\frac{-4\ln 2}{a_{FBG}^{\ 2}}(\lambda_S - \lambda_{B0})^2\right)\right] \\ &= 0\end{aligned} \tag{2.12}$$

From Equation (2.12), the corresponding λ_C value can be obtained as:

$$\lambda_C = \lambda_S = \lambda_{B0} \pm \frac{\alpha_{FBG}}{\sqrt{8\ln 2}} \tag{2.13}$$

Using Equations (2.11) and (2.13), the maximum and minimum value of $G(\lambda_S, \lambda_{B0})$

can be determined respectively. The maximum and minimum value of $G(\lambda_S, \lambda_{B0})$ has the opposite sign and same absolute value as:

$$|G(\lambda_S, \lambda_{B0})|_{\max} = \frac{\sqrt{8\ln 2}\exp(-\frac{1}{2})}{\alpha_{FBG}}\beta k I_0 R_0 \tag{2.14}$$

In addition, from Equations (2.5) and (2.9), it is obvious that:

$$\begin{aligned}\frac{\partial U(\lambda_S, \lambda_B)}{\partial \lambda_S}|_{\lambda_B=\lambda_{B0}} &= \frac{-8\ln 2}{a_{FBG}^{\ 2}}\beta k I_0 R_0 \exp(\frac{-4\ln 2}{a_{FBG}^{\ 2}}(\lambda_S-\lambda_{B0})^2)(\lambda_S-\lambda_{B0}) \\ &= -\frac{\partial U(\lambda_S, \lambda_B)}{\partial \lambda_B}|_{\lambda_B=\lambda_{B0}} = -G(\lambda_S, \lambda_{B0})\end{aligned} \tag{2.15}$$

and

$$\frac{\partial U(\lambda_S, \lambda_B)}{\partial(\lambda_S)}|_{\lambda_B=\lambda_{B0}} = \frac{\partial U(\lambda_S, \lambda_B)}{\partial(v_d)}\frac{\partial(v_d)}{\partial(\lambda_S)}|_{\lambda_B=\lambda_{B0}} = \frac{1}{k_1}\frac{\partial U(\lambda_S, \lambda_B)}{\partial v_d}|_{\lambda_B=\lambda_{B0}} \tag{2.16}$$

Therefore, from Equations (2.15) and (2.16) we can get:

$$\|G(\lambda_{B0}, \lambda_S)\| = \left\| \frac{1}{k_1}\frac{\partial U(\lambda_S, \lambda_B)}{\partial(v_d)}|_{\lambda_B=\lambda_{B0}} \right\| \tag{2.17}$$

and

$$\|G(\lambda_{B0}, \lambda_S)\|_{\max} = \left\| \frac{1}{k_1}\frac{\partial U(\lambda_S, \lambda_B)}{\partial(v)}|_{\lambda_B=\lambda_{B0}} \right\|_{\max}$$

In order to simplify the calculation process, we calculate G with respect to v_d instead of λ_B using the reference spectral curve. Also, we regard the driving voltage by which the maximum gradient is achieved as the reference driving voltage. Therefore, Equation (2.10) can be rewritten as:

$$\Delta\lambda_B = k_1\Delta v_d = \frac{\Delta U(\lambda_S, \lambda_B)}{G_{\max}(\lambda_S, \lambda_{B0})} = k_1\frac{U(\lambda_S, \lambda_B)}{\left|\frac{\partial U(\lambda_S, \lambda_B)}{\partial(v)}\right|_{\max}} \tag{2.18}$$

The proposed demodulation method can be described in the following steps:

1. The FP tunable filter is driven by driving voltages to conduct an individual scanning process within the FSR of the FP filter. Then we record the output voltages $U(t)$ and corresponding driving voltages $v(t)$. This process is used to determine the reference driving voltage.
2. We calculate the gradient of $U(t)$ with respect to $v(t)$.
3. Then we find the maximum gradient value $\left| \frac{\partial U(t)}{\partial (v)} \right|_{\max}$ and record the relevant two driving voltages. We regard one of these two driving voltages as the reference driving voltage.
4. Then the FP tunable filter is set to the operation points with the corresponding driving voltage and the output voltages are recorded for a few seconds.
5. Using Equation (2.18), the variation of $U(t)$ is first transformed to variation of driving voltage, and then to the perturbation of Bragg wavelength λ_B. Also, the information of vibration/dynamic strain can be determined.

2.3.3 Multipoint measurement using multiplexed FBG sensors

For practical applications, we need to use multiplexed sensors to reduce system costs. Assume that the multiplexed sensors we used are composed of *N* individual sensors whose pass bands are separated from each other. Because the pass bands of the sensors do not overlap, if we continuously scan the whole spectrum, the output spectral curve will be simply the sum of the spectral curves of each Bragg grating. Obviously, the spectral curve of multiplexed sensors has multiple peaks, and every peak corresponds to a Bragg wavelength of one of the gratings in the sensor set. A typical spectral curve of multiplexed FBG sensors is shown in Figure 2.4.

According to the proposed method for single sensor measurement, when we are tracking the perturbation of the $i-th$ sensor, we must make the measurement at the selected point λ_{C_i}, as shown in Figure 2.4. Since point λ_{C_i} is only within the pass

band of the *i-th* sensor, the measured output voltage will depend only on the perturbation of the Bragg wavelength of the *i-th* sensor. Moreover, if we want to know the status of all the sensors, we must sequentially tune the FP filter to different operation points. Therefore, at the beginning of every measurement period, similar as the measuring of a single sensor, we have to scan the spectrum to obtain the spectral curve, by which the *N-th* operation points for *N-th* sensors can be determined individually.

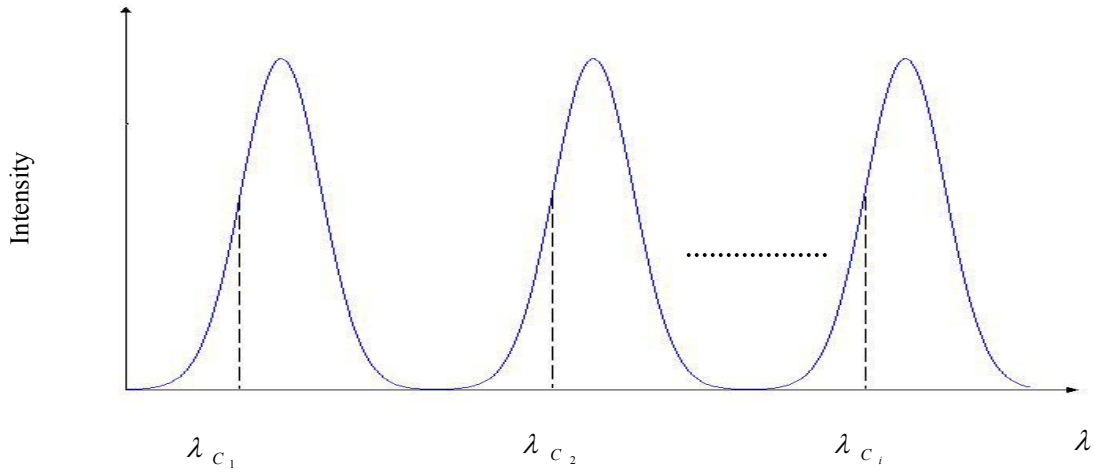

Figure 2.4 spectral curves of multiplexed FBG sensors

Meanwhile, assume that in a certain measurement period we need to track the perturbation of each sensor for a time slot of *T*. As the operation points of the sensors are different from each other, at the beginning of the $i-th$ time slot, we will tune the FP filter to the operation point of the $i-th$ grating, and then track the output voltage perturbation of the $i-th$ FBG until the end of the time slot. The output voltage perturbation of the sensors will be recorded one by one until the end of this measurement period. For the next measurement period, the same operations will be repeated. The flow chart of the measurement scheme for multiplexed sensors is shown in Figure 2.5

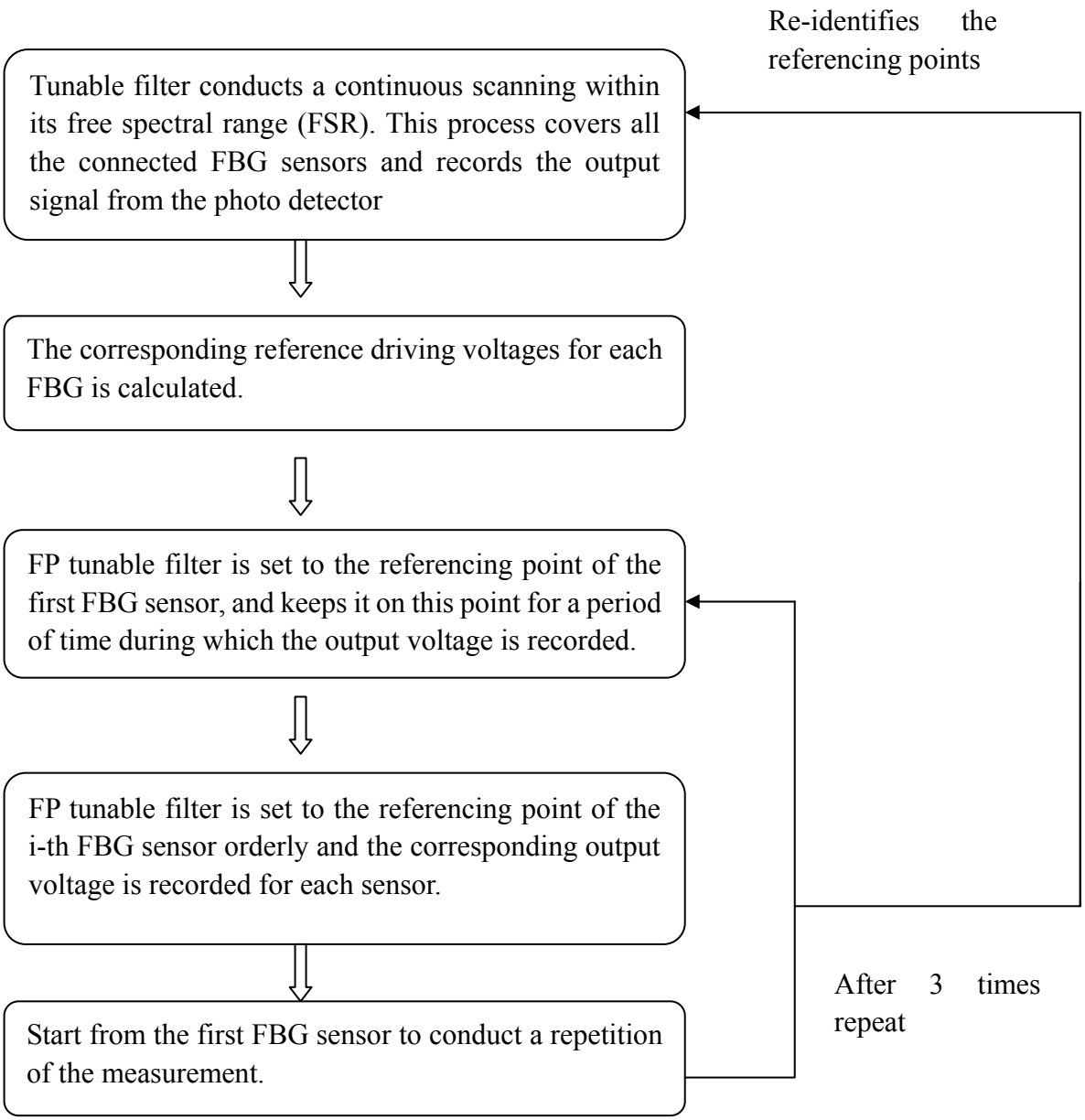

Figure 2.5 The flow chart of the measurement scheme for multiplexed sensors

2.4 System Implementation and Experimental Results

2.4.1 System setup

The system setup used in our experiment is shown in Figure 2.6. An amplified spontaneous emission (ASE) source is used as a broadband light source. Two FBG

sensors with different Bragg wavelengths are connected to an optical circulator. The broad band light from a broadband optical source is transmitted to the FBG sensors via a three-port circulator. The FBG sensors reflect the light of the relevant Bragg wavelength to the circulator along the transmission optical fiber and reach the tunable F-P filter. The tunable FP filter connects to a power meter that is used to transform the photocurrent signal into an electrical signal. Then the data acquisition unit gathers the electrical signal. The desktop computer controls both the tunable filter and the data collection unit by the Labview program.

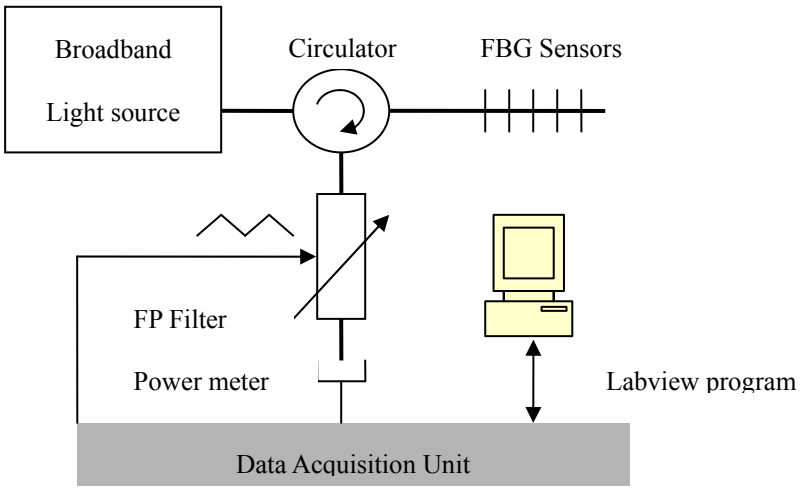

Figure 2.6 Schematic diagram of FBG vibration detection system

2.4.2 Vibration measurement by single FBG sensor

In order to test the proposed demodulation method, we conduct a dynamic strain measurement using a single FBG at different operation points. A 3 *KHz* vibration with fixed amplitude is applied to the second FBG sensor by a PZT vibrator. First, the desktop computer generates a series driving voltage (0.1~2 *volt* with the interval of 0.002 *volt*) to drive the tunable filter to scan the effective spectrum range. The relationship between the driving voltages and the output voltages from the optical receiver is made, as shown in Figure 2.7.

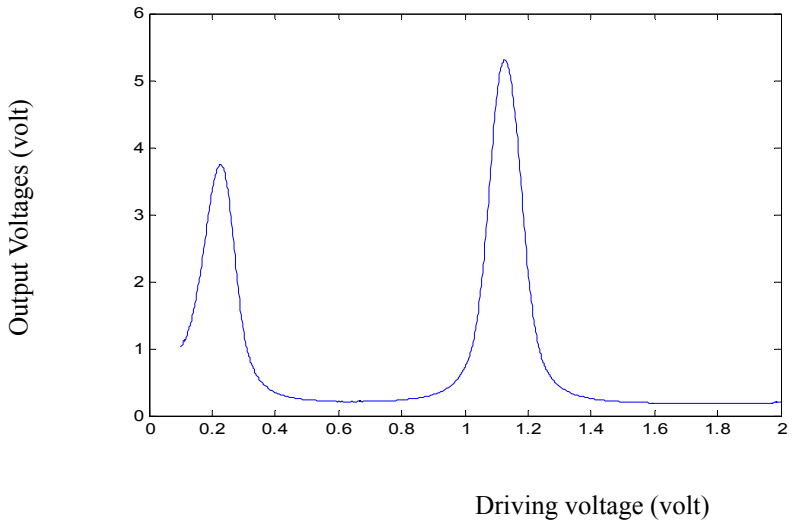

Figure 2.7 The output voltages of FP tunable filter during the scanning process for two FBG sensors

Four reference driving voltages (1.20 *volt*, 1.22 *volt*, 1.24 *volt*, 1.26 *volt*) located at the falling edge of the second FBG's spectrum shape are set to the F-P tunable filter at intervals of 20 seconds. After each reference driving voltages is set for 5 seconds, the output voltages are recorded for 100*ms* at the sampled rate 30 *KHz* as shown in Figure 2.8. The output voltages recorded from the optical receiver at different operation point appear with different mean values and AC amplitudes due to the different gradient value of the operation point. Then the gradient for these four operation points were calculated separately. The vibration of output voltage is transformed to the perturbation of the driving voltage.

In order to obtain accurate information about the dynamic strain, we need to analyse the frequency domain characteristics of the driving voltage signal of the different operation points. It is found that the vibration consists of one fundamental wave and several noise signals. The frequency of the fundamental wave stands for the frequency of the vibration which is calculated as 2.97 *KHz*. This result fulfills the initial setup of the vibration. The amplitude of the vibration can be acquired by integrating the spectrum of the fundamental wave. According to the different operation points, we get the following

vibration amplitude of the driving voltage:

Operation point	Vibration amplitude of driving voltage (*volt*)	Mean value of driving voltage (*volt*)
1.20v	0.000345	1.19
1.22v	0.000356	1.195
1.24v	0.000352	1.2
1.26v	0.000350	1.21

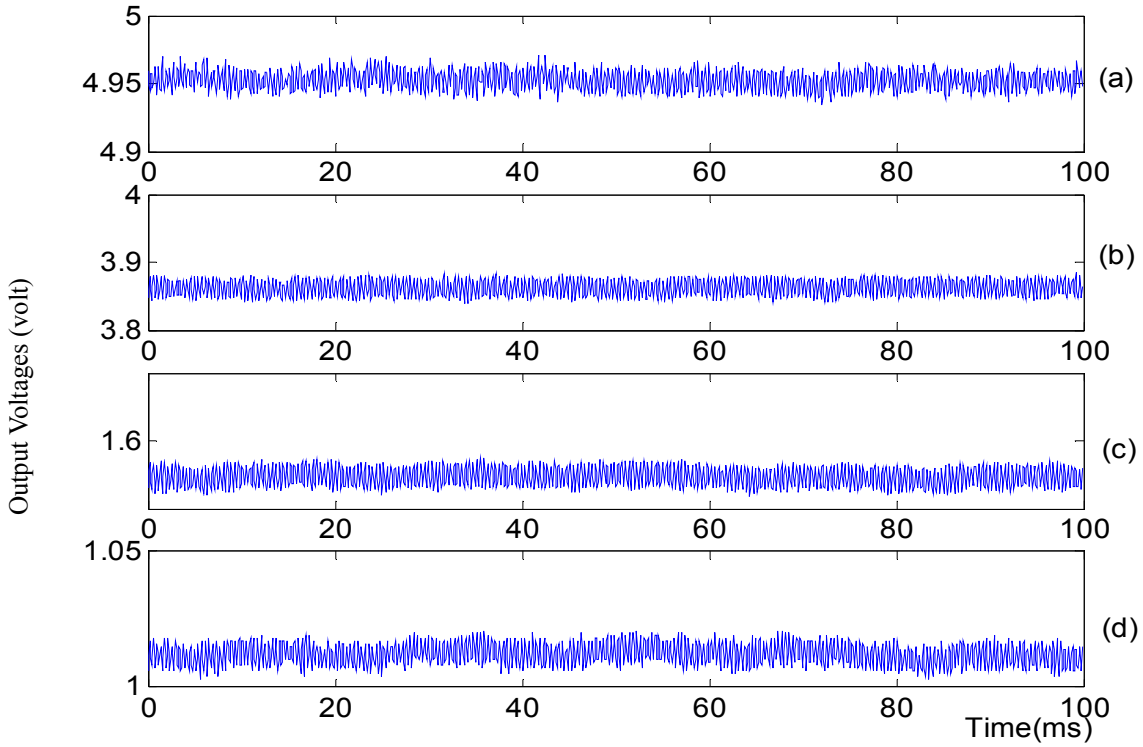

Figure 2.8 Output voltage obtained at different reference driving voltage:

(a) 1.20 *volt* (b) 1.22 *volt* (c) 1.24 *volt* (d) 1.26 *volt*

The result indicates that the vibration measured at different operation point has the same frequency and approximately the same amplitude, which accords with the experiment setting. Further, in order to test the influence of different optical power levels, 5dB attenuation was given to the optical source. As expected, the measured frequency and

amplitude of vibration remains the same. Therefore, the experiment result proves that the theoretical model is correct and the vibration information can be measured accurately at different operation points.

2.4.3 Multipoint vibration measurement using multiplexed FBG sensors

In this section, the vibration measurement using multiplexed FBG sensor is made. The scanning process, operation point calculating process and vibration detection process for two FBG sensors are implemented using Labview program. A 3 *KHz* generator is connected to these two sensors and the output voltages from the photo detector are recorded at the sampled rate 30 *KHz* by the data acquisition unit. First, the desktop computer generates a series of driving voltages (0.1~2 *volt* with the interval of 0.002 *volt*) to drive the tunable filter to conduct a continuous scanning. Then, the relationship between the driving voltages and the output voltages is built, as shown in Figure 2.7. Also, the Labview program calculates the operation point for each sensor and sets the FP tuanble filter to the operation point sequentially. The output voltage is recorded for 1 second after the FP tunable filter is set to each operation point. If the response of the FP tunable filter is fast enough, i.e. as soon as the driving voltage is adjusted to a new value, the wavelength of the FP filter can be instantaneously set to the expected point, the variation of the output voltage will depend only on the perturbation of the sensor we are measuring. However, in practical application, the transient process of the FP tunable filter is rather long. The two curves in Figure 2.9 show the output voltages for two FBG sensors after the driving voltage is set to the respective operation points. It can be seen that after the voltage is set to the selected driving voltage, it takes relative long time until the output voltage become stable.

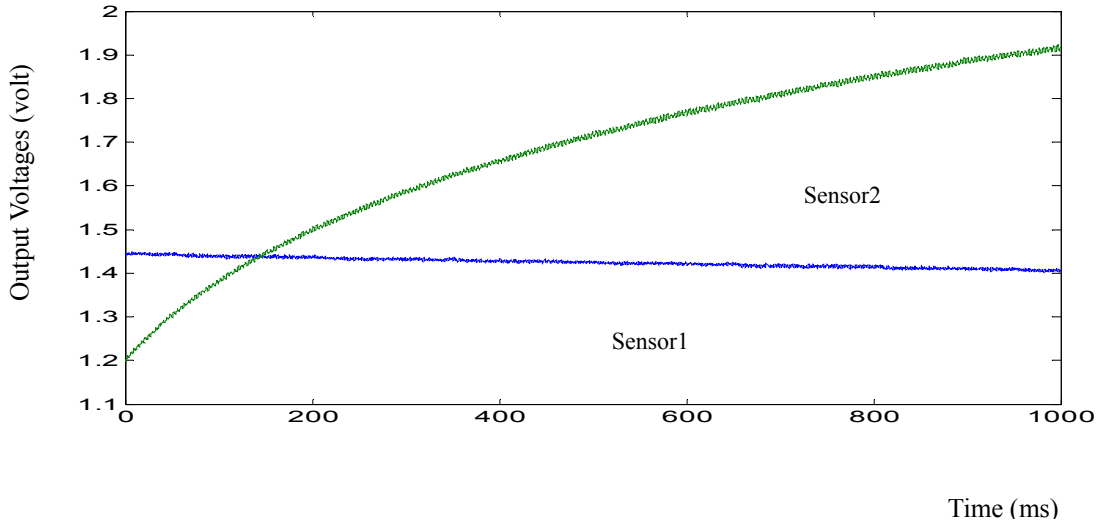

Figure 2.9 Output voltages of FP tunable filter for two FBG sensors

During the transition process, output voltages are slowly moving to the expected voltage with additional variation. In order to extract the variation signal from the transition process, in the following sections, we discuss the response characteristic of the system output and present signal processing methods in order to address the accurate information of the vibration.

.

2.4.3.1 Response of system output to step driving voltage

In this section, we evaluate the response characteristic of system output. A step driving voltage is set to the FP tunable filter. By observing the output voltage from the photo detector, we can obtain the raising time of the step response of system output. The step signal of driving voltage and corresponding output voltage are shown in Figure 2.10. We can find that the system needs approximately 2 seconds to reach the stable statement, which is the same as the response time of the FP tunable filter.

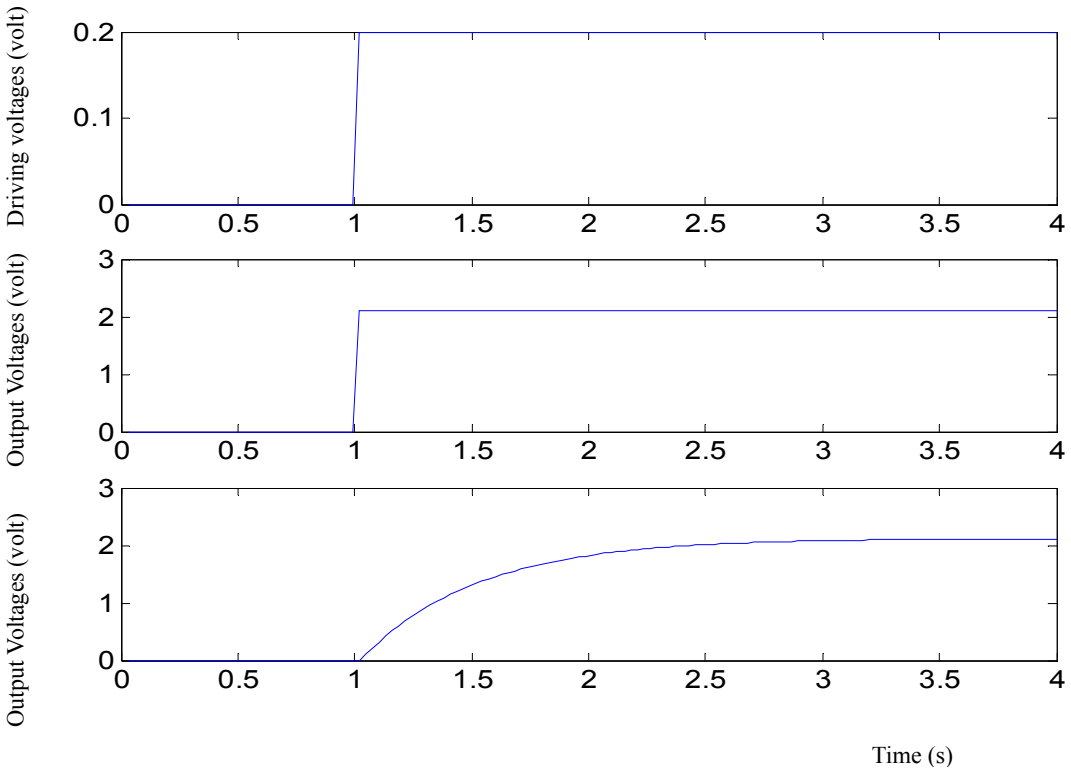

Figure 2.10 The step response of FP tunable filter

(a) Driving voltage (b) Desired output voltage (c) Actual output voltage

It is obvious that the passband central wavelength of the FP tunable filter can not be instantaneously changed with the driving voltage, due to the response time of the piezoelectric actuator of the filter. Therefore, setting an instantaneous reference driving voltage (V_R) actually results in a dynamic process so that the value of the driving voltage varies (from V_I to V_R gradually) as shown in Figure 2.11.

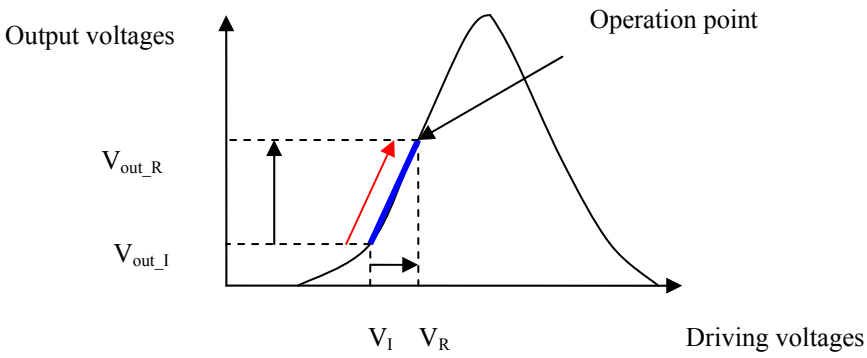

Figure 2.11 The process of setting the FP tunable filter to the operation point

Therefore, if the stable period of the FP filter is larger than the measurement time slot, the output voltages signal will be an integration of a fast time varying signal and a slow time varying signal. In this case, the peak transmission wavelength of the FP tunable filter will vary with time during the measurement process. If the gradient value of the operation point is regarded as the only proportion constant between the Bragg wavelength and the output voltage, measurement error will occur.

2.4.3.2 Signal separation and adjustment for addressing accurate vibration information

In order to address the accurate vibration information, signal separation and adjustment for the measured vibration signal is necessary. One method is first to separate the fast time varying and slow time varying signals for each measured output voltage signal using a digital filter. A section of the output voltages of the first FBG sensor that we obtained in last section is shown in Figure 2.12. The fast time varying signal stands for the output voltages perturbation induced by variation of Bragg wavelength, and the slow varying signal represents the response characteristic of the FP tunable filter

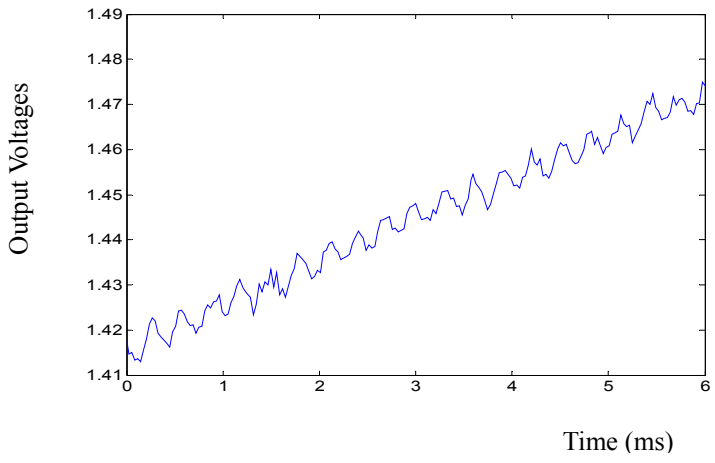

Figure 2.12 Output of the FP tunable filter including fast time varying vibration and low frequency DC offset

In order to design the proper filter for the combined signal indicated in Figure 2.12, the frequency spectrum of the signal is acquired using DFT analysis. The filter was designed based on the spectrum character of the signal. The order of the filter can be

estimated by the following Equation (Leland, *et al.*, 1995):

$$N \approx \frac{-10\ \lg(\delta_1\delta_2) - 13}{14.6\Delta\omega} \tag{2.19}$$

where δ_1 is passband ripple, δ_1 is stopband ripple, $\Delta\omega$ is the width of the normalized transition bandwidth. For this combined signal, we design a filter with δ_1=0.05, δ_2=0.005, $\Delta\omega$=0.03. Therefore, a 150 order FIR low pass filter is applied to the combined signals. The separated signals are shown in Figure 13 (a) and (b).

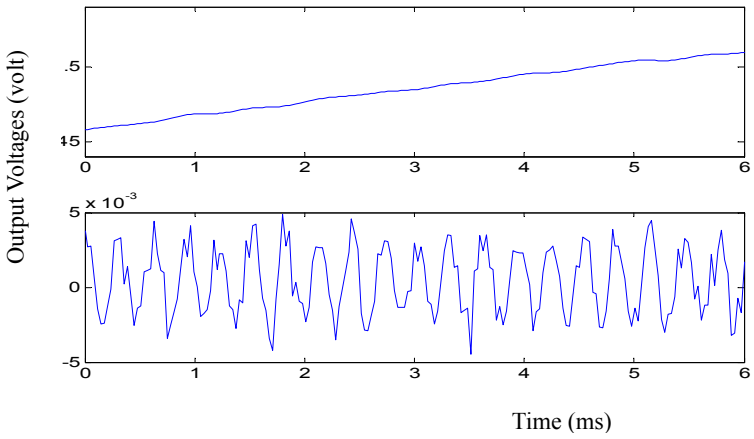

Figure 2.13 Filtered output signal. (a) DC component and (b) AC component

From Figure 2.13(b), it is shown that the amplitude of the AC component of the output voltage changes along the time axis. The reason is that the gradient between the driving voltages and the output voltages from the FP filter is varying continuously during that time. Therefore, the gradient value of the operation point cannot be regarded as a constant coefficient between the output voltage and driving voltage. To solve this problem, S_{AC} is divided into *n* small pieces and a gradient series will be used to represent the relationship between the Bragg wavelength and the output voltages.

$$S_{AC} = S_1 \left| S_2 \right| S_3 \ldots \left| S_n \right. \tag{2.20}$$

For each section of signal S_i, the gradient value can be regarded as a constant. Therefore, by using different gradient values in different sections of the signal, the output voltages can be transformed into the corresponding driving voltages perturbation that has invariable amplitude. The vibration frequency and amplitude of driving voltages signal can be obtained by frequency domain analysis. The frequency of the scanning voltages

signal is the same as the frequency of the vibration/dynamic strain. And the amplitude of the vibration/dynamic strain is calculated utilizing the known relationship.

The other processing method is to describe the relationship between the driving voltage and the output voltage as a formula instead of a gradient calculation. According to the Gaussian distributions, the expressions for the output voltage from the FP filter can be expressed as:

$$U(v, v_0) = A + U_0 \exp(\frac{-4\ln 2}{\alpha^2}(v - v_0)^2) \tag{2.21}$$

where A is the offset due to the dark noise, α is the FWHM of the scanned output voltage shape, U_0 is the peak value of the output voltages, and v_0 presents the driving voltage corresponding to U_0.

Using Equation (2.21), the output voltage signal is transformed into the corresponding driving voltages. It still is an integration of a fast time varying signal and a low frequency signal. However, the amplitude of the AC signal will not change along the time axis because the slope changes have been compensated for by the formula. It only needs to separate the fast time varying signal from the low frequency signal. Using this method, large amplitude dynamic strain can be measured more accurately. The reason is that the output voltage has non-linear relationship with λ_B, if the amplitude of dynamic strain is large enough. Therefore, as the gradient value is regarded as the proportion coefficient to calculate the variation of λ_B, measurement error will take place.

2.4.3.2 Processing result of the measured vibration signals

The first processing method is used on the output voltage signal. A 150 order FIR low pass filter is used to separate the fast time varying and slow time varying signals for each sensor. The vibration signal S_{AC} is divided into a number of small sections (10 samples each). Then, the variation of the output voltage signal can be transformed into

the corresponding driving voltages by different gradient value. In order to obtain accurate information about the vibration source, we must analyse the frequency domain characteristics of the driving voltage signal.

In this case, the vibration frequencies measured by the two sensors are 2.97 *KHz* and 2.93 *KHz* respectively, which is almost the same as the actual vibration frequency. Without the signal processing method, the vibration amplitudes of the driving voltage measured in sensor 1 and sensor 2 using the gradient of operation points are 4.73 *mv* and 3.98 *mv* respectively. The relative measurement error is up to 20%. With the first processing method, the vibration amplitude for sensor 1 is 5.32 *mv*, and at sensor 2 it is 5.41 *mv*. The experiment results accord with the experiment expectations that the amplitudes of the driving voltage signal measured at different sensors should be the same.

Then the second processing method is implemented. The relationships of output voltages and driving voltage for the two FBGs are expressed as a formula, as in Equation (2.21):

$$U_1(t) = 0.3 + 3.826 \ \exp(-167\ (v(t) - 0.238)^2) \tag{2.23}$$

And

$$U_2(t) = 0.3 + 5.008 \ \exp(-170\ (v(t) - 1.126)^2) \tag{2.24}$$

Using these expressions, the driving voltage signal can be obtained directly after filtering. A section of the driving voltage signal is shown in Figure 2.14. The measured vibration frequency is 2.97 *KHz*, 2.95 *KHz* and the vibration amplitudes are 5.25*mv*, 5.36*mv* for the two FBG sensors respectively, which is very similar to the result we obtained by the first method.

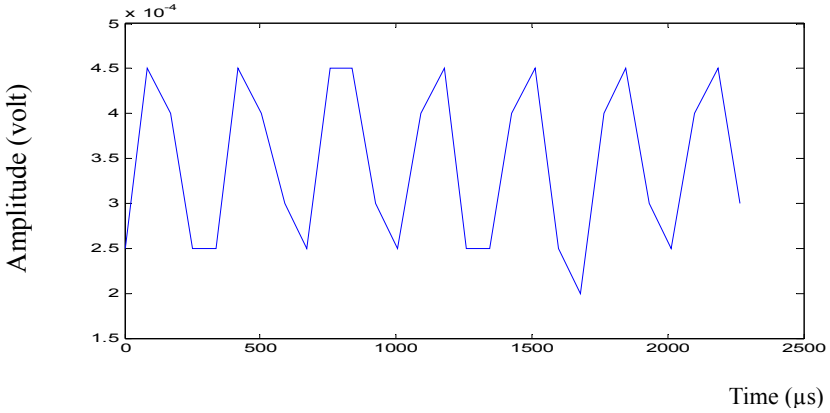

Figure 2.14 A section of driving voltages signal using curve-fitting method

2.5 Conclusions

In this chapter, a novel demodulation method has been proposed and experimentally demonstrated to interrogate fast time varying vibration signals acting on FBG utilizing the FP tunable filter. The proposed system is suitable for measuring fast time varying vibration or dynamic strain. Compared with conventional approach, the proposed method has three advantages. One is that it releases from the restricted scanning rate of FP filters which plague the dynamic performance of the conventional approach. Another advantage of this method is that it yields a higher wavelength resolution of the Bragg wavelength. As the conventional method is based on reconstructing the spectral shape of the reflected light, it requires a FP filter with very narrow bandwidth. In contrast, using the new method to measure the perturbation of the Bragg wavelength means that we need not reconstruct the spectral shape of reflected light. Therefore, it improves the measurement resolution. Last but not least, because the continuous wavelength range scanning process is implemented after each measurement process, the operation point is updated in real time. Therefore, measurement error introduced by the slow wavelength variation can be avoided.

In addition, two signal processing methods were introduced to deal with the measured signal in order to obtain stable measurement of the vibration/dynamic strain. During

the real-time vibration monitoring, the response time of FP tunable filter will cause the fluctuation of the sensors' sensitivity, and the fluctuation of the sensitivity will result in measurement errors. The experimental result demonstrates that the proposed processing method can remove such errors. Combing these signal processing methods, the FP tunable filter based sensing system can be successfully utilized to measure multipoint fast time varying vibrations or dynamic strain.

CHAPTER 3 SIGNAL PROCESSING METHODS FOR IMPROVING MEASUREMENT PRECISION OF FBG SENSING SYSTEM

3.1 Introduction

It is very important to measure strain/temperature variations with high accuracy in long-term applications. Therefore, the ability to detect small shifts in Bragg wavelengths is an essential requirement for a FBG sensing system. In practical applications, various types of noise will occur that significantly limit the accuracy of wavelength detection. For the FBG sensing system using the broadband sources as we described in last chapter, the power of reflected signal is always low. This phenomena result in low signal to noise ratio (SNR), especially for the sensing system which using time division multiplexing (TDM) technique. Recently, tunable narrow band laser source have been introduced as the light sources for interrogating Bragg wavelength. The advantage of using the tunable laser source is that it can achieve relatively high signal power. However, interferometric noise will be introduced to this kind of system. In this chapter, signal processing algorithms are developed to improve the detection accuracy of a tunable laser source based FBG sensing system.

This chapter is organized as follows. In Section 3.2, the system model of FBG sensing system using tunable laser source is described. Also, the signal model of the measured spectrum is built, which contains the unwanted interferometric signal. In Section 3.3, classical digital filters are used to improve the detection accuracy of Bragg wavelength. Also, we point out the limitations of this technique. In section 3.4, adaptive filters are applied to overcome the limitations of digital filters. In section 3.5, back propagation (BP) neural network is applied to the same task and the conclusion is presented in section 3.6.

3.2 System Model

3.2.1 Principle of FBG sensing system using tunable laser source

A typical FBG sensing system based on tunable laser source is shown in Figure 3.1. The narrowband laser light is transmitted to the sensor FBGs via a directional coupler. A FBG sensor reflects the light to the coupler along the transmission optical fiber and reaches the photo detector. The tunable laser source is driven by a laser PZT actuator to scan over the spectral range which includes the spectrum of FBG sensor. During an individual scanning process, the central wavelength of laser light varies with time, it can be expressed as:

$$\lambda\ (t) = \lambda_0 + Kt \tag{3.1}$$

where λ_0 is the initial wavelength of the laser light, K is a proportional constant. Because the linewidth of tunable laser source is much narrower than that of FBG. The spectrum of the laser light during the scanning process can be regarded as an impulse sequence $I_0\delta(\lambda - \lambda\ (t))$. As the tunable laser source scans across the spectrum of FBG, the light intensity at the photo detector can be expressed as:

$$I_{FBG}(\lambda(t)) = \frac{1}{4} I_0 \delta(\lambda - \lambda\ (t)) R_{FBG}(\lambda, \lambda_B) = \frac{1}{4} I_0 R_{FBG}(\lambda\ (t), \lambda_B) \tag{3.2}$$

where I_0 is the intensity of the light source, 1/4 is the coupler coefficient, $R_{FBG}(\lambda, \lambda_B)$ is the reflective spectrum of FBG. Therefore, $I_{FBG}(\lambda\ (t))$ has a waveform that is the same as the shape of $R_{FBG}(\lambda, \lambda_B)$. Furthermore, by recording the central wavelength of laser light when a peak in the reflected intensity is detected, we have

$$\lambda_B = \lambda\ (t_p) \tag{3.3}$$

where $I_{FBG}\ (\lambda\ (t))_{t=t_p} = Max\ (I_{FBG}\ (\lambda(t)))$. Using this method, Bragg wavelength can be detected.

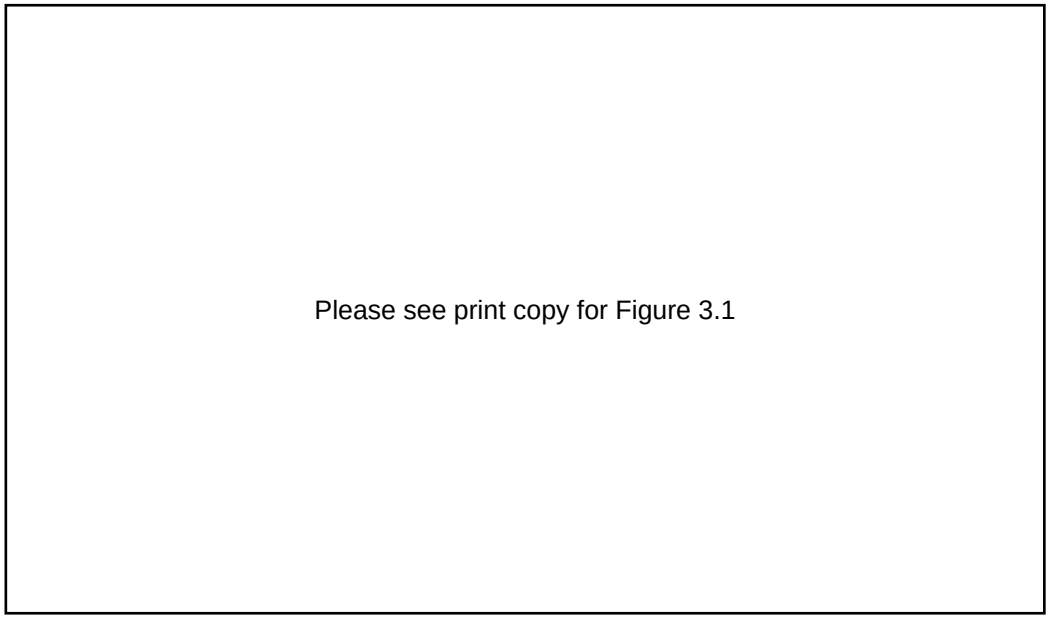

Figure 3.1 System diagram (Jin *et al.*, 1998)

However, unwanted interferometric noise will occur in this system (Chan *et al.*, 1999). This kind of noise is caused by the interference between the FBG signal (reflected from the FBG) and the residual reflected signal (reflected from fiber connectors, i.e. the "reflection point" as shown in Figure (3.1). The interferometric signal can be expressed as (Jin *et al.,* 1998):

$$I_{noise}(\lambda(t)) = \frac{I_0}{2}\sqrt{R_{FBG}(\lambda(t),\lambda_B)\beta^2}(1 - R_{FBG}(\lambda(t),\lambda_B))\cos(\frac{2\pi}{\lambda}n\Delta L) \qquad (3.4)$$

where β^2 is the intensity reflectivity of reflection point, and $n\Delta L$ is the optical path difference between the FBG and the reflection point. If there are multiple reflection points in the system, multiple interferometric noise will also appear. The total contribution of these interferometric signals can be regarded as the sum of them. As the interferometric signal appears in the system, the detector will detect a combined signal $I_{noise}(\lambda(t)) + I_{FBG}(\lambda(t))$ and wavelength detection accuracy will be affected. Therefore, signal processing methods are required for improving the measurement precision of Bragg wavelength.

3.2.2 Signal model for simulations

The reflection spectrum of the FBG can be expressed by Gaussian distributions as (Nues *et al.*, 2004):

$$R_{FBG}(\lambda, \lambda_B) = R_0 \exp(-4\ln 2(\frac{(\lambda - \lambda_B)^2}{\alpha^2}) \tag{3.5}$$

where α is the spectral full width at half-maximum (FWHM) of FBG. The spectrum of the reflected light measured by photo detector can be expressed as:

$$I_{FBG}(\lambda(t), \lambda_B) = \frac{I_0 R_0}{4} \exp(-4\ln 2(\frac{(\lambda(t) - \lambda_B)^2}{a^2}) \tag{3.6}$$

In order to apply digital signal processing algorithm to the combined signal, we sample the FBG signal $I_{FBG}(\lambda(t))$ and interferometric signal $I_{noise}(\lambda(t))$ in time domain, then we obtained two discrete sequence:

$$I_{FBG}(n) = \frac{I_0 R_0}{4} \exp(-4\ln 2(\frac{(\lambda(n\Delta t) - \lambda_B)^2}{a^2}) \tag{3.7}$$

and

$$I_{noise}(n) = \frac{I_0}{2}\sqrt{R_{FBG}(\lambda(n\Delta t)\ , \lambda_B)\beta^2}(1 - R_{FBG}(\lambda(n\Delta t), \lambda_B))\cos(\frac{2\pi}{\lambda(n\Delta t)} n\Delta L) \tag{3.8}$$

where Δt is sample interval. In the following section, Equations (3.7) and (3.8) are used to represent the FBG signal and noise signal. Thus, the signal processing algorithms in this chapter are based on these two discrete sequences.

3.3 Improving the Measurement Precision Using Classical Digital Filters

Compared with analogue filters, digital filters have many advantages: they are cheap, easy to implement, easy to upgrade, require no additional hardware equipment and can be applied for real time application. There are two main types of classical digital filters: finite impulse response (FIR) and infinite impulse response (IIR) filters. Classical digital filtering has been used to improve the measurement accuracy of FBG

sensors (Chen *et al.*, 1999). In this section, the performance of these two types of digital filters for improving wavelength detection accuracy is examined.

In order to demonstrate the effect of digital filters for improving measurement precision, a computer simulation was employed. Equations (3.7) and (3.8) are used to construct combined signal $I_{noise}(n) + I_{FBG}(n)$. In simulation, the coefficients have been assumed as (Chen *et al.*, 1999): I_0=5 *mw*, R_0=0.8, λ_B=1530 *nm*, α=0.1 *nm*, $n\Delta L$ = 2 *m* and β^2=0.1. The combined signal is sampled into 500 samples in 0.5 nm spectral range as shown in Figure 3.2. Before applying the digital filter, the peak of the spectrum and corresponding Bragg wavelength are difficult to be identified.

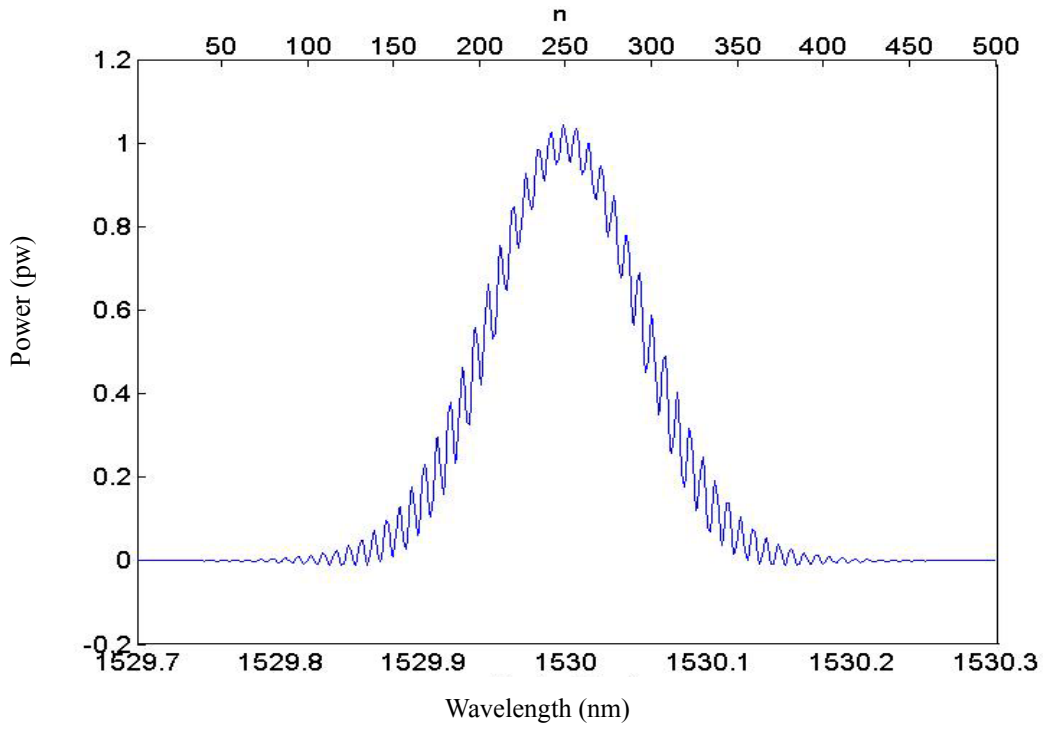

Figure 3.2 Spectrum of the combined signal

In order to develop the appropriate filter, we first need to analyze the frequency spectrum of the combined signal as shown in Figure 3.3. Then we develop the FIR and IIR filter according to the frequency spectrum of the combined signal. The order of

the FIR filter can be estimated by the following Equation (Leland *et al.*, 1995)

$$N_{FIR} \approx \frac{-10\ \lg(\delta_1 \delta_2) - 13}{14.6\,\Delta\omega} \tag{3.9}$$

where δ_1 is the passband ripple, δ_1 is the stopband ripple, and $\Delta\omega$ is the width of a normalized transition bandwidth. The order of the IIR filter can be determined by

$$N_{IIR} \approx \lg \sqrt{\frac{10^{\alpha_S/10} - 1}{10^{\alpha_P/10} - 1}} / \lg \lambda_S \tag{3.10}$$

where α_P is pass band attenuation, α_S is stop band attenuation, and λ_S is normalized cut off frequency. For the combined signal shown in Figure 3.2, we design a 45th order FIR low-pass filter and a 2nd order IIR low-pass filter to eliminate the interference signal.

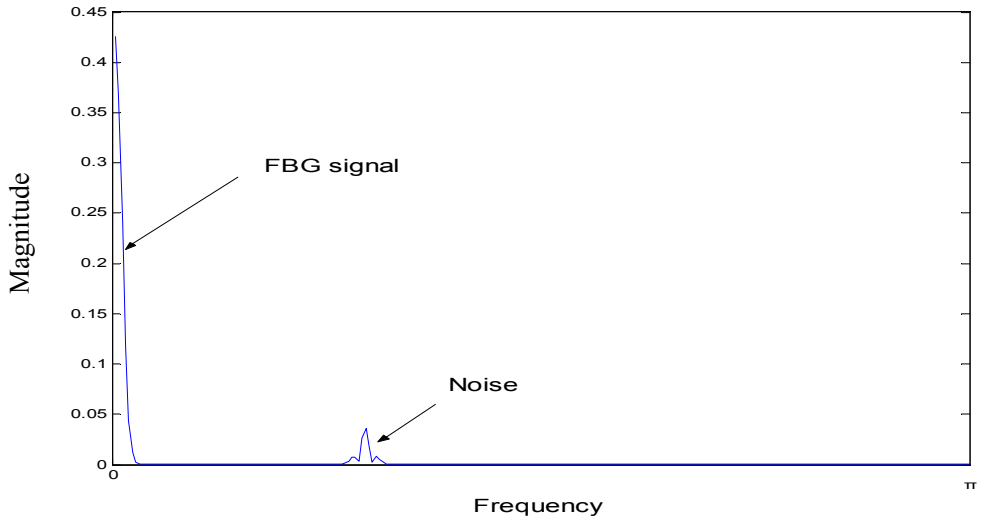

Figure 3.3 Frequency spectrum of the combined signal

The filtered signal is shown in Figures 3.4 (a) and (b). It is clear that the SNR of the signal is increased. Then we use ten combination signals with different λ_B and different $n\Delta L$ (from 1.0 *m* to 1.9*m* with interval of 0.1*m*) to test the performance of the filters. The resulting measurement errors were 0.4 *pm* (RMS value) for FIR filter and 1.3 *pm* (RMS value) for IIR filter. Therefore, FIR filter can achieve better performance than IIR filter in eliminating the interference signal.

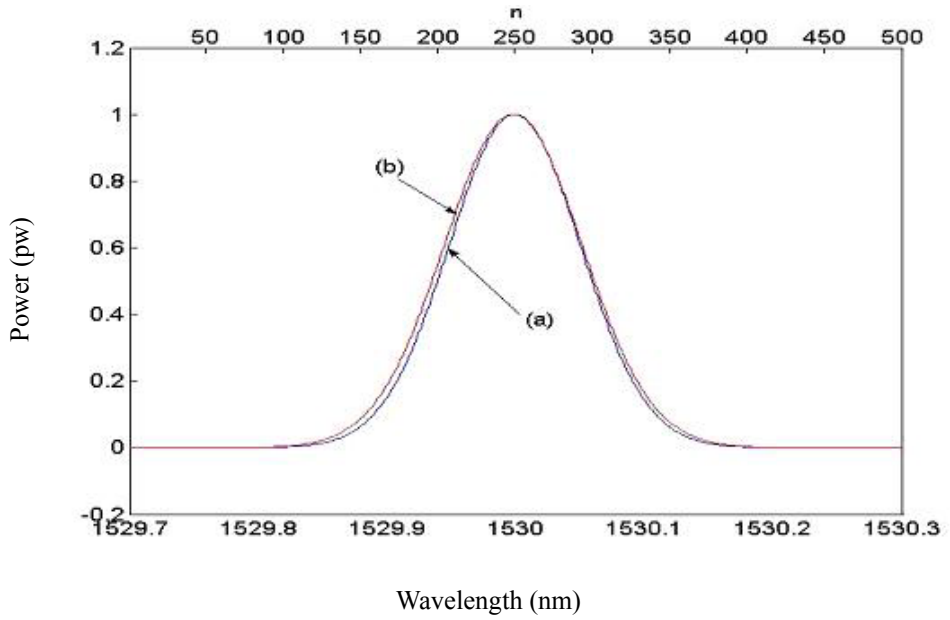

Figure 3.4 Spectrum of the filtered signal: (a) after using FIR (b) after using IIR

However, as the optical path difference between the FBG and the reflection point becomes shorter, the frequency spectrum of the noise signal will move towards the frequency spectrum of the FBG signal. If the optical path difference $n\Delta L$ is less than 10 *cm*, their frequency spectrums will overlap each other, as shown in Figure 3.5. If the classical digital filter is still applied to the combination signal, then the measurement error will reach 15*pm*. Therefore, in this case, the classical digital filter can not remove the noise signal.

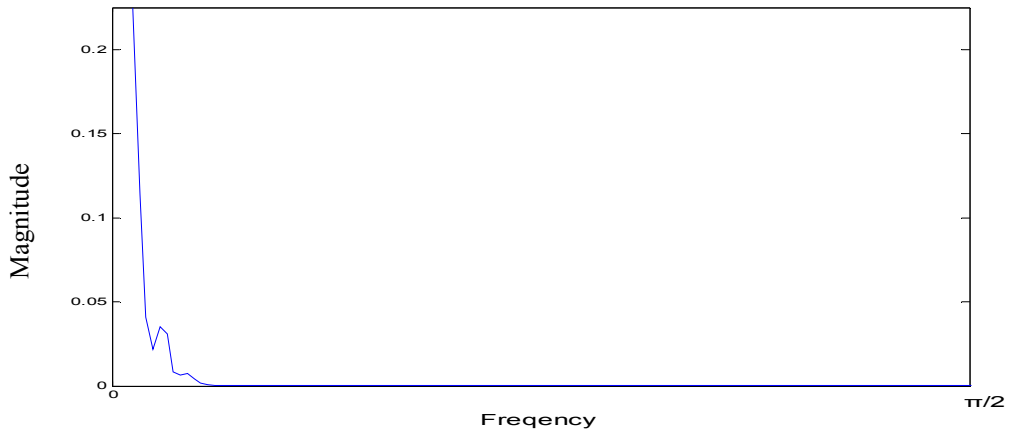

Figure 3.5 Frequency spectrum of the combined signal as $n\Delta L$=7 cm

3.4 Improving the Measurement Precision Using Adaptive Filters

In the last section, digital low-pass filters were used to improve the measurement precision of FBG sensors. This is an efficient technique for eliminating the noise signal if the $I_{FBG}(n)$ and $I_{noise}(n)$ have independent frequency spectrum. However, the performance is limited if the noise components overlap with the Bragg signal in the frequency domain. In order to solve this problem, in this chapter, we use adaptive filtering technique to improve the wavelength detection accuracy for FBG sensors.

An adaptive filter is defined as a self-designing system that has the ability to design itself using a recursive algorithm. With such a device we can process signals whose complete statistical information is unknown. The most widely used adaptive filtering algorithm is the least mean squares (LMS) algorithm. The advantage of this algorithm is that it is computationally simple, but it has the drawback of slow convergence. Advanced algorithms such as the normalized least mean square (NLMS) algorithm, affine projection algorithm (APA), NLMS with orthogonal correction factors (NLMS-OCF) and normalized data-reusing LMS (NDR-LMS) algorithm have been developed to solve this problem. In this section, these algorithms are used to eliminate the unwanted interferometric signal in the FBG sensing system.

3.4.1 Principles of operation

The operation mode of adaptive filtering is shown in Figure 3.6. Where $x(n)$ is the input signal, $y(n)$ is the output signal, $d(n)$ is the desired output signal, $e(n)$ is the estimated error.

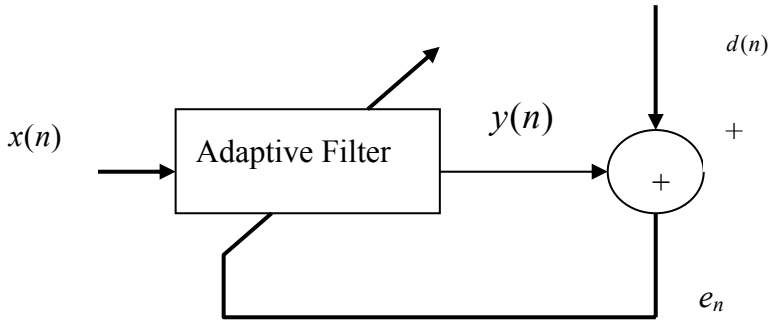

Figure 3.6 Block diagram of adaptive filter

The significance of the adaptive filter is its time variant characteristic. In contrast to the non-adaptive filters, which are linear time invariant, adaptive filters allow the coefficient used in the filter to vary according to some predetermined optimization criterion. The structure of an adaptive filter is shown in the block diagram form in Figure 3.7.

Please see print copy for Figure 3.7

Figure 3.7 Structure of adaptive filter (Haykin *et al.*, 1986)

Then, we can describe the relationship of the input signal and output signal as:

$$y(n) = \sum_{k=1}^{M} x(n-k+1)w_k(n) \tag{3.11}$$

and

$$e(n) = d(n) - y(n) \tag{3.12}$$

where M is the order of the filter, $w^T(n) = [w_1(n), w_2(n), ...w_M(n)]$ is the adjustable tap weight vector at nth instant. The adaptive algorithm is the mechanism for adjusting the tap weight vector along the time axis. The most widely used LMS algorithm adjusts the weight as follows (Haykin *et al.*, 1986):

$$w(n+1) = w(n) + 2\mu e(n)x(n) \tag{3.13}$$

where $x^T(n) = [x(n), x(n-1)...x(n-M+1)]$, μ is a constant called step size and $0 < \mu < \frac{2}{L * InputPower}$. The input power refers to the sum of the mean-square values of tap inputs $x(n)$, $x(n-1)$, … , $x(n-M+1)$.

LMS algorithm is simple, but it has the drawback of converging slowly with the average mean square error (MSE), because its convergence depends on the input signal and the order of filter (Ramani *et al.*, 1996). The advanced adaptive algrithms, such as NLMS, APA, NLMS-OCF and NDR-LMS, have faster rates of convergence than LMS. Their weight adaptation algrithms are expressed as follows:

NLMS (Haykin *et al.*, 1996):

$$w(n+1) = w(n) + 2\frac{\mu}{\|x(n)\|^2} e(n)x(n) \tag{3.14}$$

APA: (K. Ozeki *et al.*, 1984)

$$D_n = [d(n), d(n-1), ..., d(n-M+1)] \tag{3.15}$$

$$X_n = [x(n), x(n-1), ..., x(n-M+1)],\ x^T(n) = [x(n), x(n-1)...x(n-M+1)] \tag{3.16}$$

$$E_n = D_n - w_n^H X_n \tag{3.17}$$

$$w(n+1) = w(n) + \mu X_n [X_n^T X_n]^{-1} E_n \tag{3.18}$$

where ^{T} and ^{H} denote the transposition and complex conjugate transposition.

NLMS-OCF:

$$w(n+1) = w(n) + \mu_0 x_n + \mu_1 x_n^1 + ... + \mu_M x_n^M \tag{3.19}$$

where x_n is the input vector at the nth instant, x_n^k (k=1,2…M) is the component of x_{n-kD} that is orthogonal to $x_n, x_{n-D}, x_{n-2D}, ...x_{n-(k-1)D}$.

$$e_n = d_n - w_n^H x_n \tag{3.20}$$

$$e_n^k = d_{n-kD} - w_n^{kH} x_{n-kd}, \qquad (k = 1,2.....M) \tag{3.21}$$

$$w_n^k = w_n + \mu_0 x_n + \mu_1 x_n^1 + ... + \mu_{k-1} x_n^{k-1} \tag{3.22}$$

$$\mu_k = \begin{cases} \dfrac{\mu e_k^*}{x_n^H x_n} \ for \qquad k = 0, if \left\| x_n^k \right\| \neq 0 \\ \dfrac{\mu e_n^{k*}}{x_n^{hH} x_n^k} \ for \qquad k = 1, 2, ..., M, if \left\| x_n^k \right\| \neq 0 \\ 0 \qquad Otherwise \end{cases}$$

where * denotes the complex conjugate

(3.23)

NDR-LMS (B. A. Schnaufer *et al.*, 1993):

$k_0 = w_n$

For i=0,1,…,R-1

$k_{i+1} = k_i + \mu_{0,i} x_n + \mu_{1,i} x_{n-1} + ... + \mu_{M,i} x_{n-M}$

$$w_{n+1} = k_R$$

where $\mu_{j,i} = \dfrac{(d_{n-j} - k_i^T x_{n-j})}{\left\| x_{n-j} \right\|^2}$, $x_n^T = [x\ (n), x\ (n-1) \ldots x(n-M+1)]$

3.4.2 Implementation of adaptive filter

In this section, we will provide the detail of implementation the adaptive filter for eliminating the unwanted interferometric signal. Using Equations (3.7) and (3.8), $I_{noise}(n) + I_{FBG}(n)$ is generated as the input signal $x(n)$. A Bragg signal $I'_{noise}(n)$ with a different Bragg wavelength compared with $I_{FBG}(n)$ is regarded as the desired signal $d(n)$. The input signal is filtered by the adaptive filter operating on a recursive algorithm. After the weight value converged, the expected output signal is obtained.

3.4.3 Simulations

Computer simulation was carried out to demonstrate the effectiveness of adaptive filter techniques for noise reduction in a FBG sensor system. In simulation, the coefficients of the input signal were assumed as (Chen *et al.*, 1999): I_0=5 *mw*, R_0=0.8, λ_B=1550 *nm*, α=0.1 *nm*, $n\Delta L$ = 5 *cm* and β^2=0.01, in which case the frequency spectrum of the $I_{noise}(n)$ is overlapped with that of $I_{FBG}(n)$. A Bragg signal $I'_{noise}(n)$ with a Bragg wavelength of 1530 *nm* is regarded as the desired signal. The input signal and desired signal were sampled into 500 samples in 0.5 *nm* spectral range as shown in Figure 3.8.

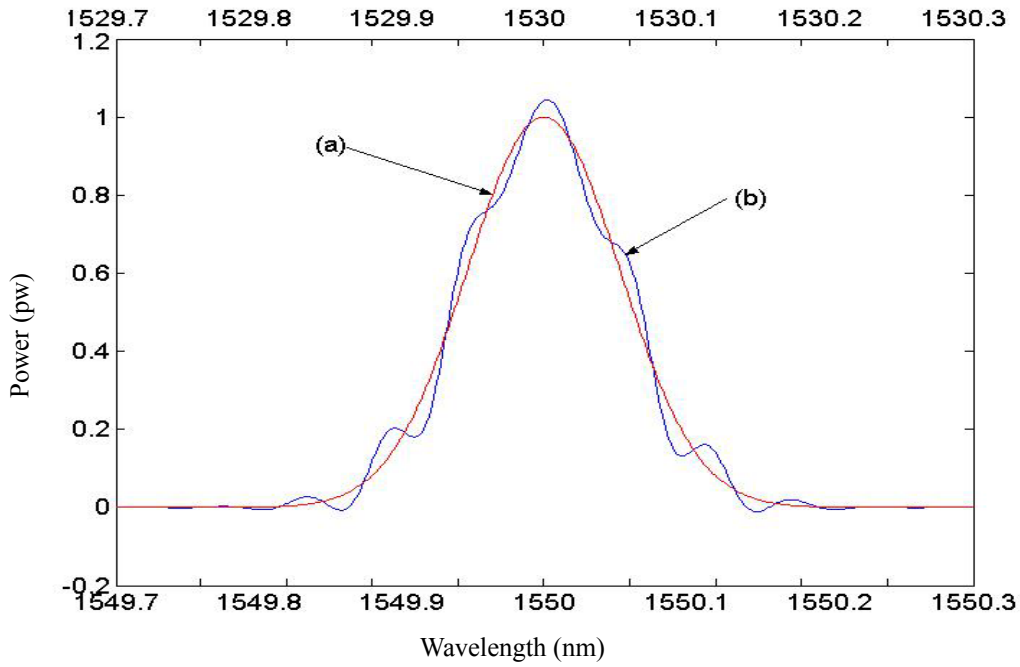

Figure 3.8 Input signal (a) and desire signal (b) for adaptive filtering

We can establish an adaptive filter using LMS algorithms. To begin with, we need to select the proper step size and order of the filter, which determine the speed of convergence and the stability of the algorithm. Large step size and low filter order imply fast convergence speed but large misadjustment in steady-state. In contrast, a small step size and high filter order lead to little misadustment in steady-state but a slow convergence speed. After using different coefficients to test the convergence speed and misadjustment in steady-state, we selected the coefficients of filter as: μ=0.006, M=12. Then the input signal is applied to the LMS adaptive filter. After the MSE is converged to a constant, the filter stops working and the output signal is shown in Figure 3.9. The measurement error of the Bragg wavelength is 4 pm. Then, ten $I_{FBG}(n)$ with different Bragg wavelengths are added to the different $I_{noise}(n)$ (using $n\Delta L$ from 5cm to 10 cm with an interval of 0.5cm) and applied to the filter. As a result, the average measurement error is 3.7 pm (RMS value), which is much lower than that of the classical digital filter: 15pm (Chen *et al.*, 1999) under the condition where the frequency spectrum of the noise overlaps that of the FBG signal.

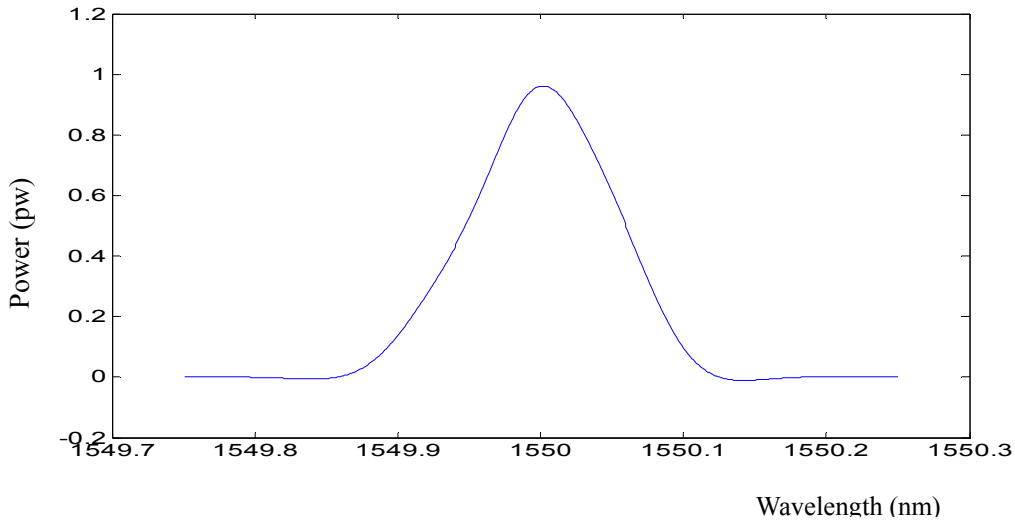

Figure 3.9 Filtered signal by LMS additive filter

In order to compare the performances of NLMS, NLMS-OCF, APA, and NDR-LMS with of LMS, these four adaptive algorithms with the same order were used for noise reduction using the same input signal. The measurement error of the Bragg wavelength using NLMS, NLMS-OCF, APA, and NDR-LMS are 4.6pm, 3.8pm, 3.9pm and 4.3pm respectively. Figure 3.10 shows the learning curves of the algorithms corresponding to the given system. It is evident that NLMS-OCF has the fastest convergence and that LMS has the slowest convergence among the algorithms being compared.

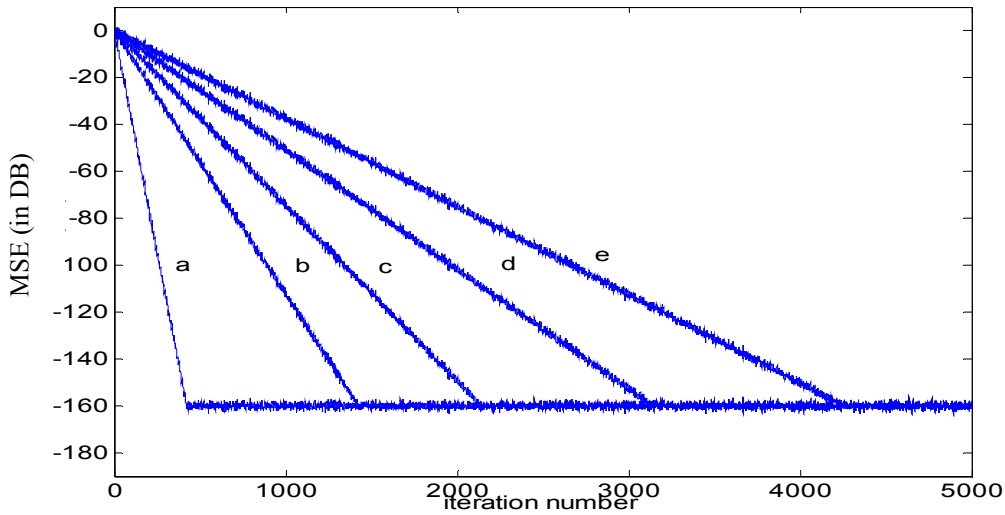

Figure 3.10 Learning Curves for five algorithms:

(a)NLMS-OCF, (b) APA, (c) NDR-LMS, (d)NLMS and (e) LMS

3.5 Noise Cancellation Using Back Propagation Neural Network

In the last section, adaptive filters were applied to improve the measurement precision of FBG sensors. They provided better performance than classic digital filters in eliminating the noise signal if the $I_{noise}(n)$ overlap with $I_{FBG}(n)$ in the frequency domain. However, the measurement error of locating the Bragg wavelength is still great, up to 4 pm under some conditions. In this section, we report on the use of a back propagation (BP) neural network to achieve greater measurement precision.

3.5.1 Principles of operation

BP is the most widely applied neural network technique. The typical structure of the BP neural network is shown in Figure 3.11. It is configured with three layers: an input layer, hidden layer and an output layer. The Input Layer receives input data and passes these to the network for processing. The Hidden Layer receives data from the input layer and processes them in a hidden way. The hidden layers are not directly connected to the outside world (inputs or outputs). The Output Layer receives processed data from hidden layer and sends output signals out of the system. According to different applications, a number of neurons are selected for each layer.

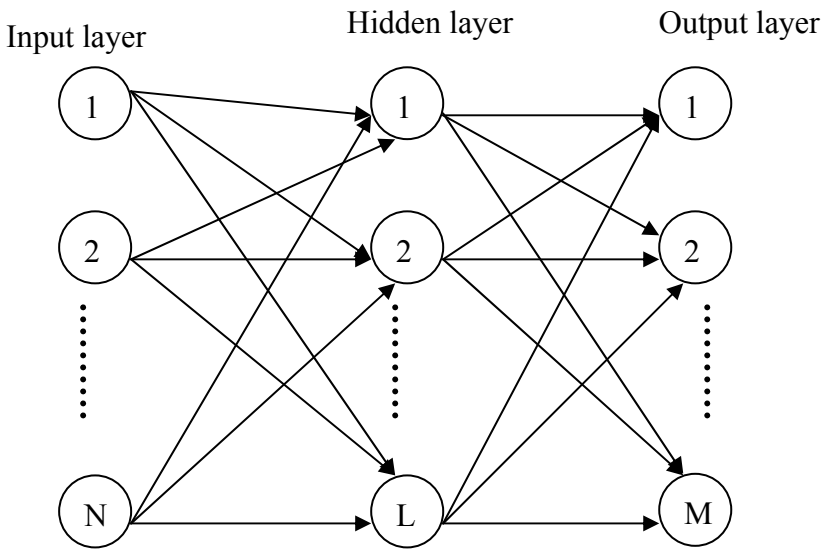

Figure 3.11 Structure of BP neural networks

The most important advantage of BP neural networks compared with traditional linear model such as digital filer lie in its powerful ability to represent non-linear relationships and in their ability to learn both linear and non-linear relationships directly from the modeled data. Traditional linear models are inefficient while it process data which contains non-linear characteristics. Another advantage of BP neural network is its high tolerance to noisy data (Otair *et al.*, 2004). In addition, BP neural network can classify patterns on which they have not been trained.

The operation process of a BP neural network is as follows (James *et al.*, 1991): Firstly, an input pattern is applied to the input layer. This input pattern is multiplied by separate weight values and forward propagation through the entire upper layer until the output pattern is generated. Then the desired output is compared to the output pattern, then the error signal is produced by each output neuron. The error signals are transmitted backward to each neuron in the hidden layer. It should be noticed that each neuron receives only a part of the total error signal, according to its contribution to the output pattern. This process is repeated, until each neuron in the network has received a particular error signal. According to the different error signal received by each neuron, connection weights are updated to make the network converge toward a desired state.

This operation process is called training process. It repeats over and over again until the error lever is at a low enough level. After the training process, the neurons in the hidden layer learn to organize different features of the input patterns. Thus, if a new input pattern enters the network, the hidden layer will respond with an active output if the input contains the feature. Otherwise, the hidden layer neurons will inhibit their output. The output patterns can be regarded as a feature map that indicates the presence or absence of many different features of the input. Therefore, the BP neural network has the ability to examine the noisy data patterns and reconstruct the desired data pattern.

The detailed mathematical description of the BP network is presented in James (1991).

Here, we present only the simple approach, as follows:

1. Apply $X_N = (x_1, x_2, ..., x_N)$ to the input layer.
2. Calculate the net-input value of the hidden layer:

$$net_j^h = \sum_{i=1}^{N} w_{ji}^h x_i + \theta_j^h \tag{3.24}$$

where θ_j^h is the bias term of the j neuron of the hidden layer. This term is a weight on a connection whose input is always equal to 1.

3. Calculate the output from the hidden layer:

$$O_j^h = f(net_j^h) = \frac{1}{1 + \exp(-net_j^h)} + \theta_j^h \tag{3.25}$$

4. Calculate the net input value of the output layer:

$$net_k^o = \sum_{j=1}^{L} w_{kj}^o O_j^h + \theta_j^h \tag{3.26}$$

5. Calculate the outputs:

$$O_k^o = f(net_k^o) = \frac{1}{1 + \exp(-net_k^o)} + \theta_k^o \tag{3.27}$$

6. Calculate the error for output units

$$\delta_k^o = (d_k - O_k^o) f_k^{'}(net_k^0) \tag{3.28}$$

where d_k is the desired output.

7. Calculate the error for hidden neurons:

$$\delta_j^h = f_j^{'}(net_j^h) \sum_k \delta_k^o w_{kj}^o \tag{3.29}$$

8. Update the weight for the output layer

$$w_{kj}^o(t+1) = w_{kj}^o(t) + \eta \delta_k^o O_j^h \tag{3. 30}$$

where η is the learning rate of the net work

9. Update the weight for the hidden layer

$$w_{ji}^{h}(t+1) = w_{ji}^{h}(t) + \eta \delta_{j}^{h} x_{i} \tag{3. 31}$$

10 Calculate the error term:

$$E_N = \frac{\sum_{k=1}^{M} \delta_k^2}{2} \tag{3.32}$$

If E_N is smaller than a specified value γ, training will stop. Otherwise the training process will repeat from step 1.

3.5.2 Implementation of BP neural network

A BP neural network is constructed to achieve greater measurement precision of FBG sensors. The network is shown in Figure 3.12 with *N=M=L=500*. Using Equations (3.7) and (3.8), the input signal $I_{FBG}(n) + I_{noise}(n)$ and the desired output signal $I_{FBG}(n)$ can be derived for the training process.

3.5.3 Simulations

In simulation, we first test the performance of the BP neural network in eliminating the noise with a frequency spectrum that overlaps that of the FBG signal. Ten FBG signals with different Bragg wavelengths were generated as the desired signal and the coefficients have been assumed as (Chen *et al.*, 1999): I_0 =5 *mw*, R_0 =0.8, λ_B=1529.85, 1529.88, 1529.91, 1529.94, 1529.97, 1530, 1530.03, 1530.06, 1530.09, 1530.12 *nm*, α=0.1 *nm*. $I_{noise}(n)$ is generated with $n\Delta L$ = 7 *cm* and β^2=0.01, in which case the frequency spectrum overlaps that of the FBG signal. Then ten pairs of input signals and desired signals were then sampled into 500 samples in 0.5 *nm* spectral range. One of these training data pairs of Bragg wavelength 1530 *nm* is shown in

Figure 3.12

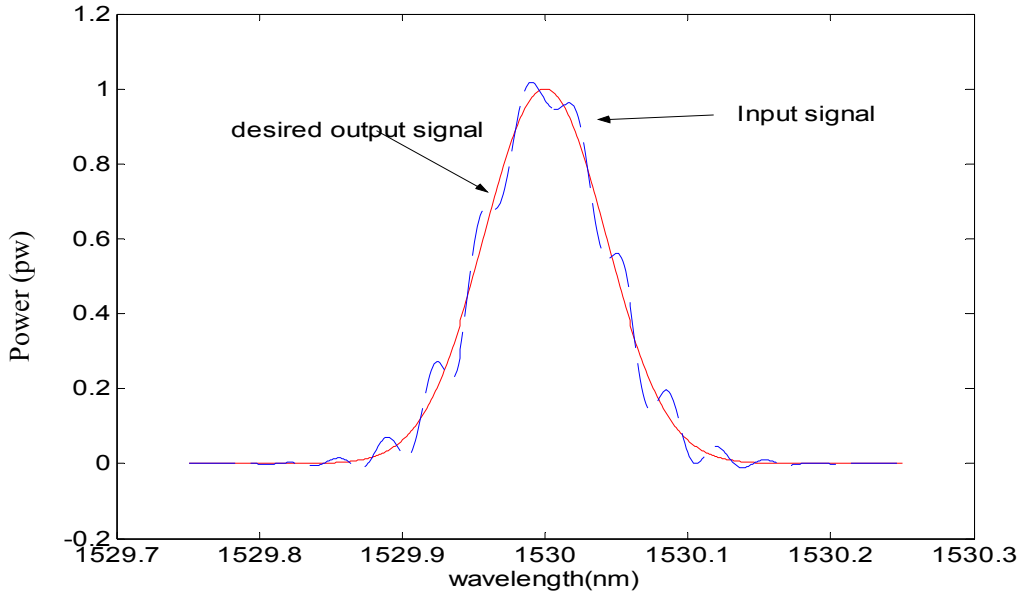

Figure 3.12 A pair of data used to train the network

Then the training process of BP neural network starts. Usually, the learning rate η must be a small value to ensure the performance of the network. However, a small value indicates that the network will have a large number of iterations. In this application, η is set to a small value 0.005 to guarantee the network performance. The value γ for the termination of the training process is set to 10^{-6}. The BP neural network is well-trained after 1321 iterations, then terminated. After training, we use a new FBG signal $I'_{FBG}(n)$ with Bragg wavelength $1530.15nm$ added to $I'_{noise}(n)$ as the input signal to test the performance of neural network. The noise signal $I'_{noise}(n)$ is generated using $n\Delta L = 5cm$ which is not within the training data. The input and output signals of the network are shown in Figure 3.13.

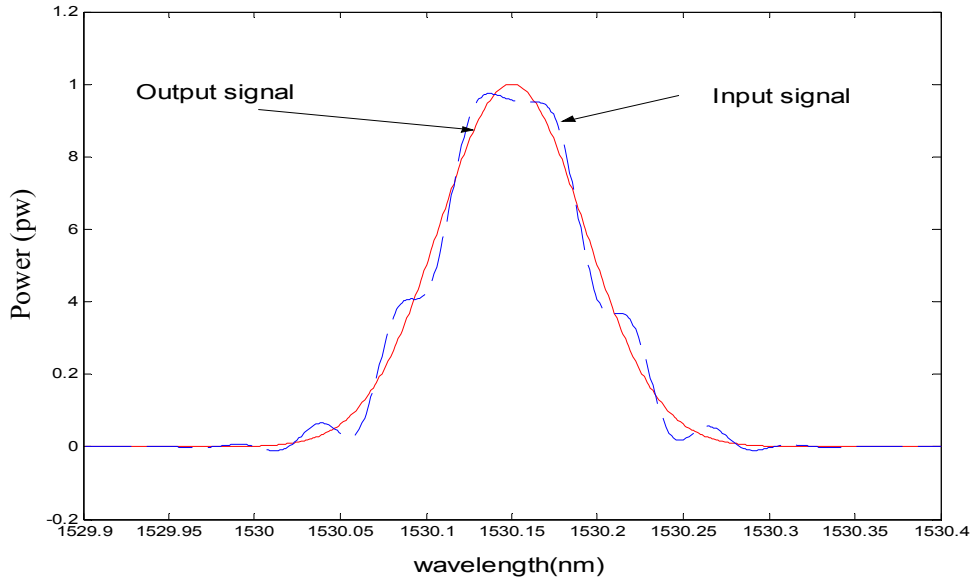

Figure 3.13 Input and output from the well-trained network

The measurement error of the Bragg wavelength is 1 *pm* which is much lower than that of the classical digital filter (Chen *et al.*, 1999). Then, ten FBG signals with different Bragg wavelengths are added to the same noise signal (using $n\Delta L$=5cm) and applied to the input layer of the network. As a result, the average measurement error is 0.9 *pm* (RMS value). Therefore, a BP neural network can improve the accuracy of detecting Bragg wavelength under the condition that the frequency spectrum of the noise overlaps that of the FBG signal. In order to examine the performance of the network in eliminating different noise signals, we vary the optical path difference $n\Delta L$ of the noise signal from 2 *cm* to 30 *cm* with an interval of 1cm. After that we set the optical path difference $n\Delta L$ to 50cm, 100cm and 150cm respectively. Then these noise signals were added to a FBG signal respectively and applied to the input layer of the BP neural network, the measurement errors for different $n\Delta L$ are shown in Figure 3.14.

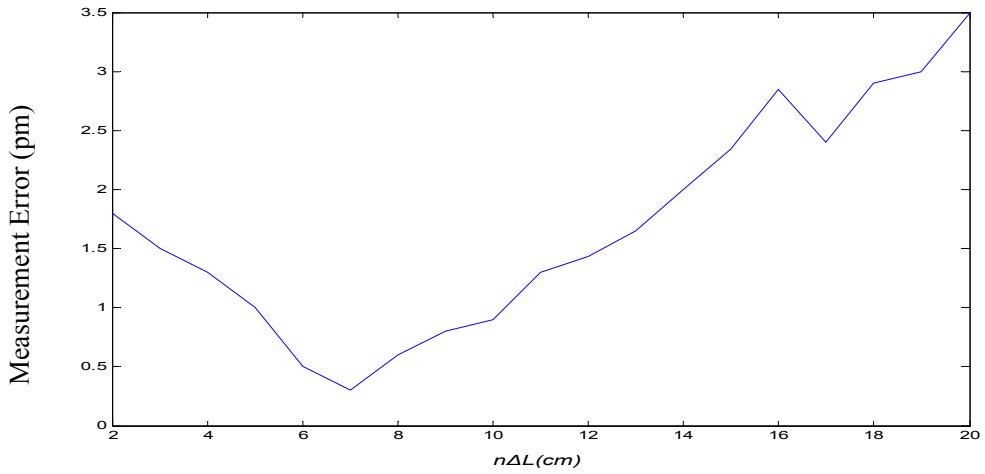

Figure 3.14 Measurement errors versus optical path difference $n\Delta L$ of the noise signal

Figure (3.14) shows that the measurement error depends on the noise component of the test signal. If the noise component of the input signal is similar to that of the training data, the measurement precision is high. In order to testify this phenomenon, we train the neural network using another ten signal pairs. The desired signals of the training pairs are the same as we used above and the optical path difference $n\Delta L$ of the noise signal is set to 20 *cm*. After training the network, we applied the same test signals on the input layer of the neural network and the corresponding measurement error of the Bragg wavelength is shown in Figure 3.15.

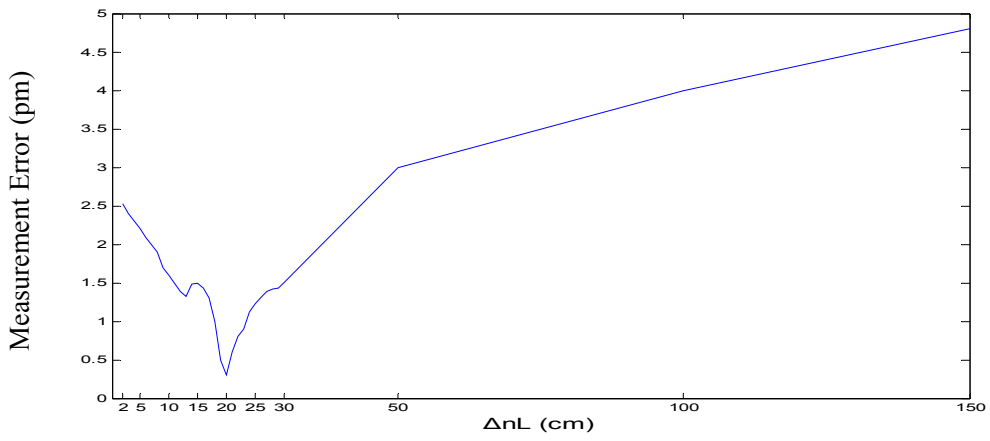

Figure 3.15 Measurement errors versus optical path difference $n\Delta L$ of the noise signal

As a result, we observe the same phenomenon: the measurement error is small if the noise component of the test signal is correlated with that of the training signal. Otherwise, the measurement error will be relatively greater. Therefore, correctly evaluating the noise signal is very important for achieving high measurement precision using a BP neural network.

3.6 Conclusions

Classical digital filters, adaptive filters and neural network have been used to improve the measurement precision of the FBG sensors. The simulation results show that classical digital filter is efficient in improving measurement accuracy if the noise signal and the FBG signal have independent frequency spectrum. However, the improvement will be limited if the noise components overlap with the Bragg signal in the frequency domain. Under that condition, the measurement error is greater than 15 *pm*.

The adaptive filter provides better performance than the classical digital filter. In the simulation, we applied 5 different adaptive algorithms to this task. The results indicate that the measurement error is around 4*pm* - much smaller than that of the classical digital filter. In addition, the filter with NMLS-OCF adaptive algorithm performs faster convergence than the other algorithms.

Moreover, a BP neural network is used to further improve the measurement accuracy. As a result, the measurement error is reduced to 1 *pm* under the condition that the frequency spectrum of FBG signal overlaps that of the noise signal. However, to achieve such a performance requires that the noise component of measured signal be correlated with that of the training signal. Otherwise, the measurement error will increase.

CHAPTER 4 IMPROVING THE PERFORMANCE OF IWDM-BASED FBGS SENSING SYTEMS

4.1 Introduction

The multiplexing of sensors is a particularly important technology of a FBG sensing system that can provide a distributed measurement along a single fiber. Currently, many advanced multiplexing techniques are developed to improve the multiplexing capacity of FBG sensing systems. In particular, intensity and wavelength-division multiplexing (IWDM) techniques have the advantages of low complexity and enabling the system to contain twice the number of FBGs as a conventional WDM technique. In addition, with a demodulation technique called minimum variance shift (MVS), the IWDM scheme can be implemented using common FBG sensors (Gang *et al.*, 2002). However, this technique requires long processing times to gain high detection accuracy. In this chapter, three optimization algorithms are developed to improve the performance of the IWDM-based FBG sensing system.

The chapter is organized as follows: In section 4.2, the system model and principle of MVS demodulation technique are introduced. Also, we point out the limitations of this technique. In section 4.3, a gradient-based algorithm is used to improve the performance of the IWDM-based FBG sensing system. In section 4.4, a global optimization algorithms-tabu search (TS) is introduced to overcome the local minima problem of gradient algorithm. In section 4.5, an improved tabu–gradient algorithm is applied to reduce the computation time of TS, and the conclusion is given in section 4.6.

4.2 System Model

In order to show the principle of MVS we consider a sensing system with two FBG sensors shown in Figure 4.1. The two FBG sensors of the system have different reflectivity. The measured spectrum is the combinations of the lights reflected by these two FBGs which can be expressed as:

$$R(\lambda) = R_1 g_1(\lambda - \lambda_{B1}) + R_2 g_2(\lambda - \lambda_{B2}) + N(\lambda) \tag{4.1}$$

where $g_1(\lambda)$ and $g_2(\lambda)$ are the reflection spectrums, λ_{B1} , λ_{B2} and R_1, R_2 ($R_1 \neq R_2$)are the Bragg wavelengths and the peak reflectivity of the two FBGs respectively, $N(\lambda)$ is a random spectral fluctuation which is introduced by the noise that occurs in the system.

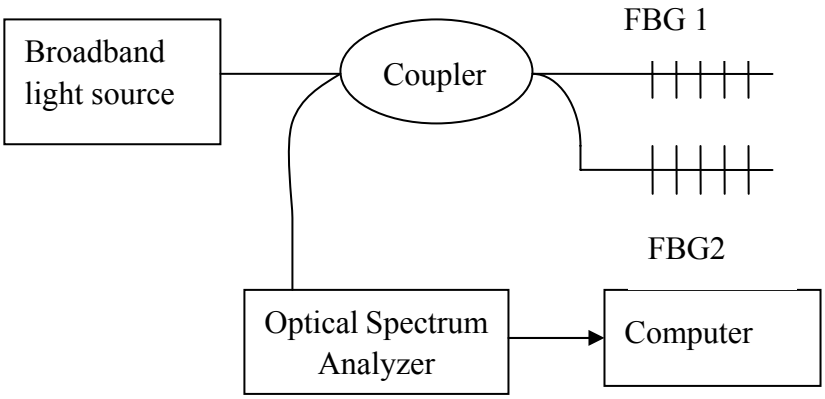

Figure 4.1 System diagram

We assume the reflection spectrums $g_i(\lambda)$ have a Gaussian shape. By using $\hat{\lambda}_{B1}$ and $\hat{\lambda}_{B2}$ to evaluate Bragg wavelengths of the two sensors, an evaluated spectrum is constructed as (Gong *et al.*, 2002) :

$$R_m(\lambda, \hat{\lambda}_{B1}, \hat{\lambda}_{\mathbf{B}2}) = R_{m1}(\lambda, \hat{\lambda}_{B1}) + R_{m2}(\lambda, \hat{\lambda}_{B2}) = R_1 g_1(\lambda - \hat{\lambda}_{B1}) + R_2 g_2(\lambda - \hat{\lambda}_{B2}) \tag{4.2}$$

where $g_i = \exp(-4\ln 2(\frac{(\lambda - \hat{\lambda}_{Bi})^2}{\alpha_i^2})$, α_i is the spectral full width at half-maximum

(FWHM) of i-th FBG sensor, $\hat{\lambda}_{Bi}$ is corresponding evaluated Bragg wavelength. A series of spectrum can be acquired by varying $\hat{\lambda}_{B1}$ and $\hat{\lambda}_{B2}$ as:

$$R_m(n) = R_m(\lambda, \hat{\lambda}_{B1}(n), \hat{\lambda}_{\mathbf{B2}}(n)) \tag{4.3}$$

These spectrums cover all possible combinations of $R_1 g_1(\lambda)$ and $R_2 g_2(\lambda)$. The average variance between actual spectrum and constructed spectrum is:

$$D(\hat{\lambda}_{B1}, \hat{\lambda}_{B2}) = \frac{1}{t_2 - t_1} \int_{t_1}^{t_2} [R(\lambda) - R_m(\lambda, \hat{\lambda}_{B1}, \hat{\lambda}_{B2})]^2 \, d\lambda \tag{4.4}$$

where $[t_1, t_2]$ is the wavelength range, $D(\hat{\lambda}_{B1}, \hat{\lambda}_{B2})$ will be minimized when $\hat{\lambda}_{B1} = \lambda_{B1}$, $\hat{\lambda}_{B2} = \lambda_{B2}$. Therefore, by scanning $\hat{\lambda}_{B1}$ and $\hat{\lambda}_{B2}$ through specified ranges with a small step size, the minimum $D(\hat{\lambda}_{B1}, \hat{\lambda}_{B2})$ and corresponding λ_{B1} and λ_{B2} can be determined.

$$D(\hat{\lambda}_{B1}, \hat{\lambda}_{B2})_{\min} = D(\hat{\lambda}_{B1}, \hat{\lambda}_{B2})\big|_{\hat{\lambda}_{B1} = \lambda_{B1}, \hat{\lambda}_{B2} = \lambda_{B2}} \tag{4.5}$$

Using this method, the Bragg wavelengths of the multiplexed FBG sensors can be accurately located even when their reflection spectrums completely overlap. Therefore, by alternately placing a series of Bragg wavelength stepped sensors with high reflectivity and low reflectivity along a fiber, the system can contain twice the number of FBGs as the conventional WDM sensor array. However, the computational burden of this algorithm is heavy. Assuming that the step size $\Delta\lambda$ of scanning $\hat{\lambda}_{B1}$ and $\hat{\lambda}_{B2}$ is *1 pm,* the wavelength range $t_2 - t_1 = 1$ *nm,* we need to calculate $(\frac{t_2 - t_1}{\Delta\lambda})^2 = 10^6$ times $D(\hat{\lambda}_{B1}, \hat{\lambda}_{B2})$ to locate the exact position of λ_{B1} and λ_{B2}. In the following section, optimal algorithms are developed to solve this problem.

4.3 Improving the Performance of IWDM-Based FBG Sensing Systems Using Gradient Optimization Algorithm

As mentioned in the previous section, the demodulation technique of an IWDM-based FBG sensing system is based on a theoretical model to calculate every possible Bragg wavelength of multiplexed FBG sensors, in order to achieve the best data-to-model match. This technique needs a long processing time to achieve an accurate result, especially where a number of sensors are involved. In this section, we propose a gradient optimization algorithm for improving the performance of IWDM-based FBG sensing systems.

4.3.1 Principles of operation

Gradient algorithm is an widely used optimization technique. Reconsidering the system discussed above, we defined the mean square error between $R_{m1}(\lambda,\hat{\lambda}_{B1})$, $R_{m2}(\lambda,\hat{\lambda}_{B2})$ and $R(\lambda)$ as the cost function as:

$$J_1 = E(e_1^2) = E\left([R(\lambda) - R_{m1}(\lambda,\hat{\lambda}_{B1})]^2 \right) \tag{4.6}$$

and

$$J_2 = E(e_2^2) = E\left([R(\lambda) - R_{m2}(\lambda,\hat{\lambda}_{B2})]^2 \right)$$

where $E(.)$ denotes the expectation. As discussed in the last section, it is expected that:

$$Min(J_1(\hat{\lambda}_{B1})) = J_1(\hat{\lambda}_{B1})_{\hat{\lambda}_{B1}=\lambda_{B1}} \tag{4.7}$$

and

$$Min(J_2(\hat{\lambda}_{B2})) = J_2(\hat{\lambda}_{B2})_{\hat{\lambda}_{B1}=\lambda_{B2}}$$

Therefore, by minimizing the mean square error with respect to $\hat{\lambda}_{B1}$ and $\hat{\lambda}_{B2}$ we may obtain λ_{B1} and λ_{B2}. Using gradient algorithm, $\hat{\lambda}_{B1}$ and $\hat{\lambda}_{B2}$ are estimated in an

iterative way:

$$\hat{\lambda}_{B1}(n+1) = \hat{\lambda}_{B1}(n) - \mu\nabla J(\hat{\lambda}_{B1}(n)\ ), \quad \hat{\lambda}_{B2}(n+1) = \hat{\lambda}_{B2}(n) - \mu\nabla J(\hat{\lambda}_{B2}(n)\ ) \tag{4.8}$$

where μ is a constant value called step size, $\nabla J()$ represents the gradient of function with respect to variable $\hat{\lambda}_{B1}$ and $\hat{\lambda}_{B2}$, and the subscript *n* denotes the n-th iteration. $\nabla J(\hat{\lambda}_{B1}(n))$ can be obtained by:

$$\begin{aligned}
&\nabla J(\hat{\lambda}_{B1}(n)) \\
&= \nabla\left(E([R(\lambda) - R_{m_k}(\lambda, \hat{\lambda}_{B1}(n))]^2)\right) \\
&= E\left(\frac{\partial(\ [R(\lambda) - R_{m_k}(\lambda, \hat{\lambda}_{B1}(n))]^2\ )}{\partial \hat{\lambda}_{B1}}\ \right) \\
&= 2E\left(\ (R_{m_1}(\lambda, \hat{\lambda}_{B1}(n)) - R(\lambda)) \cdot \left(\frac{\partial(R_{m_1}(\lambda, \hat{\lambda}_{B1}(n)\ ))}{\partial \hat{\lambda}_{B1}}\right)\ \right) \\
&= -2E(e_1(\hat{\lambda}_{B1}(n)) \cdot \frac{8\ln 2}{\alpha^2} R_{m_1}(\lambda, \hat{\lambda}_{B1}(n))(\lambda - \hat{\lambda}_{B1}(n))) \\
&= -\frac{16\ln 2}{\alpha^2} E(e_1(\hat{\lambda}_{B1}(n)) \cdot R_{m_1}(\lambda, \hat{\lambda}_{B1}(n)) \cdot (\lambda - \hat{\lambda}_{B1}(n)))
\end{aligned} \tag{4.9}$$

Similarly, $\nabla J(\hat{\lambda}_{B2}(n))$ can be obtained by:

$$\nabla J(\hat{\lambda}_{B2}(n)) = \frac{16\ln 2}{\alpha^2} E(e_2(\hat{\lambda}_{B2}(n)) \cdot R_{m_2}(\lambda, \hat{\lambda}_{B2}(n)) \cdot (\lambda - \hat{\lambda}_{B2}(n))) \tag{4.10}$$

Therefore, by repeat estimating $\hat{\lambda}_{B1}$ *and* $\hat{\lambda}_{B2}$ using Equation (4.8), $\hat{\lambda}_{B1}$ and $\hat{\lambda}_{B2}$ will converge to λ_{B1}' and λ_{B2}' which correspond to the minimum mean square error. Meanwhile, we can obtain approximately λ_{B1} and λ_{B2} by:

$$\lambda_{B1} = \lambda_{B1}', \quad \lambda_{B2} = \lambda_{B2}' \tag{4.11}$$

4.3.2 Simulations

Computer simulation is conducted for the two FBG sensing systems as shown in Figure 4.1. In simulation, the spectrum of the measured signal $R(\lambda)$ is generated using Equation (4.1) and the coefficients of $R(\lambda)$ are assumed as (Gong *et al.*, 2002): λ_{B1}=1530 *nm*, λ_{B2}=1530.2, R_1=0.8, R_2=0.5, $\alpha_1 = \alpha_2$=0.2 *nm*, $N(\lambda)$ is white noise with signal to noise ratio (SNR) about 12 *db*. The original Bragg wavelengths of two FBG sensors are assumed as: $\hat{\lambda}_{B1}$=1529.5 *nm*, $\hat{\lambda}_{B2}$ = 1530.5*nm*. The measure spectrum and original spectrum are sampled into 2000 samples within the spectral range from 1529 *nm* to 1531 *nm*. Therefore, the spectral resolution of the input spectrum is 1 *pm*. The constructed measured spectrum and original spectrum of two FBG sensors are shown in Figure 4.2.

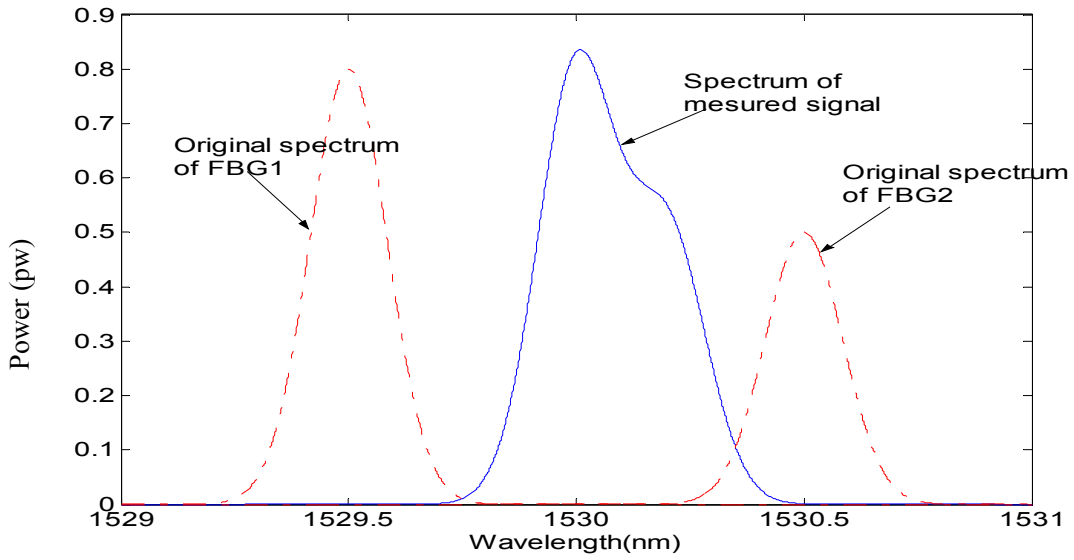

Figure 4.2 Measured and original spectrums for two FBG sensors

It is obvious that the spectrums of the two FBG sensors overlap and the Optical Spectrum Analyser can not identify the Bragg wavelength directly. Using Equations (4.8), (4.9) and (4.10), we repeat the estimations of $\hat{\lambda}_{B1}$ *and* $\hat{\lambda}_{B2}$ until they converge to constant values λ_{B1}' and λ_{B2}'. Here, we set μ to a small value, 0.05.

The learning curve of $J_1 + J_2$ is shown in Figure 4.3. After $J_1 + J_2$ converge to steady state values, we can approximately obtain the Bragg wavelength λ_{B1} and λ_{B2}. In simulation, the resulting λ_{B1} and λ_{B2} are 1530.003 *nm* and1530.096 *nm* respectively. The measurement error is 3*pm* for FBG1 and 4 *pm* for FBG2. In order to find the relationship between μ and the measurement error, we varied the value of μ from 0.05 to 0.005 with step of 0.001. The measurement errors will reduce to 2*pm* when μ is set to 0.02, after which the measurement error remains unchanged even when μ is set to a very small value.

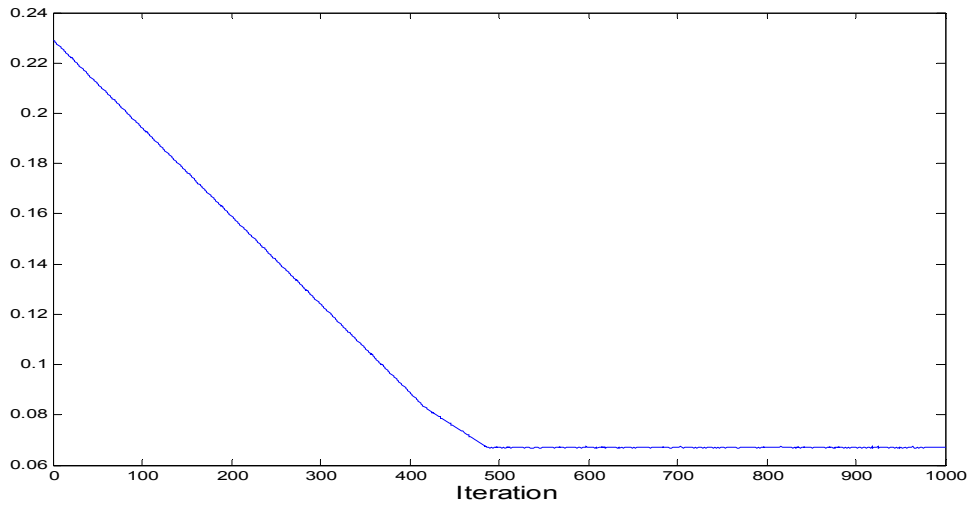

Figure 4.3 learning curve of $J_1 + J_2$

Then we repeat the simulation ten times using a different constructed measured signal with $\mu = 0.02$. As a result, the average measurement error is 2.1 *pm* and the average iterative number is 946 for the convergence of $J_1 + J_2$. In contrast, if we use the conventional IWDM method to locate the Bragg wavelengths of the measured spectrum, we must make 4×10^6 iterations. Therefore, by using the MVS technique with the gradient optimization algorithm, the Bragg wavelength of the sensors can be quickly and accurately determined.

4.3.3 Discussion

It should be noted that the MVS technique is based on prior information about the original spectrums of the FBG sensors, ie. R_i and α_i are known. If these parameters are not available, they need to be evaluated as well. Therefore, the computation time required to achieve highly accurate Bragg wavelength detection will be much longer. Assumed that the measured spectrum has *C* sampling points, R_i and α_i have *M* and *N* possible values respectively. As the two FBG sensing systems mentioned above, using the conventional MVS technique, Equation (4.3) must be calculated $C^2 M^2 N^2$ times.

Under these conditions, the cost functions J_1 and J_2 become multimode because they contain a number of uncertain parameters and exhibit multiple local minima. However, only one global minimum exists, which is the best solution for the function. Reconsidering the working principle of gradient optimization algorithm, we find that it starts from a pre-determined starting solution and converges to the closest local minimum of the cost function. Unfortunately, this closest local minimum is not guaranteed to be the global minimum of the cost function. Thus, if multiple local minima exist, the gradient algorithms fail to find the global minimum of the object function.

Therefore, the gradient algorithm is inefficient for determining the Bragg wavelength if the original uncontaminated spectrums of the FBG sensors can not be constructed exactly. To solve this problem, we need to introduce a global algorithm for optimizing the computation process of MVS.

Global optimization is the algorithm used to find the absolutely optimal solution of the cost function. It has much a better chance than local optimization algorithms to converge to the global minimum and it requires less computation time. In the next

section, we report on the use of a global optimization algorithm–tabu search for detecting the Bragg wavelengths for IWDM-based FBG sensing system.

4.4 Improving the Performance of IWDM-Based FBG Sensing System Using Tabu Search Algorithm

In the last section, we discussed the limitation of gradient algorithm for optimizing the MVS technique when the original spectrums of FBG sensors can not be pre–determined. In this section, the global optimization algorithm–tabu search (TS) is introduced to solve this problem.

4.4.1 Principles of tabu search

TS is a probabilistic global search algorithm aimed at solving combinatorial optimization problem. TS have been used in many fields including telecommunication, resource planning, financial analysis, energy distribution, molecular engineering and mineral exploration (Glover *et al.*, 1989). This optimization method is structured to search the entire solution space of the objective function and find the region where the global minimum is likely to exist. The distinguishing feature of TS is its intensive use of additional memory, which helps to prevent cycling during the search process.

The basic working principle of TS is shown in Figure 4.4. The aim of the search is to find an optimum solution $i = i^*$ in the whole solution space *S*. To begin with, a starting solution *i* is randomly generated from *S*. Also, *i* is evaluated by a object function $f(i)$. Then a neighbourhood solution $N(i)$ is produced according to the current solution *i*. A local search algorithm is then carried out to find the best solution *j* for the object function in this subset neighbourhood $N(i)$. j will be recorded as the best new neighbour and the starting point for the next iteration if it is not on the tabu list. This process repeats until the stopping condition is met.

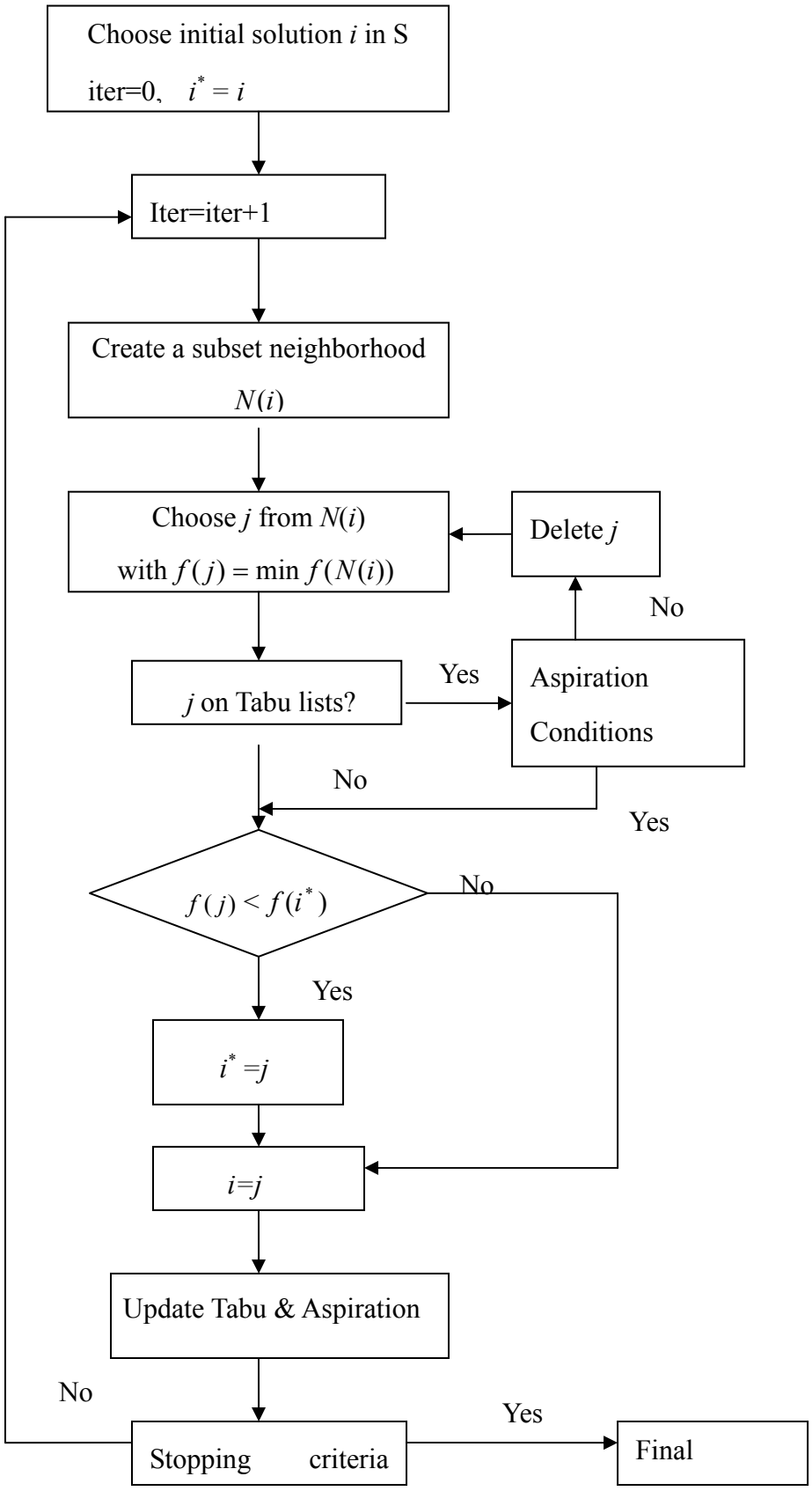

Figure 4.4 Flowchart of a Standard Tabu Search

The tabu list is used to implement tabu restrictions based on regency or frequency (Glover *et al.*, 1997). The most widely used tabu list is based on regency which records the latest visit solutions and maintains them for a given time, called tabu tenure. This type of tabu list is often called short term memory. In contrast, the tabu list which is managed according to frequency is call long term memory. This type of tabu list records the solutions that have been searched most often. According to the tabu list, the local search algorithm will not reuse the solutions recorded on the tabu list. Because Ts can accept non-improving solutions and thus escape from local minima, it is possible to find the global optimum of the objective function. Typically, the length of a tabu list is pre-specified and the tabu list is stored in a memory. At each iteration, the tabu list is updated by adding a new solution and removing other solutions, using a FIFO (first-in-first-out) discipline.

Other important elements of a tabu search are intensification and diversification strategies. Intensification and diversification strategies are used to intensify the search around the areas which have been found to contain many elite solutions. A diversification strategy encourages the search in regions not previously explored. Usually, intensification is implemented for a few iterations, followed by the diversification.

In order to avoid losing a good solution within the search process, an aspiration criterion is used to determine if the tabu restriction can be overridden. The continued optimization process always classifies the regions close to the tabu solution as tabu areas, within which all the solutions will be forbidden. This strategy leads to the best neighbour of the current tabu solution being missed. With an aspiration criterion, the best neighbour in the tabu list can be accepted beyond the tabu restriction if it is much better than the current best solution. Otherwise, it will be deleted and the second best solution will be accepted as the best neighbour.

The criteria for stopping the search process can be describes as follows:

1. The maximum iteration number is reached
2. The number of iterations since the last update of i^* is larger than a specified number.
3. The optimum solution is obtained.

4.4.2 Implementation of TS for optimizing MVS technique

In this section, we provide details of the implementation of TS algorithm to solve the exhausted computation problem of the MVS technique, which consists of the following issues:

1. Parameters of a solution

As discussed in last section, if information of the original uncontaminated spectrums of FBG sensors is unknown, then six parameters [$\hat{R}_1, \hat{R}_2, \hat{\alpha}_1, \hat{\alpha}_2, \hat{\lambda}_{B1}, \hat{\lambda}_{B2}$] need to be determined in order to detect λ_{B1} and λ_{B2}.

2. Search Space

Search space depends on the type of parameter. For instance, $R_1, R_2 \in (0,1)$, $\alpha_1, \alpha_2 \in (0,0.5)nm$. The search range of $\hat{\lambda}_{B1}$ and $\hat{\lambda}_{B2}$ are decided according to the experimental requirement.

3. Neighbourhood generation

In this particular application, we adopt a single parameter generation strategy. Using this strategy, new solutions are generated by varying only one parameter and keeping the others fixed. The parameter is varied using a random coefficient β:

$$\beta = \delta \quad r_i(X_t - X_b) \tag{4.12}$$

where δ is a [-1,1] random number, r_i is a constant factor according to different parameters which decide the estimation precision and $X_t - X_b$ is the search space of the parameter. Thus,

$$X_{new} = X_{old} + \beta \tag{4.13}$$

4. Object function

The object function is the mean square function

$$f = \frac{1}{L}\sum_{\lambda=n_1}^{n_2}[R(\lambda) - (\hat{R}_1\, g_1(\lambda - \hat{\lambda}_{B1}) + \hat{R}_2\, g_2(\lambda - \hat{\lambda}_{B2}))]^2 \tag{4.14}$$

where [n_1, n_2] is the wavelength range, L is the sampled number of wavelength range.

5. Memory type

In this application, we use short term memory and a tabu list is employed based on recency. The length of the tabu list is set to 20. Therefore, the ten most recently changed variables are kept in the tabu list.

6. Criteria for stopping the search

The search will stop as F<10^{-4} or when the iteration number is larger than 10^5

4.4.3 Simulations

Computer simulation is carried out using two FBG sensing systems as shown in Figure 4.1. In the simulation, the spectrum of the measured signal $R(\lambda)$ is generated using Equation (4.1) and the coefficients of $R(\lambda)$ were assumed as (Gong *et al.*, 2002): λ_{B1}=1530 *nm*, λ_{B2}=1530.1, R_1=0.8, R_2=0.5, $\alpha_1 = \alpha_2$=0.2 *nm*, $N(\lambda)$ is white noise with a signal to noise ratio (SNR) of about 10db. The measured spectrum is sampled into 2000 samples within the spectral range from 1529 *nm* to 1531 *nm*.

Simulation is conducted to detect the Bragg wavelength λ_{B1} and λ_{B2} using TS. The search range of $\hat{\lambda}_{B1}$ and $\hat{\lambda}_{B2}$ is [1529, 1531] *nm*. The constant factors of the movement of the parameters are selected as $r_{\hat{\lambda}_{B1}} = r_{\hat{\lambda}_{B2}} = 10^{-4}$, $r_{R_1} = r_{R_2} = 0.01$, $r_{\alpha_1} = r_{\alpha_2}$ 0.01. The TS procedure is described as follows:

1. The TS is started from a random initial solution $i_0 = [\hat{R}_{10}, \hat{R}_{20}, \hat{\alpha}_{10}, \hat{\alpha}_{20}, \hat{\lambda}_{B1}, \hat{\lambda}_{B2}]$, then set for the best solution $i^* = i_0$.
2. The neighbourhood solutions *N(i)* of i_0 are generated by randomly moving only one of the parameters of i_0 using Equations (4.12)and (4.13).
3. Choosing the best neighbourhood *j* from *N(i)* and checking whether it is on the tabu list.
4. If $f(j) < f(i)$, $i=j$; If $f(i) < f(i^*)$, $i^* = i$
5. If $f(i) > f(i^*)$ 3 times, go to step 2 and generate the neighbourhood solutions by moving another parameter of *i* randomly.
6. Repeat steps 2-5 until the criteria for stopping the search is met.

As a result, the TS is finished after 6,3815 iterations, it takes 17 minutes running on a Pentium III 600 MHz 512-M computer. The result of the search is

	R_1	R_2	α_1 *(nm)*	α_2 *(nm)*	λ_{B1} *(nm)*	λ_{B2} *(nm)*
Real value	0.8	0.5	0.2	0.2	1530	1530.1
TS	0.813	0.571	0.183	0.209	1529.9943	1530.0969

The detection error for the Bragg wavelengths of FBG1 and FBG2 are 5.7 pm and 3.1pm respectively. We repeat the tabu search 8 times from different initial solutions. The measurement error is shown in Figure 4.5

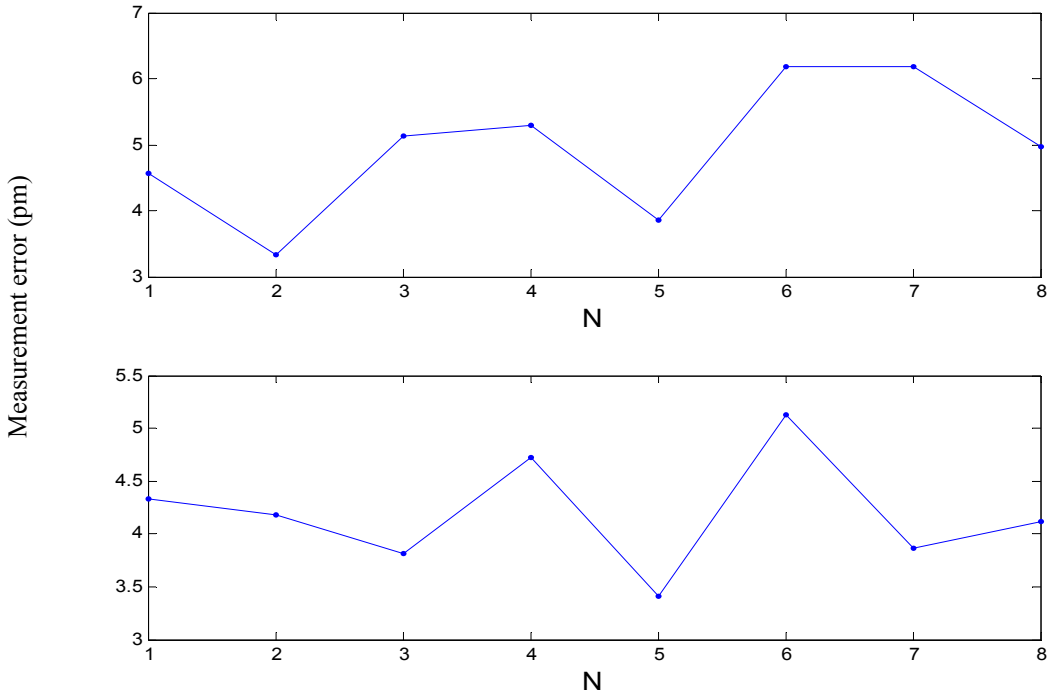

Figure 4.5 Bragg wavelength detection error for FBG1 (upper diagram) and FBG2 (lower diagram)

The root mean square (RMS) values for Bragg wavelength detection error for FBG1 and FBG 2 are 5.09 and 4.33 *pm* respectively. The result indicates that the proposed TS algorithm can accurately detect the Bragg wavelength on the condition that the original spectrums of the FBG sensors can not be pre–determined.

However, the computation time for applying the TS is still too long, although it is much better than the MVS method. In order to further reduce computation time and achieve higher detection accuracy, we introduce a tabu-gradient optimization algorithm in the next section.

4.5 Improving the Performance of IWDM-based FBG Sensing System using tabu–gradient Optimization algorithm

In this section an improved TS algorithm: tabu-gradient (TG) optimization algorithm is introduced to further solve the optimization problem of MVS.

4.5.1 Principles of operation

In the previous section, by using TS algorithm we could accurately detect the Bragg wavelength. However, it still takes a relatively long time to reach the best solution. The reason is that the TS may miss some near global solution during the search process. For instance, as shown in Figure 4.6, solutions *A* and *B* are neighbourhoods of *C*, which is the starting point of iteration. By TS algorithm, solution A may be selected as the best neighbourhood solution for $f(A) < f(C)$ although *B* is the global minimum. This phenomenon is due to the random move principle of the TS, by which the TS may lose the nearby global minimum.

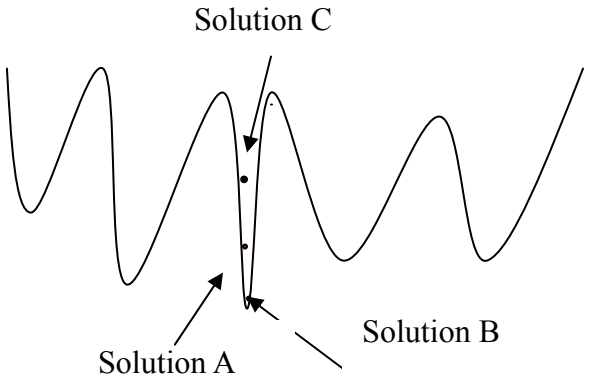

Figure 4.6 The reason that TS may miss a close global minimum Bragg wavelength

To solve this problem and further improve the performance of TS, a tabu-gradient

combination optimization algorithm is proposed. The implementation of TG algorithm is very simple. Based on TS algorithm, the best neighbourhood is applied as the initial solution of the gradient algorithm. The flow chart of TG algorithm is shown in Figure 4.7. Using gradient based algorithm, the solution is estimated in an iterative way and converges to a constant value, which minimizes the object functions:

$$\begin{aligned}
\hat{R}(n+1) &= \hat{R}(n) - \mu\nabla f(\hat{R}(n)) \\
\hat{\alpha}(n+1) &= \hat{\alpha}(n) - \mu\nabla f(\hat{\alpha}(n)) \\
\hat{\lambda}_{B1}(n+1) &= \hat{\lambda}_{B1}(n) - \mu\nabla J(\hat{\lambda}_{B1}(n)) \\
\hat{\lambda}_{B2}(n+1) &= \hat{\lambda}_{B2}(n) - \mu\nabla J(\hat{\lambda}_{B2}(n)) \ ,
\end{aligned} \tag{4.15}$$

where μ is the step size, $\nabla f(\hat{\alpha}(n)) = \frac{\partial f}{\partial \alpha}|_{\hat{\alpha}=\hat{\alpha}(n)}$, $\nabla f(\hat{R}(n)) = \frac{\partial f}{\partial \hat{R}}_{\hat{R}=\hat{R}(n)_m}$,

$\nabla f(\hat{\lambda}_{B1}(n)) = \frac{\partial f}{\partial \hat{\lambda}_{B1}}|_{\hat{\lambda}_{B1}=\hat{\lambda}_{B1}(n)}$, $\nabla f(\hat{\lambda}_{B2}(n)) = \frac{\partial f}{\partial \hat{\lambda}_{B2}}|_{\hat{\lambda}_{B2}=\hat{\lambda}_{B2}(n)}$,

The solution obtained from the gradient algorithm is then the best neighbourhood solution within $N(i)$, because it achieves minimum value of the object function compared with its neighbour. The neighbours of this solution will be evaluated in the next iteration unless they are not in the tabu list. By using TG algorithm, the search process will not miss the global minimum nearby.

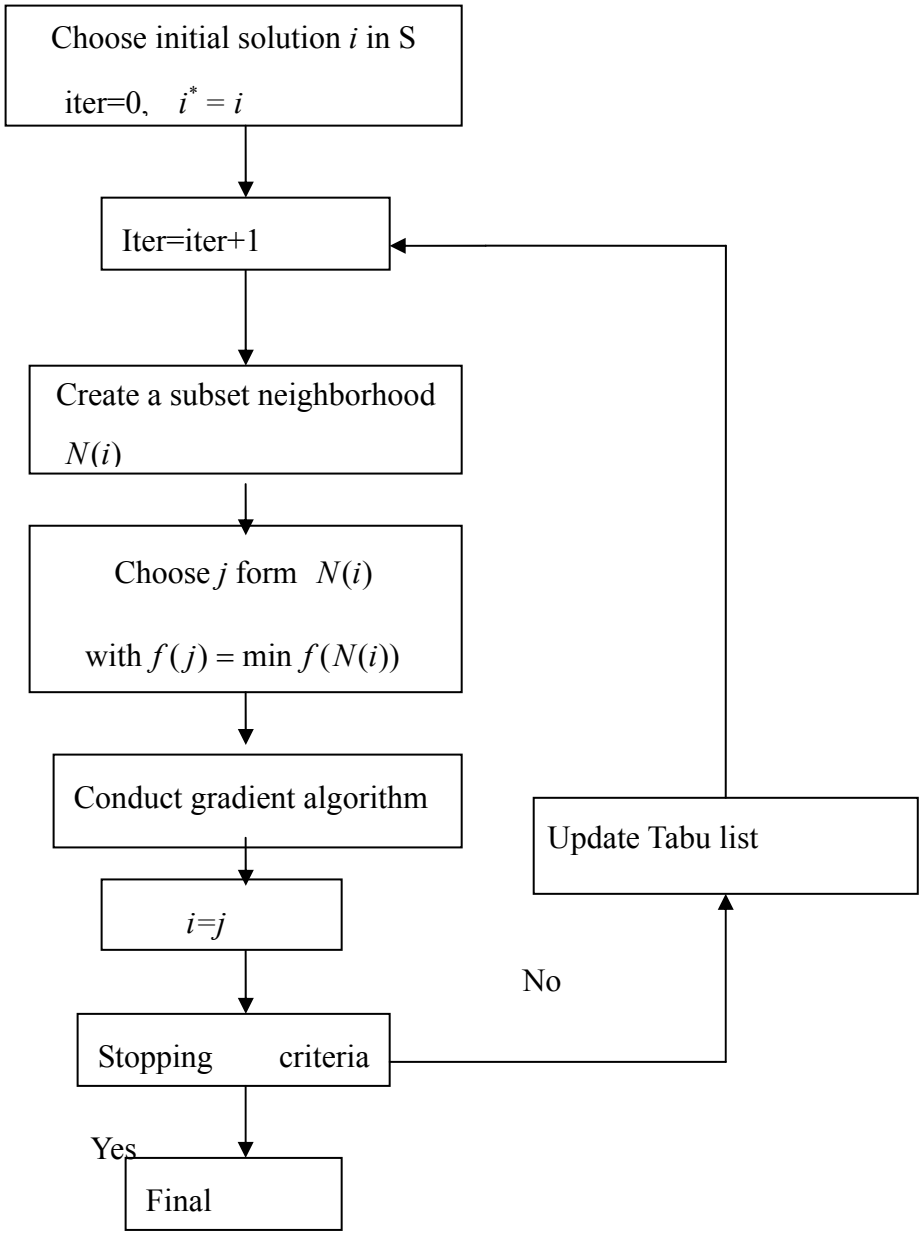

Figure 4.7: Flowchart of tabu-gradient search

4.5.2 Simulations

In order to compare the performance of TS and TG, a computer simulation is carried out with two FBG sensing systems using the same simulation set-up as described above in the previous section. As a result, TG is finished after 1,154 iterations, taking 36 seconds running on the same computer. The results of search are shown in the following table.

	R_1	R_2	$\alpha_1(nm)$	$\alpha_2(nm)$	λ_{B1} (nm)	λ_{B2} (nm)
Real value	0.8	0.5	0.2	0.2	1530	1530.1
TS	0.783	0.518	0.198	0.187	1529.9961	1530.1027

The detection error for the Bragg wavelength of FBG1 and FBG2 are 3.9 pm and 2.7pm respectively. We repeat the tabu-gradient search 8 times from different initial solutions, and the measurement error is shown in Figure 4.8.

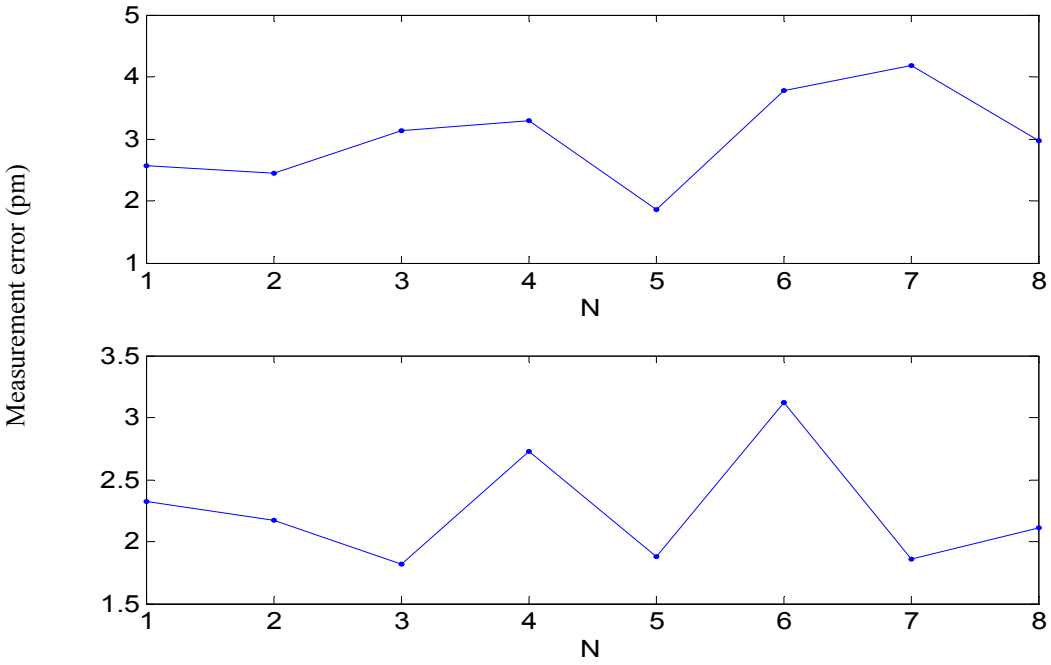

Figure 4.8 Bragg wavelength detection error for FBG1 (upper diagram) and FBG2 (lower diagram) using TG algorithm

The root mean square (RMS) values for Bragg wavelength detection error for FBG1 and FBG 2 are 3.027 and 2.26 *pm* respectively, and the average processing time is 41 seconds. Therefore, the proposed TG algorithm can achieve a better performance than TS on detection Bragg wavelength. Not only does it reduce the computation time

dramatically, but it also improves the detection accuracy.

4.6 Conclusions

In this chapter, we used gradient algorithm, tabu search algorithm and tabu-gradient algorithm for improving the performance of IWDM-based FBG sensing system. Gradient algorithm provides quick and accurate detection of Bragg wavelength if the spectrums of the original uncontaminated FBG sensors can be pre-determined. This method can identify the Bragg wavelengths on condition that the reflection spectrums completely overlap. However, it is invalid where more than one parameter of the uncontaminated spectrum of FBG sensors are uncertain due to the local minima problem.

The global optimization algorithm TS has the ability to avoid the attraction of local minima. The simulation results indicate that by using TS algorithm we can accurately detect Bragg wavelength on condition that the original spectrums of FBG sensors can not be pre–determined. However, the computation time for applying TS is still relatively long, although it is an improvement over the MVS method.

Finally, an improved tabu -gradient algorithm is presented. Compared with TS, it can reduce computation time dramatically and maintain or even improve detection accuracy at the same time.

CHAPTER 5 CONCLUSIONS AND FUTURE WORK

5.1 Conclusions

The main aim of this thesis was to improve the performance of the FBG sensing system. The research work have been performed which included evaluating the performance of existing techniques and developing a number of new techniques. In particular three issues are considered in this thesis.

One dealt with improving the dynamic measurement capability of the FBG sensing system. We presented a novel demodulation system based on wavelength-multiplexed FBG sensors and the FP tunable filter for vibration/dynamic strain measurement (Chapter 2). Using such a system, the restricted scanning frequency of tunable filter is released and it is suitable for multipoint vibration/dynamic strain detection. Furthermore, detection of the Bragg wavelength using this technique is independent of the reconstruction of the spectral shape of reflected light. Therefore, it provides a higher wavelength resolution than the conventional FP tunable filter demodulation system, which requires FP filters having a very narrow bandwidth to reconstruct the spectral shape of the reflected light.

The second aspect considered in this thesis is to improve the measurement precision of FBG sensing systems. In this work, classical digital filters, adaptive digital filters and neural networks are applied to this task (Chapter 3). The classical digital filters are efficient at improving measurement accuracy if the noise signal and the FBG signal have independent frequency spectrums. However, the improvement is limited if the noise components overlap with the Bragg signal in the frequency domain. Then, adaptive filter with 5 different adaptive algorithms is used to overcome the limitation of the classical digital filter. The simulation result shows that it achieves better performance than the latter. In addition, the filter with NMLS-OCF adaptive algorithm

performs faster convergence than the other algorithms. Finally, a BP neural network is used to further improve measurement accuracy. As a result, measurement error is reduced to 1 pm under the condition that the frequency spectrum of the FBG signal overlaps that of the noise signal.

The third and last issue of this thesis is the improvement of the performance of IWDM-based FBG sensing systems using gradient algorithm, tabu search (TS) algorithm and tabu-gradient algorithm (Chapter 4). Gradient algorithm provides quick and accurate detection of the Bragg wavelength, where the spectrums of the original uncontaminated FBG sensors should be pre-determined. However, it is invalid when more than one parameters of the uncontaminated spectrum of FBG sensors are uncertain due to the local minima problem. By using TS algorithm we can accurately detect the Bragg wavelength on condition that the original spectrums of FBG sensors can not be pre–determined. However, the computation time for applying TS is still long, although much better than with the MVS method. Therefore, an improved tabu-gradient algorithm was proposed to solve this problem. Compared with TS, it can reduce computation time dramatically and improve detection accuracy at the same time.

5.2 Suggestions for Future Research Work

The proposed FBG sensing system in Chapter 2 can perform multipoint vibration/dynamic strain measurement based on wavelength division multiplexed FBG sensors. However, the capacity of the WDM technique is limited that the maximum number of FBG sensors in a single fiber is less than ten. Therefore, it would be very useful to apply a new multiplexing technique on our system in order to enlarge capacity and reduce cost.

Another issue for the FBG sensing system is simultaneous measurement of strain and temperature. The FBG sensing system presented in Chapter 2 is suitable for both

dynamic and static strain measurement. However, it can not differentiate the temperature or strain introduced Bragg wavelength change. Currently, a number of techniques address this issue, but most of them need specific grating and special techniques. Therefore, a practical strain-temperature discrimination technique based on our proposed system needs to be developed.

In addition, the performance of our proposed tabu-gradient algorithm may be improved by combined some elicitation algorithm. Thus, the computation time for accurately locating Bragg wavelength will be further shortened.

Finally, the simulation results of Chapter 3 and 4 should be verified by the experiments in the future.

REFERENCES

Alferness R.C. *et al*.(1986), "Narrowband grating resonator filter in InGaAsp/InP waveguides," *Applied Physics Letters*, Vol.49, 1986.

Ball B. A, Morey W.W (1992), "Continuousl tunable single –mode erbium fiber laser", *Optics Letters*, Vol. 17, 1992.

Ball G A., Menlz, and Morey W.W (1993), "Polarunetuc heterodyning Bragg grating fiber laser sensor," *Optics letter*, Vol.18, pp.1976-1978, 1993.

Bhatia V, Vengsarkar AM.(1996), "Optical fiber long-period grating sensors," *Opt Lett*, Vol.21, pp. 692–4,1996.

Berkoff T. A. *et al*. (1995), "Hybrid time and wavelength division multiplexed fiber grating array," *Proc. SPIE*, Vol. SPIE-2444, pp. 288, 1995.

Chien P.-Y., Chang Y.-S, Chang M.-W.(1996), "Vibration suppression in a flexible structure based on fiber optics Michelson interferometric sensor," *J. Intelligent Mater. Syst. Struct.* Vol.7, pp. 65–70, 1996.

Chan P. K. C., Jin W., and Demokan M. S. (2000), "FMCW multiplexing of fiber Bragg grating sensors," *IEEE J. Select. Topics Quantum Electron.*, Vol. 6, pp. 756–763, Oct. 2000.

Chan C.C., Jin W., Demokan, M.S (1999), "Enhancement of measurement accuracy in fiber Bragg grating sensors by using digital signal processing," *Optics & Laser Technology*, Vol31, 1999.

Chan C.C. *et al* (2000) "Performance Analysis of a time division multiplexed fiber Bragg grating sensor array by use of a tunable laser source," *IEEE Journal of selected topics in quantum electronics,* Vol.6, 2000.

Chavez-Pirson, NP Photonics, "The Basics of Fiber Bragg Gratings," www.sensorsmag.com/articles/0804/17/main.html.

Davis M A, Kersey A D(1994), "All-fiber Bragg grating strain-sensor demodulation technique using a wavelength division couple," *Electron, Lett*, Vol. 30, 1994.

Dandridge A., Kersey A.D.(1988), "Overview of Mach-Zehnder sensor technology and applications", in: *Proceedings of the Fiber Optic Laser Sensors VI SPIE*, vol. 985, Boston, pp. 34, 1988.

Dale Barr, JR. (2000), "Wavelength Division Multiplexing (WDM) Networks", Office of the Manager National Communications System, 2000.

Dinev P.D.(1995), "A two-dimensional fiberoptic vibration sensor," *Meas. Sci. Technol*, Vol.6, pp.1395–1398, 1995.

Du WC, Tao XM, Tam HY(1999), "Fiber Bragg grating cavity sensor for simultaneous measurement of strain and temperature," *IEEE Photon Technol Lett*, Vol.11, pp.105–7,1999.

Dong X Y, *et al* (2000), "All-fiber photonic device and system for advanced optical communications," .2000.

Dwyer M. J. *et al* (1998), "Relating the state of cure to the real-time internal strain development in a curing composite using in-fibre Bragg gratings and dielectric sensors," *Meas. Sci. Technol*. Vol. 9, pp 1153-1158, 1998.

Eggleton B, J, *et al*(1994)., "Long periodic superstructure Bragg grating in optical fibres,"*Electronics Letters* Vol.30,1994.

Fallon R.W.(1997), "Identical broadband chirped grating interrogation technique for temperature and strain sensing," *Electronics Letters*, Vol. 33, 1997.

Glover F. (1989), "Tabu search, Part I," *ORSA Journal on computing*, 1989.

Glover, F. and M. Laguna (1997), *Tabu Search*, Kluwer Academic Publishers, Boston,1997.

Grattan K.T.V. and Meggitt (2000), *Optical Fiber Sensor Technology: Advanced application Bragg Grating and distributed sensor*, Kluwer Academic Publishers, London, 2000.

Gornall W. and Amarel T. (2003), *Applications and Techniques for Fiber Bragg Grating Sensor Measurement*, EXFO Burleigh Products Group Inc., 2003

Guan B.O., Tam HY, Tao XM, Dong XY(2000), "Simultaneous strain and temperature measurement using a superstructure fiber Bragg grating," *IEEE Photon Technol Lett*, Vol.12, pp.675–7, 2000.

Gong J. M., MacAlpine J. M. K., Chan C. C., Jin W., Zhang M., and Liao Y. B. (2002), "A Novel Wavelength Detection Technique for Fiber Bragg Grating Sensors," *IEEE Photon. Technol. Lett*, Vol. 14, 2002.

Haykin S. (1986), *Adaptive Filter Theory, First Edition*, A Division of Simon & Schuster Inc., NJ, 1986.

Haykin S. (1996), *Adaptive Filter Theory*, Third Edition, Prentice Hall Inc., NJ, 1996.

Hill K.O. Fuji F., Johnson D.C., and Kawasaki, B.S.(1978), "Photosensitivity in optical fiber waveguides: Application to reflection filter fabrication," *Appl.Phys.Lett*., vol. 32, pp.674-649, 1978.

Hill K O, Malo B, Bilodeau F, Johnson DC and Albert J. (1993),"Bragg gratings fabricated in monomode photosensitive optical fibre by UV exposure through a phase mask," *Applied Physics Letters*, Vol.62, pp.1035-1037, 1993.

Hill P. C. and Eggleton B. J.(1994), "Strain gradient chirp of fiber Bragg gratings," *Electron. Lett.*, Vol. 30, p. 1172, 1994.

Jin W, Stewart G, Philip W, Culshaw B, Demokan MS. (1997), "Limitation of absorption-based fiber optic gas sensors by coherent reflections," *Appl Opt*, 1997.

Jin W. (1998), "Investigation of interferometric noise in fiber-optic Bragg grating sensors by use of tunable laser sources,"*Appl Opt,*1998, Vol.37, pp.2517-2525.

James A. Freeman, David M., Skapura (1991)*, Neural networks : algorithms, applications, and programming techniques*, Reading, Mass. : Addison-Wesley, c1991.

Jharna Mandal, et al.(2005), "Fiber laser-based temperature sensor systems using uniform wavelength-matched Bragg grating reflectors", *Sensor and Actuator*, 2005.

Kersey A. D. *et al* (1993), ".Multiplexed fiber Bragg grating stain-sensor system with a fiber Fabry-Perot Wavelength filter," *Optics Letters*, Vol. 18, pp. 1370-1372, 1993.

Kersey A. D.(1997), Davis M., Patrick A., H. P., LeBlanc, M., K. P. Koo C. G., Askins M. A., Putnam and Friebele E. J., "Fiber grating sensors," J. *Lightwave Technol.*, vol. 15, pp. 1442–1462, Aug. 1997.

Kashyap, Wyatt R. R.(1994), "Wavelength flattened saturated erbium amplifier using multiple side- tap Bragg gratings," *Electronic Letters*, Vol.29, 1994.

Koo A, Kersey AD.(1995), "Fiber laser sensor with ultrahigh strain resolution using interferometric interrogation," *Electronic Letter* 1Vol.31, pp.1180, 1995.

Koo K.P., Tveten A.B., Vohra S.T.(1999), "Dense wavelength division multiplexing of fiber Bragg grating sensors using CDMA," *Electronic. Letter*. Vol.35, pp. 165–167, 1999.

K.Zhou. *et al*, "Fiber Bragg Grating Sensor Interrogation System Using a CCD Side Detection Method With Superimposed Blazed Grating", IEEE Photonics Technology Letters, Vol.16, 2004.

Liquime M., (1997), "Fiber sensors for industrial applications," *Proceeding of the Optical Fiber Sensors conference*, Williamsburg, USA, pp.328-336, 1997.

Lin S.C., T.G. Giallorenzi (1979), "Sensitivity analysis of the sagnac-effect optical-fiber ring interferometer," *Appl. Opt*. vol18, pp.915–931,1979.

Leland B. Jackson (1994), *Digital Filters and Signal Processing*, 3nd Edition, Kluwer Academic Publishers, 1994.

Meltz G, Morey W.W., and Glenn W.H.(1989), "Formation of Bragg grating in optical fibers by a transverse holographic method," *Optical letters*, Vol.14, pp.823-825, 1989.

Malo B., *et al*. (1993),"Point-by-point fabrication of micro-Bragg grating in photosensitive fiber using single excimer pulse refractive index modification techniques," *Electronics Letters*, Vol. 29, 1993, pp.1614-1616.

Morey W, Meltz W. G (1989), "Fiber optic Bragg grating sensors," *Society of Photo optical Instrumentation Engineers, Fiber Optic and Laser Sensors*, vol.1169, 1989

Nunes L.C.S., Valente, L.C.G. Braga A.M.B (2004), "Analysis of a demodulation system for Fiber Bragg Grating sensors using two fixed filters," *Optics and Lasers in Engineering* Vol.42, pp.529–542, 2004.

Ozeki K. and Umeda T.(1984), "An Adaptive Filtering Algorithm Using an Orthogonal Projection to an Affine Subspace and Its Properties," E*lectronics and Communications in Japan*, Vol. 67-A, No. 5, pp. 19 – 27, 1984.

Othonos Andreas, Kyriacos Kalli (1999), *Fiber Bragg grating : Fundamental and applications in telecommunications and sensing*, Artech House optoelectronics library, 1999.

Othonos A..X, Lee and .Measures R.M.(1994) "Superimposed multiple Bragg gratings," *Electronics Letters*, Vol.30, 1994.

Ouellette F.,(1991), "All-fiber filter for efficient dispersion compensation," *Opt. Lett.*, vol. 16, pp. 303, 1991.

Otair, M. A. & Salameh, W. A. (2004) "An improved back-propagation neural networks using a modified non-linear function," *Proceedings of the LASTED International Conference*, 2004.

Putnam M A, Williams and E. J (1995), "Fabrication of tapered, strain-gradient chirped fiber Bragg gratings," *Electronics Letters*, Vol 31, 1995.

Rao Y J (1997), "In-fibre Bragg grating sensors," *Meas. Sci. Technol*., 1997.

Schnaufer B. A. and Jenkins W. K.(1993), "New Data-Reusing LMS Algorithms for Improved Convergence," *Proceedings of Asilomar Conference on Signals, Systems, and Computers*, Pacific Grove, CA, pp. 1584 – 1588, May 1993.

Seungin Baek, Yoonchan Jeong, and Byoungho Lee (2001) , "Characteristics of short-period blazed fiber Bragg gratings for use as macro-bending sensors," *Topical Meeting on Bragg Gratings, Photosensitivity, and Poling in Glass Waveguides*, pp.0-13, Jul. 2001.

Tapanes E. (1991), "Real-time structural integrity monitoring using a passive quadrature demodulated, localised Michelson optical fibre interferometer capable of simultaneous strain and acoustic emission sensing," *Proc. SPIE—Int. Soc. Opt. Eng*. Vol.1588, , pp. 356–367., 1991.

Weis, *et al* (1994), "A four element fiber grating sensor array with phase sensitive detection," *IEEE Photonic Technology Letters*, 1994.

Xu MG, Archambault JL, Reekie L, Dakin JP.(1994), "Discrimination between strain and temperature effects using dual-wavelength fibre grating sensors," *Electron Lett*, Vol.30, pp.1085–7,1994.

Zhang W G, Dong X Y, Feng D J., *et al*. (2000), "Linearly fiber grating-type sensing tuning by applying torsion stress," *Electronics Letters*, Vol.36, 2000.

Zhang Hong Bo, Huang Hai and Shen Zhu (2004), "Demodulation Technique of Fiber Bragg Grating," *Sensing world*, 2004.

Zhang L., Liu Y., Wiliams J. A. R, and Bennion I.(1999), "Enhanced FBG strain sensing multiplexing capacity using combination of intensity and wavelength dual-coding technique," *IEEE Photon. Technol. Lett.*, Vol. 11, pp. 1638–1641, Dec. 1999.

APPENDIX-Program Codes

1. LMS Algorithm

```
function [w,e,y] = LMS(x,d,N,mu,w1);
-------------------------------------------------------------------
% Implementation of the LMS algorithm.
% Inputs:
%   x   input signal
%   d   desired signal
%   N   filter order
%   mu  step size
%   w1  initialization of filter weights (opt)
% Outputs:
%   w   adapted filter weights
%   e   error signal
%   y   outputsignal
-------------------------------------------------------------------
if (~exist('w1')),
   w1 = zeros(N,1);
else
   if length(w1)~=N,
      error('weight initialization must match filter length');
   end;
   w = w1;
endif;
L = length(x);
  for k = 1:L
    xx = x(k+N-1:-1:k);
    y (k)= w'*xx;
    e(k) = d(k)-y(k);
    w = w+2*mu*e(k)*xx;
end
```

2. NLMS Algorithm

```
function [w,e,y] = NLMS(x,d,N,mu,alpha,w1);
%-------------------------------------------------------------------
% Implementation of the NLMS algorithm.
% Inputs:
%   x   input signal
%   d   desired signal
```

```
%   N   filter order
%   mu  step size
%   w1  initialization of filter weights (opt)
% Outputs:
%   w   adapted filter weights
%   e   error signal
%   y   outputsignal
%--------------------------------------------------------------------
if (~exist('w1')),
   w1 = zeros(N,1);
else
   if length(Winit)~=N
      error('weight initialization must match filter length');
   end;
   w = w1;
endif;
L = length(x);
for k = 1:L
   xx = x(k+N-1:-1:k);
   y(k) = w'*xx;
   e(k) = d(k)-y(k);
   p = x(k+N-1)*conj(x(k+N-1));
   w = w+(2*mu*conj(e(k))/p)*X;
end
```

3. APA Algorithm

```
function [w,e,y] = APA(x,d,N,mu,x1,W1,D1);
%--------------------------------------------------------------------
% Implementation of the Nth order affine projection algorithm algorithm.
% Inputs:
%   x   inpute signal
%   d   desired signal
%   N    order of filter
%   mu  step size
%   x1   initialization of state vector
%   w1   initialization of filter weights
%   D1   initialization of desired signal
% Outputs:
%   w   adapted filter weights (column vector)
%   e   error signal (row vector)
%   y   output signal
%--------------------------------------------------------------------
```

```
if (~exist('w1')),
   w= zeros(N,1);
else
   if length(Winit)~=N,
      error('weight initialization must match filter length');
   end;
   w = w1;
end;

L = length(x);
if (~exist('x1')),
   x = [zeros(2N,1); x];
else
   if length(Xin)~=(N)
      error('state   initialization   must   match   filter   length
appropriately');
    end;
   x = [x1; x];
end;
if (~exist('D1'))
   D1 = zeros(N,1);
else
   if length(D1)~=N
      error('error state initialization must match projection order
minus');
   end;
end;
d = [D1; d];
% ***** initialize xx *****
xx = zeros(N,N);

for j = N:-1:1,
  xx(:,N-j) = x(2N-1:-1:j);
end;
% ***** perform adaptive filtering *****
for k = 1:L,
   xx = [x(k+2N-1:-1:k+N-1) xx(:,1:N)];
   D = d(k+N-1:-1:k);
   E = D - xx'*w;
   e(k) = E(1);
   y (k)= w'*xx(1:N);
   R = inv(xx'*xx);
   w = w + mu*xx*R*E;
end;
```

4. NDR-LMS Algorithm

```
function [w,e,y] = NDR-LMS(x,d,N,R,d1,x1,W1);
%--------------------------------------------------------------------
% Implementation of the Nth order NDRL-LMS algorithm.
% Inputs:
%   x   inpute signal
%   d   desired signal
%   R    reuse factor
%   N    order of filter
%   D1   initialization of desired signal
%   x1   initialization of state vector
%   w1   initialization of filter weights

% Outputs:
%   w   adapted filter weights (column vector)
%   e   error signal (row vector)
%   y   output signal
%--------------------------------------------------------------------
if (~exist('w1')),
   w= zeros(N,1);
else
   if length(Winit)~=N,
      error('weight initialization must match filter length');
   end;
   w = w1;
end;
L = length(x);
x = x(:);
if (~exist('x1')),
   x = [zeros(2N,1); x];
else
   if length(Xin)~=(N)
      error('state   initialization   must   match   filter   length
      appropriately');
    end;
    x1 = Xin(:);
   x = [X1; x];
end;
if (~exist('D1'))
   D1 = zeros(N,1);
else
   if length(D1)~=N
      error('error  state  initialization  must  match  projection  order
```

```
minus');
   end;
end;
d = [D1; d];

for k = 1:L
    p=w;
    for i=0:R-1
     for j=1:N
         t= x(k+N-1)*conj(x(k+N-1));
         mu=(d(k+N-j)-p'*x(k+2N-j:-1:k+N-j))/t;
         h=mu*x(k+2N-j:-1:k+N-j);
         g=g+h;
     end
     p=p+g;
   end
   w=g;
   y (k)= w'*x(k+2N:-1:k+N);
   e(k) = d(k)-y(k);
end
```

5. Training Process of BP Neural Network

```
function [w_oh,w_hi,iter] = BP(x,d,B,mu,w1,w2);
%-----------------------------------------------------------------------
% Implementation trainning process of 500x500x500 neural network.
% Inputs:
%   x   inpute signal
%   d   desired signal
%   B    Stop learning once RMSE is below B
%   mu   learning rate
%   w1   initialization of  weights between outputlayer and hidden layer
%   w2   initialization of  weights between hidden layer and input layer

% Outputs:
%   w_oh   weights between outputlayer and hidden layer
%   w_hi   weights between hidden layer and input layer
%  iter   iteration of trainning
%-----------------------------------------------------------------------

if (~exist('w1')),
   w1= zeros(500,500);
end;
w_oh=w1;
```

```
if (~exist('w1')),
   w1= zeros(500,500);
end;
w_oh=w1;
[m,n]=size(x);
e=1;
while e>B,
for i=1: m
    xx=x(i,:)                          %apply x to input layer
    input_h=xx*w_hi;                    % Calculate the input value of the
hidden layer
    output_h=transf(inpt_h);            % Calculate the output value of the
hidden layer
    input_o=output_h*w_ho;              % Calculate the input value of the
output layer
    output_o=transf(input_o);           % Calculate the output value of the
output layer
    e1=err1(d,output_o,input_o);        %   Calculate   the   error   for
output units
    e2=err2(input_h,e1,w1);             % Calculate the error for hidden
units
    w_ho=w_ho+mu*e1*output_h'           %   Calculate   the   error   for
output units
    w_hi=w_ho+mu*e2*xx'                 % Calculate the error for hidden
neurons
    e=sum(e1.*e1)/2;
    iter=iter+1;
end

function output = transf(x)
   for i=1: length(x)
      output(i)=1/(1+exp(-x(i)))
   end


   function e1=err1(x,y,z)
   for i=1:length(x)
      e1(i)=(x(i)-y(i))*(1+exp(-z(i)))^(-2)*exp(-z(i));
   end

   function e2=err2(x,y,z)
   for i=1: length(x)
      z1=z(:,i)
      e2(i)=(1+exp(-x(i)))^(-2)*exp(-x(i))*(y*z1);
```

```
   end
```

7. Tabu Search Algorithm

```
function [iter,i_min]=tabu(TABUSIZE,ITERMAX,mu)

%-------------------------------------------------------------------
% Implementation of the tabu search algorithm.
% Inputs:
%   TABUSIZE     size of tabulist
%   ITERMAX       maximum lteration number
%   mu            learning rate of gradient algorithm
% outputs:
%   iter          number of iteration
%   i_min         Final solution
%-------------------------------------------------------------------

% initialize prameters
I = [0.8 0.5 0.2 0.2 10 10.1];
l = [1:2000];
l = l / 1000;
l = l + 9;
L = 2000;

Nois = 0.001;
%generate original R
R = gRa(I, l, L, Nois);

r = [0.7 0.01 0.01 0.01 0.0001 0.0001];
Xt = [1 1 0.5 0.5 11 11];
Xb = [0 0 0 0 9 9];

i_min = [0.001 0.001 0.001 0.001 9.001 9.001];
f_min = 10;
iter = 0;
Tabu = zeros(TABUSIZE, 6);
intabu = 0;
s = 1;
s_counter = 0;
i = i_min;

for iter = 0:ITERMAX
    s_counter = s_counter + 1;
    [f, j] = neibcomp(R, Xt, Xb, r, i, s, 10, l, L);    %create and compare
```

```
neighborehood
    [F, n] = min(f);
    intabu = comp(j(n, :), Tabu); %search vector in Tabu list
    while intabu ~= 0
        f(n, :) = 10;
        [F, n] = min(f);
        intabu = comp(j(n, :), Tabu);
        if F >= 10
            break;
        end
    end

    j1=gradient(j(n,:))  %implement gradient algorithm
    if(F<f_min)
        i_min = j1;
        f_min = F;
        s_counter = 0;
    end
    i = j1;
    Tabu=update(j1);    %updata tabulist

    if(s_counter>3)
        s = mod(s, 6);
        s = s + 1;
        s_counter = 0;
    end
    if(F<0.0001)
        break;
    end
end

%generate original R
function R = gRa(i, l, L, Nois);
R = gR(i(1), i(2), i(3), i(4), i(5), i(6), l, L, Nois);

function R = gR(R1, R2, a1, a2, lb1, lb2, l, L, Nois);
R = Rxx(R1, R2, a1, a2, lb1, lb2, l, L);
N = rand(1, L);
N = N * Nois;
R = R + N;

function R = Rxx(R1, R2, a1, a2, lb1, lb2, l, L);
R = zeros(1 , L);
for i = 1:L
```

```
    R(i) = Rx(R1, R2, a1, a2, lb1, lb2, l(i));
end

function R = Rx(R1, R2, a1, a2, lb1, lb2, l);
p1 = R1 * exp((-4) * log(2) * ((l - lb1)^2) / (a1^2));
p2 = R2 * exp((-4) * log(2) * ((l - lb2)^2) / (a2^2));
R = p1 + p2;

%create and compare neighborehood
%R, Xt, Xb, r, i: all arrays. s: 1~6 point out which para is being examed
n: number of subset neighborhood.
function [f, j] = neibcomp(R, Xt, Xb, r, i, s, n, l, L);
j = zeros(n, 6);
%J = i;
f = zeros(1, n);
X = i(s);
x = Nxx(X, r(s), Xt(s), Xb(s), n);
for k = 1:n
    j(k, :) = i;
    j(k, s) = x(k);
    f(k) = fxxa(R, j(k, :), l, L);
end

%create neighborehood of i
function x = Nxx(X, r, Xt, Xb, L);
x = zeros(1, L);
for i = 1:L
    b = Bx(r, Xt, Xb);
    X = X + b;
    x(i) = X;
    if(x(i)<=Xb)
        x(i) = Xb + 0.001;
    end
    if(x(i)>=Xt)
        x(i) = Xt - 0.001;
    end
end

%create beta
function b = Bx(r, Xt, Xb);
d = rand(1) * 2 - 1;
b = d * r * (Xt - Xb);

% calculate the value of object function
```

```
function f = fxxa(R, i, l, L);
f = fxx(R, i(1), i(2), i(3), i(4), i(5), i(6), l, L);

function f = fxx(R, R1, R2, a1, a2, lb1, lb2, l, L);
Rd = Rxx(R1, R2, a1, a2, lb1, lb2, l, L);
delta = R - Rd;
delta2 = delta.^2;
f = sum(delta) / L;

%search vector in Tabu list
function yn = comp(s, T);
yn = 0;
L = length(T(:, 1));
for i = 1:L
    r = s - T(i, :);
    if(sum((r.^2)) == 0)
        yn = i;
        break;
    end
    if(T(i, 1)==0)
        break;
    end
end

%updata tabulist
function Tabu = updat(j,TABUSIZE);
 for i=1:TABUSIZE-1
     Tabu(i,:)=Tabu(i+1,:)
 end
Tabu(Tabusize,:)=j;
```